RSC Sustainability

Accepted Manuscript

This article can be cited before page numbers have been issued, to do this please use: C. Fiorillo, L. Trossaert, E. Bezeraj, S. Debrie, H. Ohnmacht, P. Van Steenberge, D. R. D'hooge and M. Edeleva, *RSC Sustain.*, 2024, DOI: 10.1039/D4SU00485J.

ROYAL SOCIETY OF CHEMISTRY

View Article Online
DOI: 10.1039/D4SU00485J

A key consumer product in our society is the PET bottle for which long term circularity via polyester recycling is within reach (UN SDG 12). However, with more generations of waste being created it is unclear when which recycling technology is most suited (UN SDG 9 and 13), specifically how long mechanical recycling is a preferred technique. The current review puts forward how the quality of polyester-based materials depends on molecular changes, demonstrating that the connection of the molecular and material scale is paramount in future R&D and product design. By doing so better guidelines can be formulated regarding the ideal PET recycling route and industrial implementation, accounting for regulations and geographical constraints.

Molecular and material property variations during ideal PET degradation and mechanical recycling

Chiara Fiorillo,[1,2] Lynn Trossaert,[1] Erion Bezeraj,[1] Simon Debrie,[1] Hannelore Ohnmacht,[1]

Paul H.M. Van Steenberge,[2] Dagmar R. D'hooge,[2,3*] Mariya Edeleva[1,*]

[1] Centre for Polymer Material and Technologies (CPMT), Technologiepark 130, 9052 Zwijnaarde

[2] Laboratory for Chemical Technology (LCT), Technologiepark 125, 9052 Zwijnaarde

[3] Centre for Textile Science and Engineering (CTSE), Technologiepark 70a, 9052 Zwijnaarde

Corresponding authors: dagmar.dhooge@ugent.be mariya.edeleva@ugent.be

Abstract

Poly(ethylene terephthalate) (PET) is an important polyester utilized for a wide variety of applications such as bottles, fibers and engineering compositions. Its chemical composition depends on the use of main monomers (e.g. terephthalic acid and ethylene glycol) as well as comonomers (e.g. diethylene glycol and isophthalic acid) in low amounts, defining several reaction pathways upon degradation or (mechanical) recycling. The present work gives a detailed overview of these molecular pathways, differentiating between thermal, thermo-mechanical, thermo-oxidative, photo-oxidative, hydrolytic and enzymatic degradation reactions. Considering at most low contaminant amounts, hence, under ideal (mechanical) recycling (lab) conditions, a wide range of functional group variations is already revealed, specifically during consecutive polyester processing cycles. Moreover, as a key novelty it is explained how the molecular variations influence the material behavior, considering both rheological, thermal and mechanical properties. Supported by basic life cycle analysis, it is highlighted that our future improved assessment of the mechanical recycling potential must better link the molecular and material scale. Only such linkage will open the door to a well-balanced polyester waste strategy, including (i) the evaluation of the most suited recycling technology at industrial scale, dealing with the mitigation of contaminants, and (ii) its further adoption and design in the context of the overall virgin and recycling market variation.

Keywords: degradation reactions; sustainability; polymer circularity; (co)polyesters; viscosity

View Article Online
DOI: 10.1039/D4SU00485J

Contents

View Article Online
DOI: 10.1039/D4SU00485J

List of abbreviations

ABS	Acrylonitrile Butadiene Styrene Polymer
ASTM	American Society For Testing And Materials
BDB	Butylene Dibenzoate
BHET	Bishydroxyethyl Terephthalate
CAGR	Compound Annual Growth Rate
CF	Carbon Footprint
CFD	Computational Fluid Dynamic
CHDM	1,4-Cyclohexanedimethanol
C-PET	PET Modified With A Crosslinking Agent
DEG	Diethylene Glycol
DFT	Density Functional Theory
DMT	Dimethyl Terephthalate
DSC	Differential Scanning Calorimetry
EB	Elongation At Break
EDB	Ethylene Dibenzoate
EG	Ethylene Glycol
FTIR	Fourier Transform Infrared Spectroscopic
GO	Graphene Oxide
GPC	Gel Permeation Chromatography
HDPE	High Density Polyethylene
HFIP	1,1,1,3,3,3-Hexafluoroisopropanol
IPA	Isophthalic Acid
IV	Intrinsic Viscosity
LCA	Life Cycle Assessment
LCB-PET	PET Modified With Long Chain Branches Via Reactive Extrusion
LDPE	Low Density Polyethylene
L-PET	Linear PET
MFI	Melt Flow Index
MFR	Melt Flow Rate
MHET	Mono(2-Hydroxyethyl) Terephthalate
MHETase	Enzyme For The Hydrolysis Of MHET
NMR	Nuclear Magnetic Resonance
OECD	Organization For Economic Cooperation And Development
OOP	Onset Oxidation Peak
PBT	Polybutylene Terephthalate
PCL	Poly(Caprolactone)
PCT	CHDM-Modified PET
PCTA	CHDM-Modified PET Modified With IPA
PCW	Post-Consumer Waste
PET	Poly(Ethylene Terephthalate)
PET-btg	Bottle Grade PET
PETG	Polyethylene Terephthalate Glycol
PETg	PETG Grade With Low Amount Of Modifications
PETM	Modified Polyethylene Terephthalate
PIW	Post-Industrial Waste
PLA	Poly(Lactic Acid)
PPC	Poly(Propylene Carbonate)

View Article Online
DOI: 10.1039/D4SU00485J

PS	Polystyrene
PS	Polystyrene
RH	Relative Humidity
rPET	Recycled PET
RPET-5	PET Reprocessed For 5 Times
SAOS	Small Amplitude Oscillatory Sweep
SEC	Size Exclusion Chromatography
SSP	Solid-State Polymerization
TGA	Thermogravimetric Analysis
THF	Tetrahydrofuran
TMCD	2,2,4,4-Tetramethyl-1,3-Cyclobutanediol
TMP	Trimethylolpropane
TPA	Terephthalic Acid
TRLs	Technology Readiness Levels
TRMS	Time-Resolved Mechanical Spectroscopy
VPET	Virgin PET
xGnP	Exfoliated Graphite

View Article Online
DOI: 10.1039/D4SU00485J

Introduction

Poly(ethylene terephthalate) (PET) is a thermoplastic polymer belonging to the polyester family. It is used for applications such as synthetic fibers; beverage, food and other liquid containers, in general, packaging; thermoformed shape production; and engineering resins often in combination with glass fibers. Packaging, in particular beverage packaging, is likely the most important PET application, with a current market size larger than 20 billion $[1] and plastic bottles taking a share of more than 80%. The global PET bottle market is expected to be worth around 35.7 billion $ by 2032, growing at an annual growth rate (CAGR) of 3.3% during the forecast period from 2024 to 2032.[2]

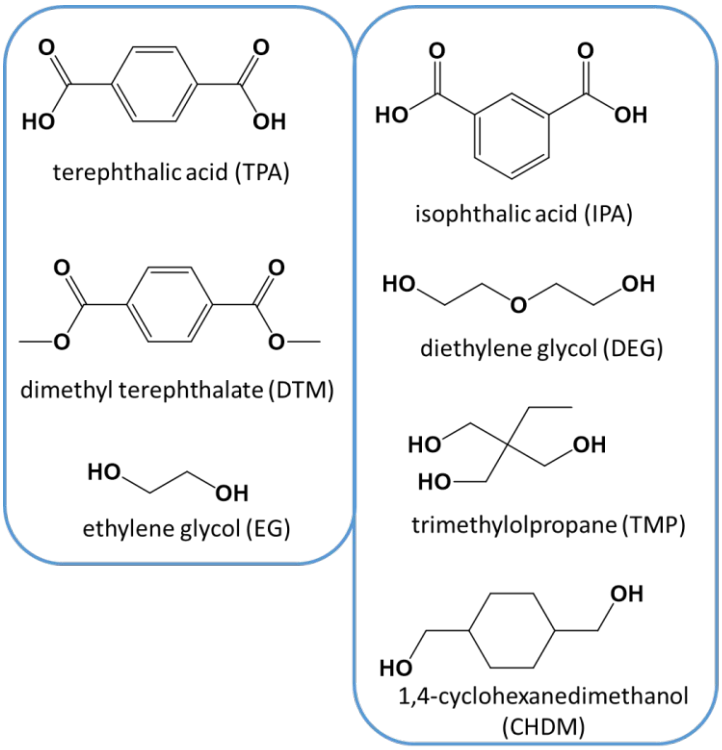

Figure 1. Left: conventional monomers for PET synthesis; Right: typical comonomers used in low amounts (e.g. a few mass %) to enable the production of bottle-grade PET (PET-btg).

In its most simple form, only two monomers are employed for PET synthesis.[3,4] Examples of such monomers are terephthalic acid (TPA), or its counterpart dimethyl terephthalate (DMT), and ethylene glycol (EG), as depicted in the left part of **Figure 1**. The reactions taking place are polycondensation reactions, releasing small molecules such as water or methanol as byproducts, considering at first sight equimolar amounts of monomers.[5] Practically, volatility issues can be encountered and a high average

View Article Online
DOI: 10.1039/D4SU00485J

chain length PET is commercially required,[6–8] implying deviations from the natural stoichiometric balance. Moreover, an injection-molded PET grade (e.g. bottle-grade PET; PET-bt)[5] needs to be synthesized employing low concentrations of comonomers alongside the aforementioned traditional (main) monomers. As shown in the right part of **Figure 1**, typical comonomers are diethylene glycol (DEG), isophthalic acid (IPA), trimethylolpropane (TMP), and cyclohexanedimethylene glycol or 1,4-cyclohexanedimethanol (CHDM).[9,10] DEG is the main comonomer used in PET-btg production and its ether groups provide more flexibility to the otherwise relatively stiff conventional backbone. Depending on the polymerization conditions, the concentration of DEG monomer units in the final polymer application changes from 1 to 4 mol%.[11]

The presence of comonomers decreases the thermal crystallization rate and improves the ductility,[11] processability and clarity of modified PET compared to conventional PET.[5,12–15] The lowering of the crystallinity is important to avoid more easily production challenges regarding shrinkage and warpage.[16] This can be further exploited in e.g. additive manufacturing applications, as exemplified by the copolyester polyethylene terephthalate glycol (PETG), being synthesized using a significant molar amount of CHDM (up to 50%) in the presence of EG and DMT.[17]

One of the largest challenges the PET industry faces is the efficient incorporation of its own waste in the value chain for many decades to come, guaranteeing an acceptable product quality at any time. Governments are taking a leading role in setting recycling boundaries, with e.g. the environmental rules of the European Commission demanding that PET-based packaging material needs to include 30% of recycled plastics by 2030.[18] Recycling of PET has been industrially realized but with increased circular usage of PET (bottles) the composition of the PET waste stream will change in a very dynamic manner, further influenced by the local collection methods, sorting strategies and process efficiencies.[19] It is thus paramount to evaluate which recycling technology and/or operating settings are most suited during a non-trivial feedstock variation for a given geographical location.

Parallel to changing regulations, societal pressure exists for the polymer production community to become more sustainable and to deliver circular innovative polymeric materials. According to the Organization for Economic Cooperation and Development (OECD), in 2022, ca. only 10% of the plastic

View Article Online
DOI: 10.1039/D4SU00485J

waste was recycled, with (i) worldwide polymer production that doubled in the last decade (to ca. 350 Mt in 2019), and (ii) ca. 66% of the produced plastics having a use lifetime below 5 years, specifically packaging items.[20] The majority of plastic waste still ends up in landfill, is incinerated or unfortunately leaks in the environment.[21] Interestingly, the global polymer production originating from recycled or secondary sources is becoming more relevant, with e.g. a reported increase from ca. 7 to 30 Mt from 2000 to 2019. However, the market share of such recycled products is still below 10%, showcasing the relevance of recycling research and design. In any case, it is advisable to work on a worldwide waste management plan, including dedicated and durable investments in waste management infrastructure.[20]

It is particularly critical to compare polymer recycling technologies and define criteria allowing a fair judgment of the preferred technology in a given geographical area, taking into account regulations and future intensions in view of scale-up and technology improvement. Notably for PET streams both mechanical and chemical recycling technologies have already been developed and adjusted.[22,23] For example, re-melting through extrusion, hence, mechanical recycling technology was originally implemented in the absence of additives but to counteract discoloration and molecular changes one has added complementary color agents, inorganic substances and chain extenders later on.[24] More recently, it has been put forward that a vacuum solid-state pre-reactor enables a better decontamination and crystallization of flakes before performing the actual re-melting.[25] Next to crushed PET waste mixing for filler replacement, incinerating PET waste for direct energy recovery (ca. 45 kJ g^{-1}), and PET waste pyrolysis for indirect energy recovery (e.g. fuels),[26,27] chemical technology has been developed exploiting the reverse nature of polycondensation reactions, by adding in excess the solvent that was a byproduct from the synthesis to induce depolymerization.[28] For these depolymerization technologies that aim at high yield monomer and oligomer formation, a distinction can be made between hydrolysis (use of water),[29], glycolysis (use of glycol),[30] and alcoholysis (use of alcohol).[31] However, stringent reactor conditions (e.g. high temperature and pressure) and dedicated separation techniques are needed. In parallel, physical recycling through dissolution and extraction has been developed.[28,32]

Mechanical recycling is a lower energy process as compared to chemical recycling but it requires clean inputs and after multiple cycles the polyester may degrade too much, which may limit its fitness for use

View Article Online
DOI: 10.1039/D4SU00485J

in certain applications, while chemical recycling can handle hard to recycle inputs and provides a virgin quality material as an output.[19,33] For example, it has been indicated that the material properties of PET post-consumer-waste (PCW) as flakes should obey the requirements as specified in Table 1. Besides requirements for molecular driven properties such as the intrinsic viscosity ([η]; also known as IV) and the melting temperature (T_m), care should be taken regarding acceptable contamination levels in the processed flakes.[19] As shown in Table 1, a process contaminant such as water need to be avoided by drying although in some industrial cases one operates wet, allow for molecular scale degradation by hydrolysis to then repair the chains later on in the production train. Hence, it is critical to understand molecular scale driven changes during PET mechanical recycling, which is less explored in detail in previous work.

Table 1. Example of minimum requirements for mechanical recycling of PET flakes[19]

Property	**Value**
intrinsic viscosity, [η]	> 0.7 dl g^{-1}
melting temperature, T_m	> 240 °C
water content	< 0.02 wt.%
flake size, D	0.4 mm < D < 8 mm
dye content	< 10 ppm
yellowing index	< 20
metal content	< 3 ppm
poly(vinyl chloride) content	< 50 ppm
polyolefin content	< 10 ppm

The primary difference between the composition of post-industrial waste (PIW) and PCW, with respect to virgin PET, is the source of the waste and the level of contamination. PIW comes from manufacturing processes and is generally clean and easily recyclable but PCW originates from products used by individuals and can be more contaminated and challenging to recycle. This is because in PCW PET, dirt, labels, glue, other polymers and various small molecule contaminants are present associated with the packaging, bottles and other applications in which the PET material has been used.[34]

View Article Online
DOI: 10.1039/D4SU00485J

In the present contribution, starting from an enumeration of the expected chemical building blocks incorporated during synthesis, we give in a first part an overview of the variations in molecular properties during PET mechanical recycling. This is done assuming that the contamination amount is low and even in many cases negligible, hence, ideal (lab) mechanical recycling conditions are covered. A distinction is made in this first part between thermal, thermo-oxidative, photo-oxidative, hydrolytic and enzymatic (degradation) reactions, including a discussion of literature data on kinetic parameters, specifically (overall/lumped) degradation rate coefficients. For the interpretation of the impact of the molecular properties on the material properties, as covered in a second part of this contribution, emphasis is on the variations of rheological, thermal and mechanical properties, as induced by environmental exposure during use and/or by mechanical recycling itself.

By connecting the discussion of the second part to the first part, a framework is set to facilitate answering two major questions of relevance for the PET recycling community and regulation authorities: (i) how does recycling of PET influences the (packaging) material properties due to (macro)molecular changes, and (ii) how we can achieve acceptable (mechanical) performance of PET products which contain recycled PET (rPET).

The novelty of this review lies in providing a PET (mechanical) recycling perspective on both the molecular and material scale and connecting both. This is opposed to most other PET-based reviews that only deal with (i) the overall chemical modification and main operational units of the manufacturing steps,[31,35–38] (ii) are focusing from a fundamental point of view only on less industrially mature (enzymatic-based) molecular alternations but not material properties,[39] or (iii) are oriented around molecular design more for chemical recycling purposes.[40]

This connection of molecular and material variations for PET mechanical recycling goes hand in hand with understanding more the chemistry behind the original polyester, in general, polymer synthesis. This synthesis is only treated in more material driven approaches to a very limited extend by for instance a (indirect) average molar mass assessment only.[41,42] It should be stressed that chain repair, being a key mitigation in the PET mechanical recycling industry, depends on having the correct functional groups and chain lengths. In other words, science-driven evaluations of mechanical recycling techniques need to account for sufficiently detailed (degradation) reaction schemes.

View Article Online
DOI: 10.1039/D4SU00485J

For comparison purposes, results on one of the most other studied polyesters, i.e. poly(lactic acid) (PLA), as well as on conceptually related thermoplastic vinyl polymers such as polystyrene (PS) and acrylonitrile butadiene styrene polymer (ABS) are included. Guidelines are also provided to better identify threshold and boundary values for PET mechanical recycling constraints and to support strategic finetuning of PET recycling policies.

The present contribution will be followed by a second contribution dealing with industrial details of the overall PET mechanical recycling process. In that contribution, the industrial challenges compared to ideal (lab) mechanical recycling are addressed, with a specific focus on the expected degree of contamination and typical mitigation strategies along the production chain as well as detailed life cycle assessment (LCA) analysis. This second contribution will target state-of-the-art insights on the impact of industrial contaminants on the most important relationships between molecular and material property variations as established in the present contribution, which is already supported by more basic LCA analysis addressing overall numbers in carbon footprints and the E-factor.

View Article Online
DOI: 10.1039/D4SU00485J

Synthesis routes and commercial grades

In line with general step-growth polymerization principles and as outlined in **Figure 2** (top), conventional PET should be obtainable from e.g. the esterification reaction between EG and TPA with water as a by-product. Alternatively, this transesterification reaction can be realized by reacting EG and DMT, releasing methanol as a byproduct (**Figure 2**; bottom).

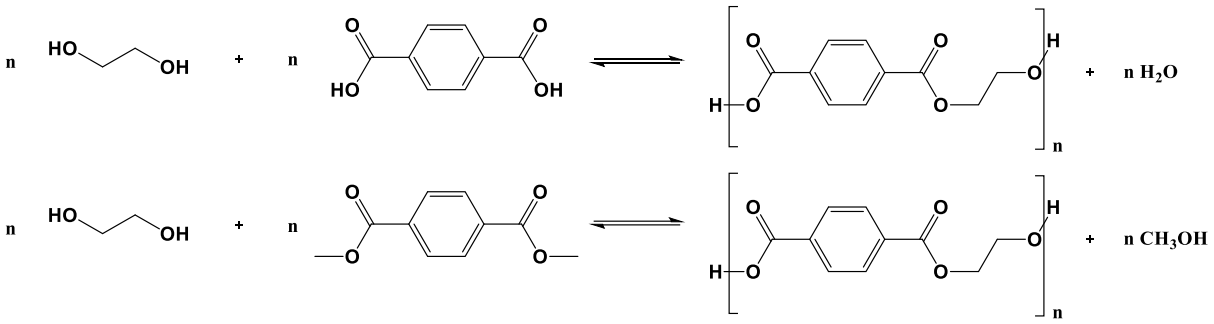

Figure 2: Basic reaction scheme for conventional PET synthesis, either via the polycondensation of EG and TPA (top) or EG and DMT (bottom) from Figure 1.

A chemical challenge is although the reversibility of the reaction and the ease of byproduct removal.[43,44] Industrially, a three stage synthesis is therefore applied with the main reactions per stage depicted in the top part of **Figure 3** (only TPA-EG route shown to not overload the subplot) and the associated (continuous) reactor configuration included in the bottom part of the same figure.

In the first stage of the commercial implementation,[8] which is known as esterification, TPA (or DMT) is reacted with an excess amount of EG to obtain bishydroxyethyl terephthalate (BHET) and possibly some oligomers. Mostly a metal acetate catalyst is employed such as zinc acetate. A temperature of 160-180 °C is applied for several hours, and in a reflux column the condensation product water (or methanol) is separated from EG as well as additives and stabilizers are utilized in the reactor.[45]

In the second stage of the commercial implementation, the BHET-rich mixture exiting the first reactor is brought in a superfine filter to remove residues related to additives. A pre-polymerization then takes place under vacuum at a higher temperature of about 270°C, defining a so-called transesterification stage. EG is removed by a vacuum pump while the polymer product is pumped to finishing reactors after a residence time of about two hours, defining the third stage typically denoted as polycondensation.

View Article Online
DOI: 10.1039/D4SU00485J

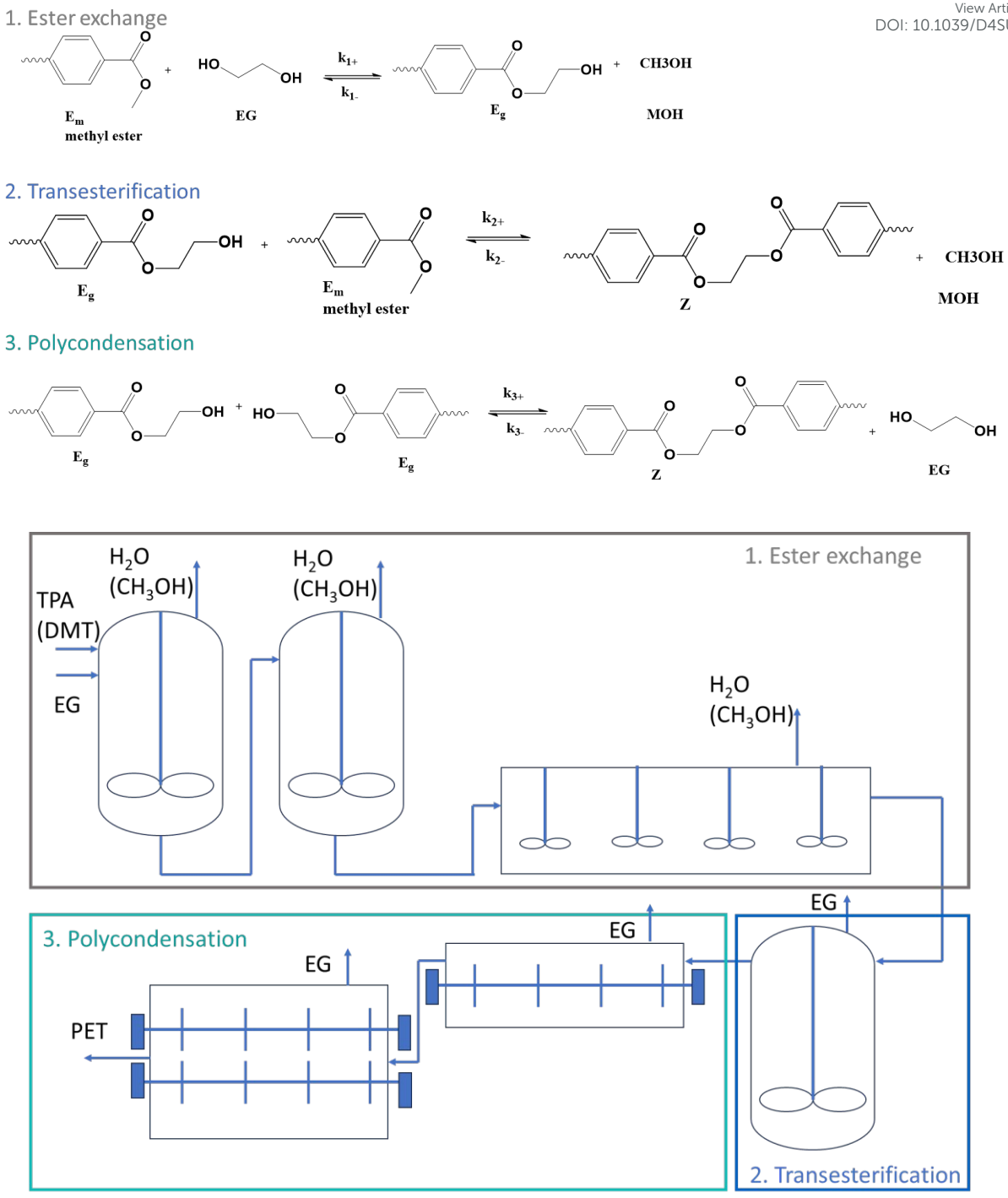

Figure 3: Industrial implementation of PET synthesis, starting either from EG and TPA or EG and DMT from Figure 1, according to three stages with at the top the main reactions per stage and at the bottom the associated continuous reactor configuration; $k_{(-)i}$ values are rate coefficients for stage *i* with kinetic equations depicted in Figure 4 also accounting for mass transfer (k_L).

This last stage of the commercial implementation in **Figure 3** is considered to increase the number average chain length x_n from e.g. 30 to 80.[8] A large surface area is needed to remove EG from the viscous

View Article Online
DOI: 10.1039/D4SU00485J

melt, with typical reactors being rotating disk, extruders, and cage reactors. If the x_n of the conventional PET needs to be e.g. above 100, solid-state polymerization (SSP) can be additionally applied in a fourth stage of the industrial implementation. Sintering of PET particles can be prevented in this stage by selecting a sufficiently high reaction time for crystallization through prior annealing.[46–49]

1. Ester exchange

$$E_m + EG \underset{k_{1-}}{\overset{k_{1+}}{\rightleftharpoons}} E_g + MOH \qquad R_1 = 2k_{1+}E_m EG - k_{1-}E_g MOH$$

2. Transesterification

$$E_m + E_g \underset{k_{2-}}{\overset{k_{2+}}{\rightleftharpoons}} Z + MOH \qquad R_2 = k_{2+}E_m E_g - 2k_{2-}Z\,MOH$$

3. Polycondensation

$$E_g + E_g \underset{k_{3-}}{\overset{k_{3+}}{\rightleftharpoons}} Z + EG \qquad R_2 = k_{3+}E_g^2 - 4k_{3-}Z\,EG$$

$$\frac{d(V\,E_m)}{dt} = -(R_1 + R_2)V$$

$$\frac{d(V\,Z)}{dt} = (R_2 + R_3)V$$

$$\frac{d(V\,MOH)}{dt} = (R_1 + R_2)V - (k_L a)_{MOH}V(MOH - MOH^*)$$

$$\frac{d(V\,EG)}{dt} = (-R_1 + R_3)V - (k_l a)_{EG}V(EG - EG^*)$$

Figure 4: Kinetic modeling principles to describe and tune the PET synthesis according to the reactions in Figure 3 (calculation of reaction rates R_i). Functional group modeling is applied with k_L being a mass transfer coefficient, a the mass transfer area and V the volume.

In any case, kinetic modeling can facilitate the reaction progress efficiency per stage, as conceptually highlighted in **Figure 4**, showcasing the differential equations to calculate variations in functional group concentrations according to the reactions in **Figure 3**. This is done accounting for volume (V) variations and byproduct removal considering mass transfer coefficients (k_L values). For the latter coefficients, correlations can be utilized depending on *e.g.* the reactor geometry, reaction system and agitation type

View Article Online
DOI: 10.1039/D4SU00485J

or in general more fundamental theories can be considered, which have a direct link with e.g. the Flory-Huggins theory.[8]

Modified PET is synthesized in a similar way as depicted in **Figure 3** but other types and/or ratios of reactants are employed, consistent with the chemical structures introduced in the right part of **Figure 1**. An overview of typical PET commercial grades for given applications is included in **Table 2**, distinguishing between the (co)monomers, additives and targeted number average molar masses (M_n values).

Table 2. Examples of grades of PET and modified PET (in general polyester) in the market and their applications as well as the main synthesis characteristics; v: virgin; r: recycled.; M_n: number average molar mass. (Co)monomers based on Figure 1.

Grade	(Co)monomers	Comonomer %	M_n (g mol^{-1})	Common additives	Applications	References
(v) PET	EG, TPA/DMT	n.a.	17.600-52.300	depending on application	disposable beverage bottles, packaging, textile fiber production, films	50–54
rPET	EG, TPA/DMT	n.a.	5.000-35.000	thermal stabilizers, antioxidant	textile production, fiber applications	50,53,55–60
PET foam	EG, TPA/DMT	n.a.	22.390-23.159	blowing agents, flame retardant	building and construction, composites	8,50,61–63
PETG	EG, TPA/DMT, CHDM	up to 50 mol.% CHDM	27.300-33.200	fibers, glass/carbon	3D printing, packaging	64–71
PBT	TPA/DMT, 1, 4 – butanediol	< 5 mol% total diol	5.000-45.000	pigments, minerals, fillers, flame retardants, fibers	electrical engineering/electronics, vehicle manufacturing, household goods	8,72–76
PCTA	TPA, IPA, CHDM	< 20 mol% total diacid	-	-	optical applications	74,77
PTT	TPA, 1,3-propane-diol, DEG	< 5 mol% total diol	-	-	textile fibers	74,78,79

The incorporation of comonomer units can significantly change the thermal stability of PET. As conventionally T_m and the glass transition temperature (T_g) are about 260 °C and 78 °C, a modified PET with a somewhat lower T_m and a moderately higher T_g would result in easier and cheaper processing, and make PET more suitable for higher temperature applications such as packaging of hot-filled

View Article Online
DOI: 10.1039/D4SU00485J

products. Furthermore, the ability to synthesize PET with a weaker tendency to crystallize by adding comonomers enlarges the ductility range for applications, with important reviews being the ones of Kint and Munoz-Guerra,[80] Demirel et al,[81] Pang et al.,[82] and Konstantopoulou et al.[83]

A key example is the use of the bulky CHDM unit, enabling a highly amorphous structure and transparency specifically for high molar amounts (e.g. 50%) as in PETG. The incorporation of the 1,4-cyclohexylene units, compared to the linear EG units, delivers higher T_m values, which is critical to certain applications but also introduces potential thermal degradation issues during processing. The initial commercialization target for PETG was extrusion blow moulding, however, its greatest success has been found in extruded sheets, for which its combination of excellent clarity, chemical resistance, and toughness is important. PETG has also gained interest because of its ease of use in 3D printing.[84] Furthermore, the modification of crystallinity in CHDM-modified PET (PCT) with IPA is the basis of the PCTA family. This family of copolyesters, based on CHDM and 2,2,4,4-tetramethyl-1,3-cyclobutanediol (TMCD) as diols, has an important practical feature of improved resistance to hydrolysis upon melt processing,[85] meaning that these copolyesters need less drying prior to processing.[16,86]

Molecular degradation reactions and variations in chemical functional groups

PET (waste) can undergo several types of degradation reactions depending on external conditions such as temperature, mechanical forces, UV intensity, and the presence of small species being for instance water, ionic, and oxygen molecules. Specifically, UV light from the sun provides energy to facilitate the incorporation of (extra) oxygen atoms into the chains, which can cause the polymer to become more brittle.[87–89] Consistent with most studies regarding (vinyl) polymer stability, for PET, most emphasis has been on the understanding of thermal and thermo-oxidative degradation for which the main reactions considering a general "purple" chain are depicted in **Figure 5**.

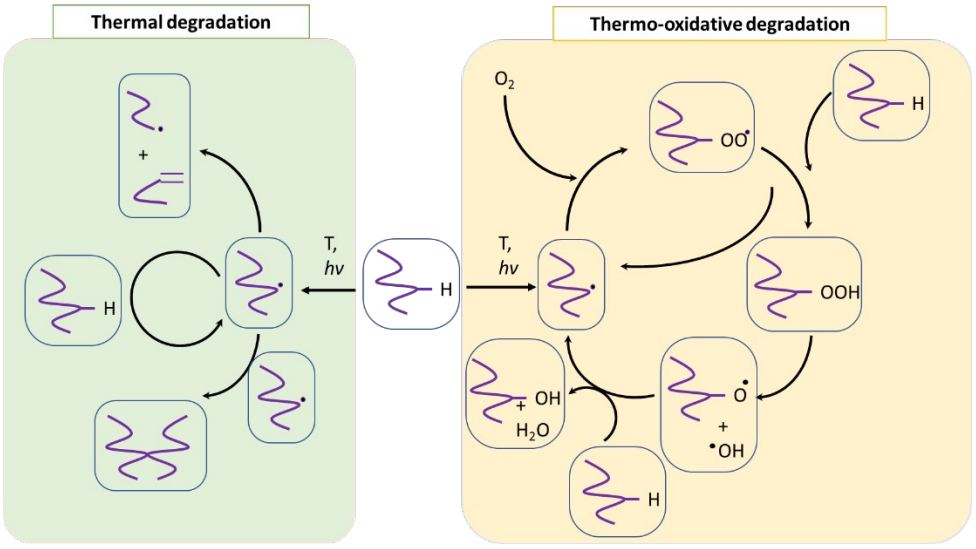

Figure 5. Typical reactions for thermal degradation (left) and thermo-oxidative degradation (right), starting from a general polymer "purple" chain depicted in the middle; *T*: temperature; *h* the Planck constant and ν the frequency.

The reaction starting the degradation in **Figure 5** is a (temperature (*T*) driven) hydrogen (H) - abstraction, delivering a (mid-chain) radical with follow-up reactions resulting either in double bound formation, crosslinking or the incorporation of oxygen-derived functional groups. Because of screw activity or UV contact with an energy h ν, with *h* the Planck constant and ν the frequency, more radicals can be even formed at a given *T* so that the overall degradation rate increases. Specifically, for PET, the presence of ester linkages makes hydrolytic and enzymatic degradation possible as well. Many authors [90–92] put forward that short oligomers with carboxylic and unsaturated ester end groups are particularly formed, due a specific role of intramolecular exchange reactions in the primary PET thermal

View Article Online
DOI: 10.1039/D4SU00485J

degradation. Mapping the balance of inter- and intramolecular degradation reactions can thus be kinetically relevant. In general, during PET mechanical recycling one needs to track variations in chain length and chemical functional groups, the latter enabling chain repair if they are reactive enough under polymerization conditions.

In what follows, an overview is given of reported thermal degradation, thermo-mechanical, thermo-oxidative, photo-oxidative, hydrolytic and enzymatic degradation reactions, with a key focus on PET as substrate. This summary is accompanied by a listing of relevant functional groups and experimental techniques to pinpoint the main molecular parameters as well as a bundling of typical (apparent) rate coefficients (or kinetic parameters) reported in the open literature.

Thermal degradation

A pioneering work for PET thermal degradation is the work of Marshall and Todd[93] at temperatures between 282 and 320 °C. These authors concluded that chain scission, which has been also denoted as fission,[94,95] takes place with an overall activation energy of 133.9 kJ mol^{-1}. Foti et al. [96] and Luderwald [97] confirmed the results of Marshall and Todd[93] by conducting PET pyrolysis experiments above 200 °C, also performing analysis of the degradation products via mass spectrometry. They reported that poly(alkylene terephthalates) are preferentially degraded by cleavage of the ester bond. Complementary, Yoda *et al.*[98] investigated thermal degradation of PET at temperatures between 263 and 300°C, showcasing that under nitrogen purging crosslinking can be neglected but in air both scission and crosslinking can occur.

Most studies on PET thermal degradation put forward that first scission of the ester group (-C(O)-O-CH_2-) occurs, delivering a -C(O)-O* and *CH_2- radical. As shown in the top part of **Figure 6** (*m*=2), subsequent disproportionation or βH-abstraction[99] results in the formation of a chain fragment with a hydroxyl functional end group and another chain fragment with a alkene functional end group. Alternatively, (β)H-abstractions with other molecules can deliver the same end groups.

Based on thermogravimetry and thermal volatilization analysis McNeill and M. Bounekhel[99] put forward several combined scission and (β)H-abstraction pathways for poly(alkylene terephthalate)

View Article Online
DOI: 10.1039/D4SU00485J

thermal degradation characterized by a general *m* (≥ 2), as highlighted in the middle and bottom part of **Figure 6**. These authors identified seven main reaction pathways. In the case of PET (*m*=2), however, diene formation (reaction pathway 2) is impossible and reaction pathway 4, formally producing vinyl alcohol, leads in practice to acetaldehyde formation via a fast reaction pathway 7.

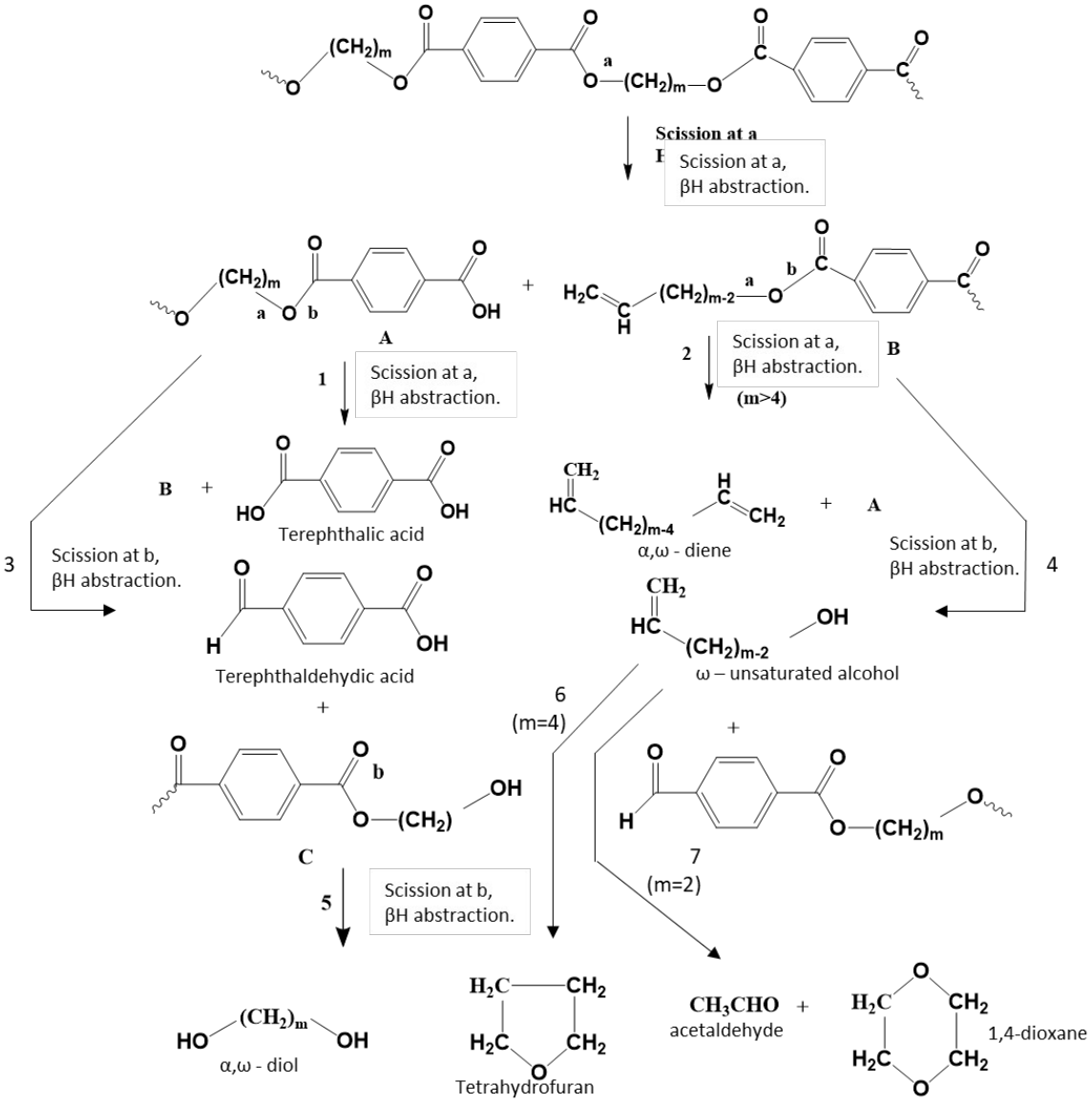

Figure 6: Thermal degradation reaction pathways for poly(alkylene terephthalate)s: ester scission (or fission) driven. Additional reaction pathways in Figure 7 and Figure 8. Figure is made based on the reactions proposed in McNeill and M. Bounekhel.[99]

In parallel with the ester scission based reactions in **Figure 6** decarboxylation reactions can take place, yielding various products as depicted in **Figure 7**. Here the scission occurs at the positions "a" and "c"

View Article Online
DOI: 10.1039/D4SU00485J

toward carbon dioxide (CO_2) formation, or at the positions "b" and "c" toward carbon oxide (CO) formation.

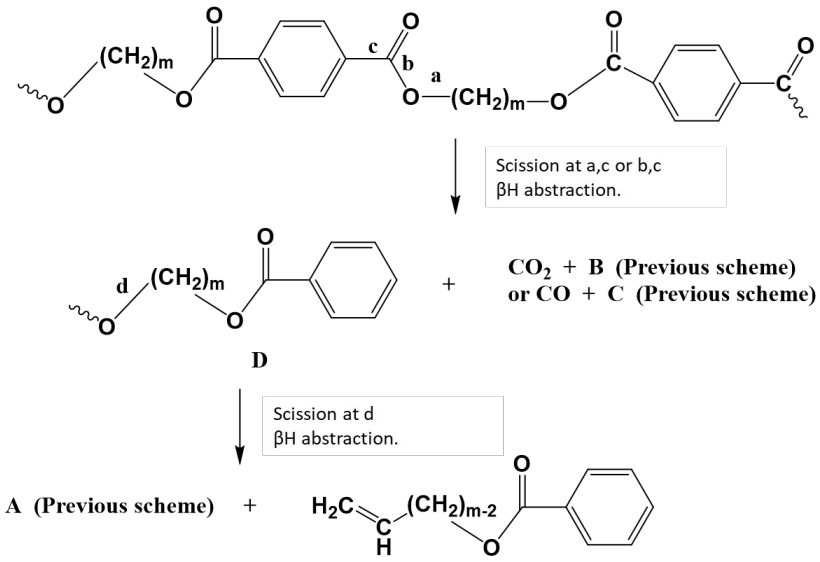

Figure 7: Thermal degradation reaction pathways for poly(alkylene terephthalate)s: carboxylation driven. Additional reaction pathways in Figure 6 and Figure 8. Figure is made based on the reactions proposed in McNeill and M. Bounekhel.[99]

It should be noted that the reaction pathways in **Figure 6** and **Figure 7** rely on homolytic cleavage of bonds, since such cleavages are assumed to occur in most polymer systems, specifically for temperatures above 300°C. Zimmermann *et al.*[92] have postulated that homolysis is not the main chain scission process, since PET degradation is not inhibited by free radical trapping reagents. This observation triggered the use of more precise analytical techniques to enable a deeper mapping of the spectrum of degradation products.

Particularly, Montaudo *et al.*[100] highlighted that cyclic compounds can be formed during PET thermal degradation in the absence of radical formation, as displayed in **Figure 8** (top). These authors put forward that ionic intramolecular exchange takes place as a cleavage process, followed by a βH-abstraction reaction to generate a series of non-cyclic oligomers. The likelihood of the ionic nature of this cyclization-based mechanism has been supported by the observation that the presence of acids increases the degradation rate not altering the degradation product types.

View Article Online
DOI: 10.1039/D4SU00485J

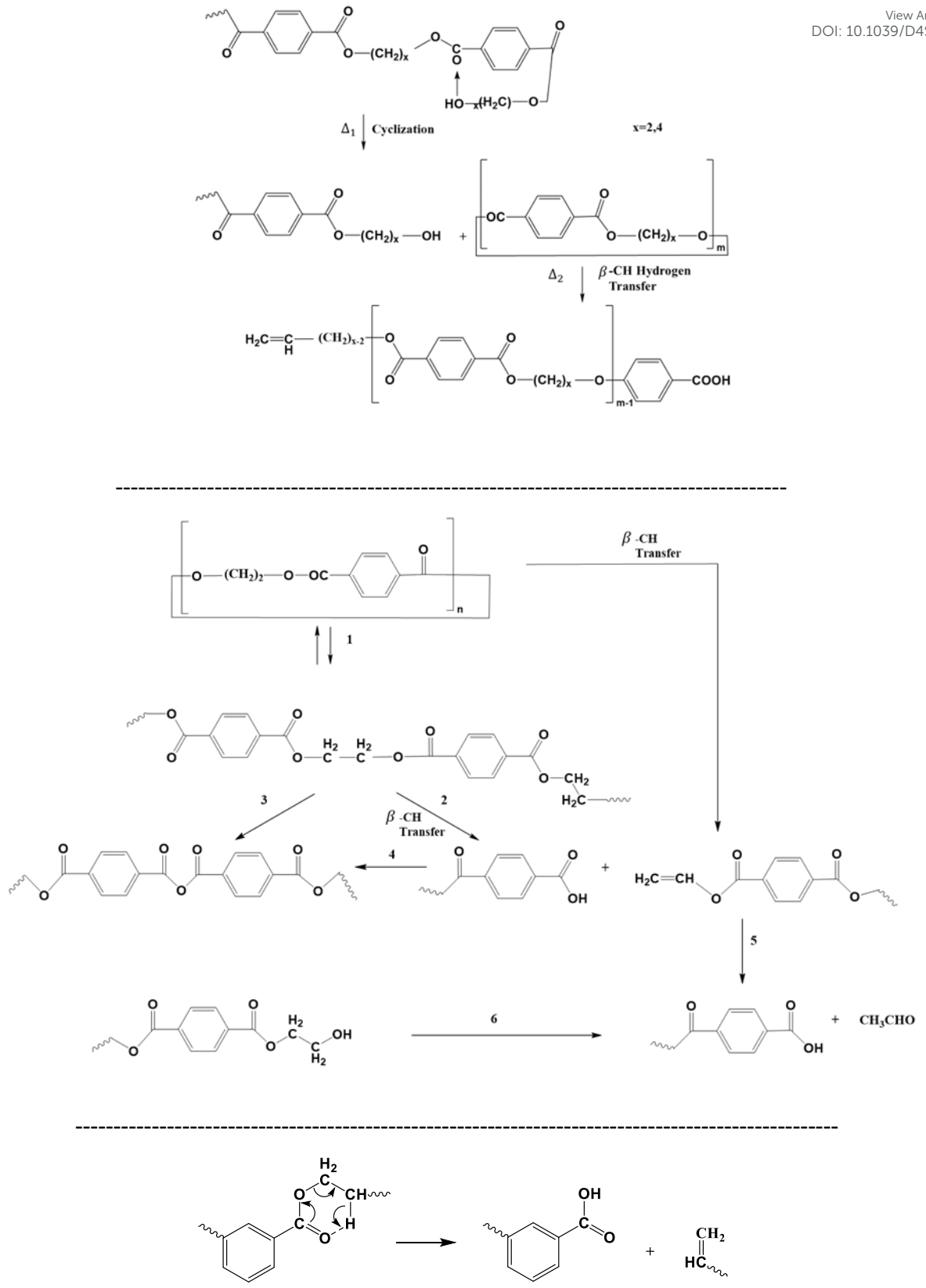

Figure 8: Additional thermal degradation reaction pathways for poly(alkylene terephthalate)s: cyclization driven (end-group) attack: top (ionic); middle: alternative representation; bottom: ester rearrangement; additional reaction pathways in Figure 6 and Figure 7. Figure is made based on the reactions proposed in following references: [99–102]

View Article Online
DOI: 10.1039/D4SU00485J

The relevance of cyclic structures has also been indicated by Samperi et al.,[101] who focused on the degradation of poly(alkylene terephthalate)s at higher processing temperatures between 270 and 370 °C. They highlighted the formation of cyclic oligomers and their further degradation according to the reactions reported in **Figure 8** (middle). Specifically, additional reactions toward the formation of small (volatile) molecule acetaldehyde have been proposed. In general, the study of volatiles is key for poly(alkylene terephthalate) thermal degradation, with in **Figure 6** (bottom) the formation of the volatile small molecules tetrahydrofuran (THF), acetaldehyde and 1,4-dioxane.[101] Moreover, ester rearrangement, as included in **Figure 8** (bottom) has been proposed by e.g. Assadi et al.[102]

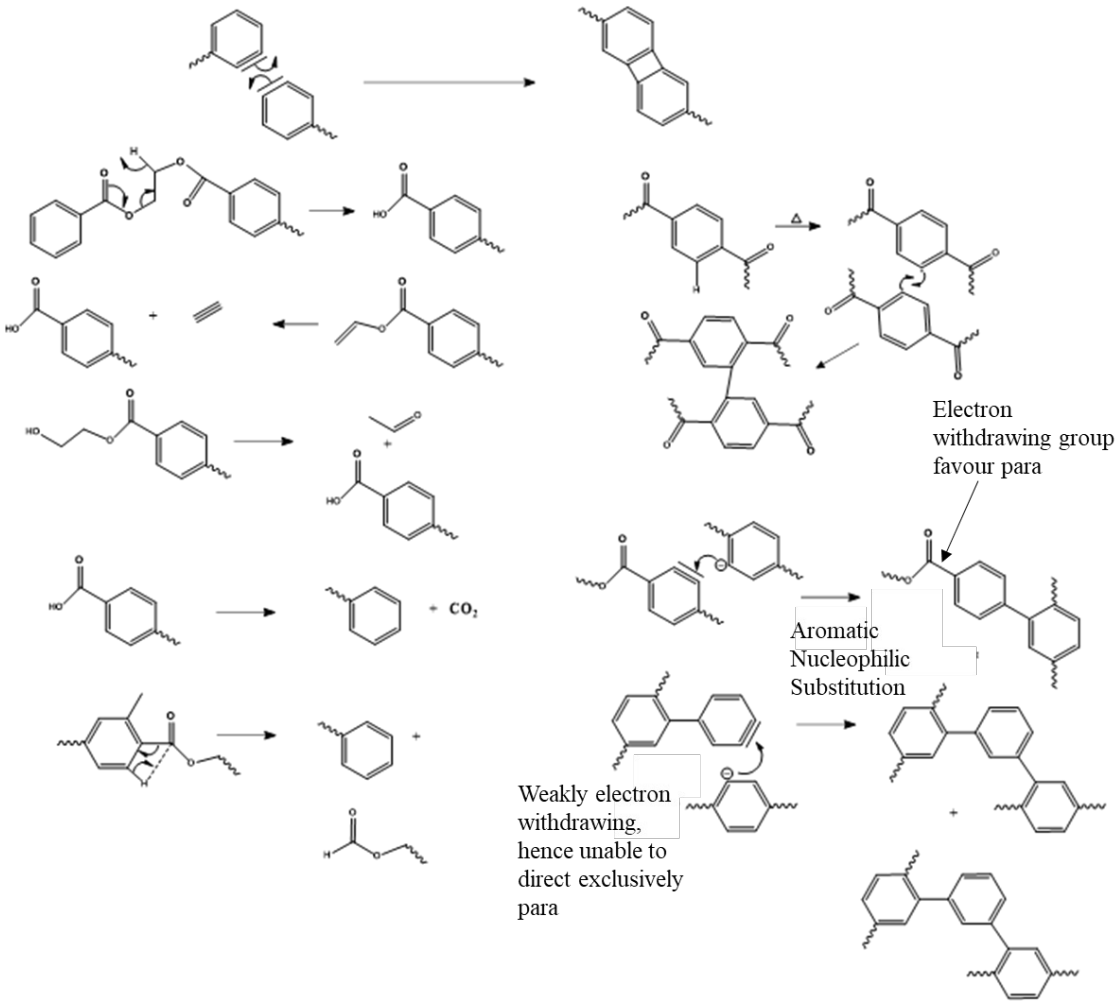

Figure 9: Additional proposed thermal degradation pathways for poly(alkylene terephthalate)s at very high temperatures toward polyaromatics. Main reaction pathways in Figure 6-8. Figure is made based on reactions of the work of Holland and Hay.[103]

Notably the Fourier transform infrared spectroscopic (FTIR) study of Holland and Hay[103] revealed the detection of polyaromatic compounds during thermal degradation in the higher temperature range

View Article Online
DOI: 10.1039/D4SU00485J

between 200 and 370 °C; an overview of typical PET labeling using FTIR is included in **Table 3**. Holland and Hay[103] proposed a series of reactions to explain the formation of such compounds, with examples depicted in **Figure 9**.

Table 3: Labeling relevant for FTIR analysis of (degraded) PET

Wavenumber (cm^{-1})	Assignment
3535	Absorbed moisture
3440	O–H stretching of diethylene glycol end-group
3060	Aromatic C–H stretching
2960, 2880	Aliphatic C–H stretching
1950	Aromatic summation band
1720	Carbonyl C=O stretching
1615, 1450, 1430, 1410	Aromatic skeletal stretching bands
1950	Aromatic summation band
1720	Carbonyl C=O stretching
1615, 1450, 1430, 1430	Aromatic skeletal stretching bands
1465	$–CH_2–$ deformation band
1270	C(=O)–O stretching of ester group
1175, 1120 and 1020	Bands in the skeletal ring region are indicative of aromatic substitution pattern, and indicates 1,4-substitution
980	$O–CH_2$ stretching of ethylene glycol segment
850	C–H deformation of two adjacent coupled hydrogens on an aromatic ring
730	Associated with the out of plane deformation of the two carbonyl substituents on the aromatic ring

It should however be mentioned that in certain cases energetically rather unlikely transition states and chemical intermediates are put forward. The formation of polyaromatics needs to be thus still further investigated, and is very likely outside the scope of PET mechanical recycling studies and design under industrially relevant conditions.

Holland and Hay[103] further highlighted that the DEG and IPA comonomer units promote thermal degradation through increased chain flexibility and the presence of more favorable bond angles, respectively. Romao et al.[104] found similar results in case DEG was used as comonomer for PET-btg production, stating that the DEG unit is formally a reactive site in PET-btg thermal degradation.

The impact of thermal degradation becomes also more evident in case PET is processed multiple times. More oligomers and volatile compounds are produced if PET is held for a longer time above its melting

View Article Online
DOI: 10.1039/D4SU00485J

temperature, contributing to a lowering of the (number) average molar mass.[105–107] Note that for a direct measurement of (the variation of) such average gel permeation chromatography (GPC), which is also known as size exclusion chromatography (SEC), is most recommended. Polyesters are however difficult to solubilize, as the high crystallinity and strong polar interactions require in practice aggressive analysis solvents and elevated analysis temperatures. PET has been analyzed in 1,1,1,3,3,3-hexafluoroisopropanol (HFIP), a polar organic solvent, considering the addition of sodium trifluoroacetate to prevent aggregation. Alternatively o-chlorophenol has been applied, which is under normal conditions a viscous solvent practically requiring analysis at elevated temperature (e.g. 110 °C) as well as careful handling being a hazardous substance. A solvent mixture of chloroform and hexafluoroisopropanol[108] (98 vs. 2 vol %) has also been applied, including UV detection and conventional calibration.

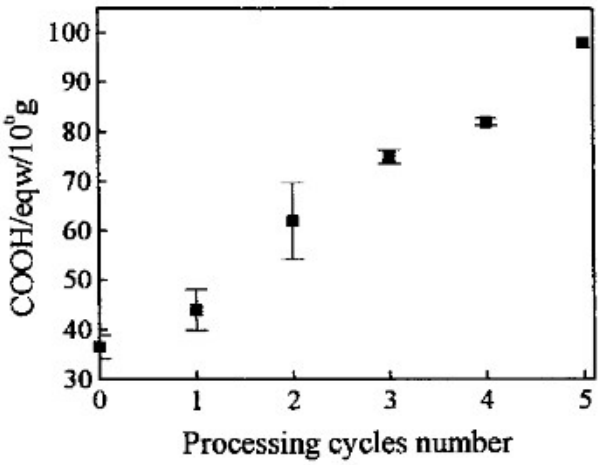

Figure 10: Variation of the carboxylic end group concentration as a function of the number of processing cycles for PET thermal degradation.[107] Reproduced with permission from the publisher John Wiley & Sons.

Parallel with chain length (molar mass) investigations via GPC, specifically considering different passes, one can perform end group analysis, focusing on the formation (or disappearance) of a specific functional group to assess the intensity of the thermal degradation ongoing. For example, Spinace and De Paoli [107] found that the carboxylic end groups concentration increases almost linearly with the number of processing cycles, changing from 36 eq. per 10^6 g for virgin PET to 100 eq. per 10^6 g after five cycles, as shown in **Figure 10**.

View Article Online
DOI: 10.1039/D4SU00485J

Thermomechanical degradation

In extrusion-based mechanical recycling high shear forces are applied to a polymer melt, which can lead to shear-induced chain scission.[109] An elevated temperature is used to realize this melt situation so that practically thermomechanical degradation reactions need to be considered. Compared to purely thermal degradation reactions these thermomechanical reactions result in the formation of extra radical types or at least in an increase of the radical concentration(s).[110,111]

This implies that more molecular changes are manifested compared to the pure thermal degradation case but to a first approximation the same set of reactions as in the previous section occur with additional mechanical forces.[112–114] From a practical point of view, in modeling studies, the Arrhenius-like behavior of a thermal degradation needs to be mathematically extended to account for these forces.[115] Specifically for larger chains and under more concentrated conditions a mechanical action stress can be formally included.

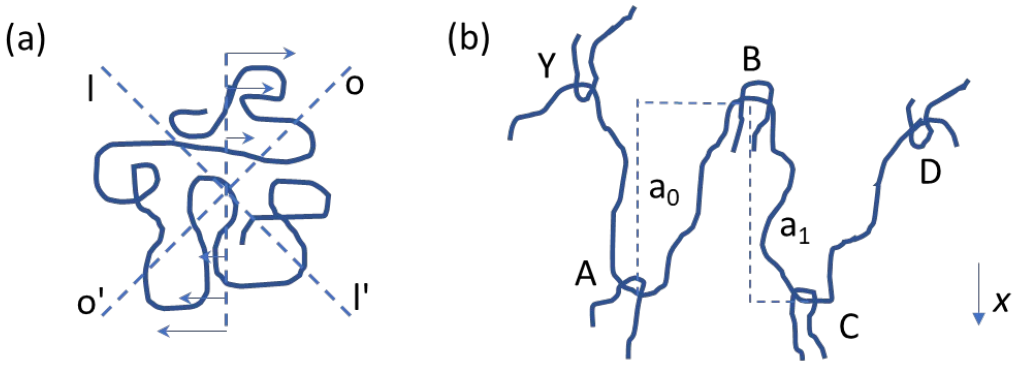

Figure 11. Conceptual illustration why melts are prone to thermomechanical degradation, with an isolated polymer chain under shear flow (left) having flexibility and a chain having entanglements in the melt (right; concentrated cases), experiencing stress points for shear-induced breakage.[116]

Polymer chains that are subjected to shear stress can be both stretched and compressed at the same time. As explained by Bueche[116] and illustrated in **Figure 11** (left), an isolated chain stretches in the OO' direction and compresses in the II' direction upon applying shear. No rupture is expected as the movement is oscillatory, with chain rotation due to shear causing the chain part that was first compressed to be stretched later on and vice versa. In contrast, for concentrated polymer systems, the entanglements between chains play a critical role. As shown in **Figure 11** (right), for one chain to be stretched, it first

View Article Online
DOI: 10.1039/D4SU00485J

needs to be liberated from such entanglements. This interactive phenomenon generates stress points, which even at rather low shear rates can lead to shear-induced degradation.

Regarding the understanding and quantifying of the thermomechanical degradation kinetics most attention has however been paid to polyolefin degradation. For example, Oblak et al.[112] deduced that reprocessing of high density polyethylene (HDPE) leads to molecular changes via competitive chemical reactions, including mechanical contributions. These authors observed a peak for the pressure and torque with an increasing number of recycling cycles, as shown in **Figure 12**. The initial increase for both properties has been associated with dominant crosslinking, implying a reduced flowability, whereas the decrease of these properties at more recycling cycles has been linked to a dominant chain fission.

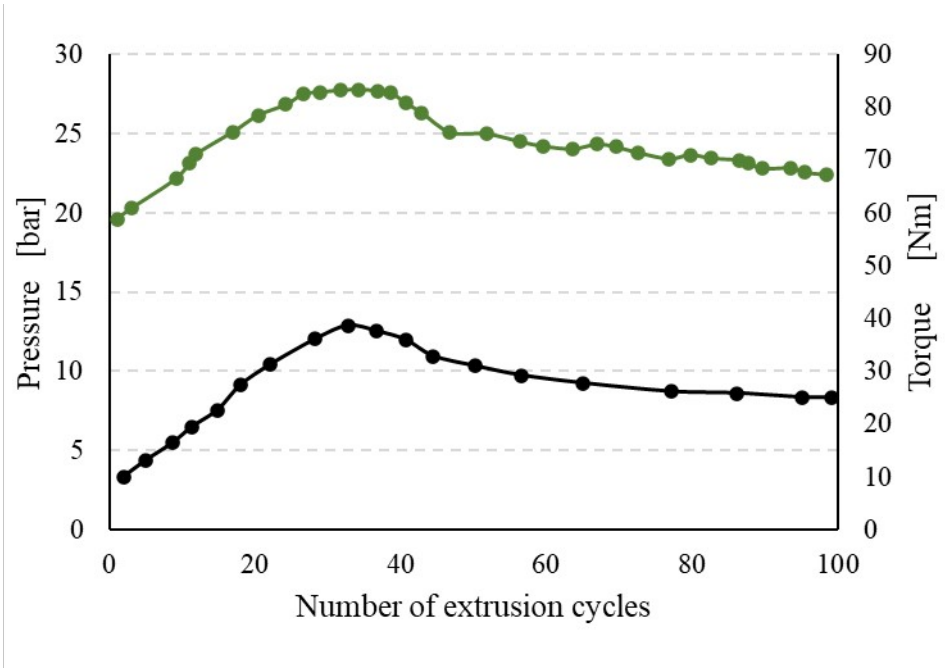

Figure 12: Impact of the number of recycling cycles in an extruder environment thus with mechanical forces. Recorded torque and pressure variation for HDPE, in general a polyolefin being the most studied polymer in view of thermomechanical degradation kinetics. Data to construct the figure taken from Oblak *et al.* [112]

For polyesters, it has been indicated that thermomechanical degradation mainly happens at the C-O bond, which has a bond energy of 109 kcal mol^{-1} comparable with the one for a C-C bond being 99 kcal mol^{-1}.[117] The presence of an ester function in close proximity further decreases the C-C bond dissociation energy to ca. 85 kcal mol^{-1} thus facilitating the scission.[118] However, to have chain rupture due to

View Article Online
DOI: 10.1039/D4SU00485J

mechanical forces sufficient energy needs to be stored in the intermolecular bond, as highlighted by Bestul [119] for other polymers.

Thermo-oxidative degradation

At first sight, the presence of oxygen initiates the typical cascade of thermo-oxidative reactions, as introduced in the right part of **Figure 5** in general terms and specified in larger detail in the right part of **Figure 13**. However, the presence of C-O linkages and phenyl rings in the PET backbone leads to some specific oxygen-induced reactions, as addressed in the present subsection further distinguishing between more overall observations and mechanistic insights based on (small) model compounds.

The presence of oxygen significantly affects the degradation of PET, as first postulated by Marshall and Todd.[120] Without mentioning a mechanism these authors highlighted that oxygen accelerates the scission process and leads to carbonyl group formation, as further exploited in follow-up studies. For example, Jabarin and Lofgren[121] showed that the (lumped) activation energy of PET degradation in the melt state is dependent on the presence of oxygen in the sample. Botelho *et al.*[122] in turn derived a more detailed thermo-oxidative mechanism, based on ethylene dibenzoate (EDB) and butylene dibenzoate (BDB) as model compounds for PET and polybutylene terephthalate (PBT).

As shown in **Figure 13**, Botelho *et al.* [122] highlighted that for BDB oxygen particularly attacks the C-H bond adjacent to the ester linkage carbon atom. In follow-up degradation reactions, peroxide decomposition, with the formation of O-centered radicals, and the subsequent cleavage reactions forming carboxyl radicals and aldehydes are essential. A carboxyl radical can abstract hydrogen and generate a carboxylic functionality but can also undergo decarboxylation similar to the case of thermal degradation (cf. **Figure 7**). The H-atom in the aldehyde group is prone to abstraction as well and the formed carbonyl radical can further react with oxygen generating superoxide species, which in the end decompose or abstract H with the formation of carboxyl acid.

View Article Online
DOI: 10.1039/D4SU00485J

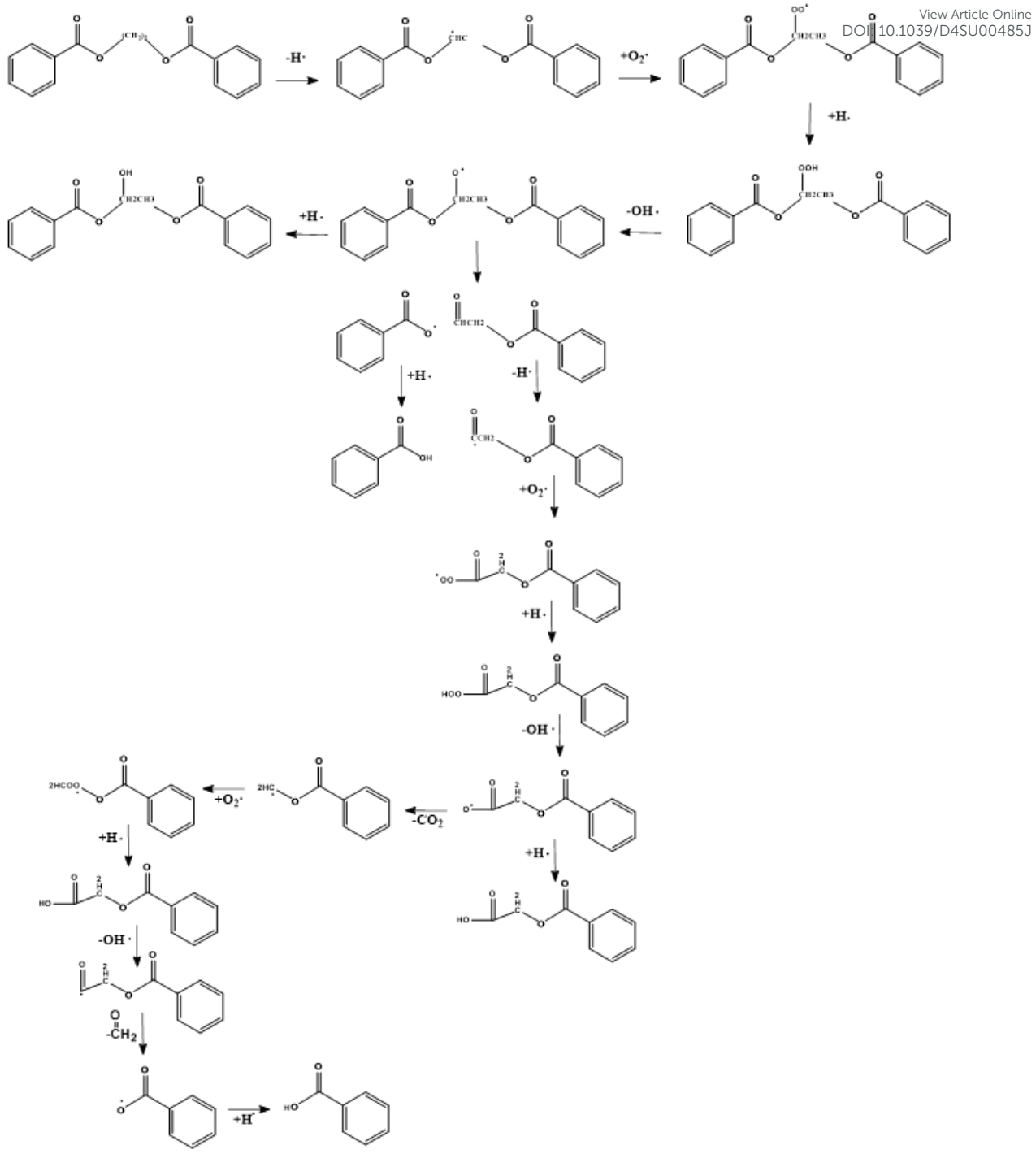

Figure 13. A first mechanism of thermo-oxidative degradation of ethylene dibenzoate (EDB) being a model compound for PET. This mechanism is based on the work of Botelho et al. [122]

Ciolacu *et al.*[123] also aimed at detailed thermo-oxidative (scission driven) mechanistic insights by studying the formation of chromophore groups via FTIR and ^{1}H nuclear magnetic resonance (NMR). They evaluated the changes of the molecular properties on the surface and in bulk, conducting a controlled degradation of PET in the presence of oxygen. These authors pointed out that oxidation of

View Article Online
DOI: 10.1039/D4SU00485J

PET initially takes place at the surface with spreading of the phenomena in the bulk of the melt due to oxygen diffusion, which is facilitated at elevated temperature. More in detail, based on the determination of the oxidation products and literature data analysis, the extensive set of reactions as included in **Figure 14** was obtained.

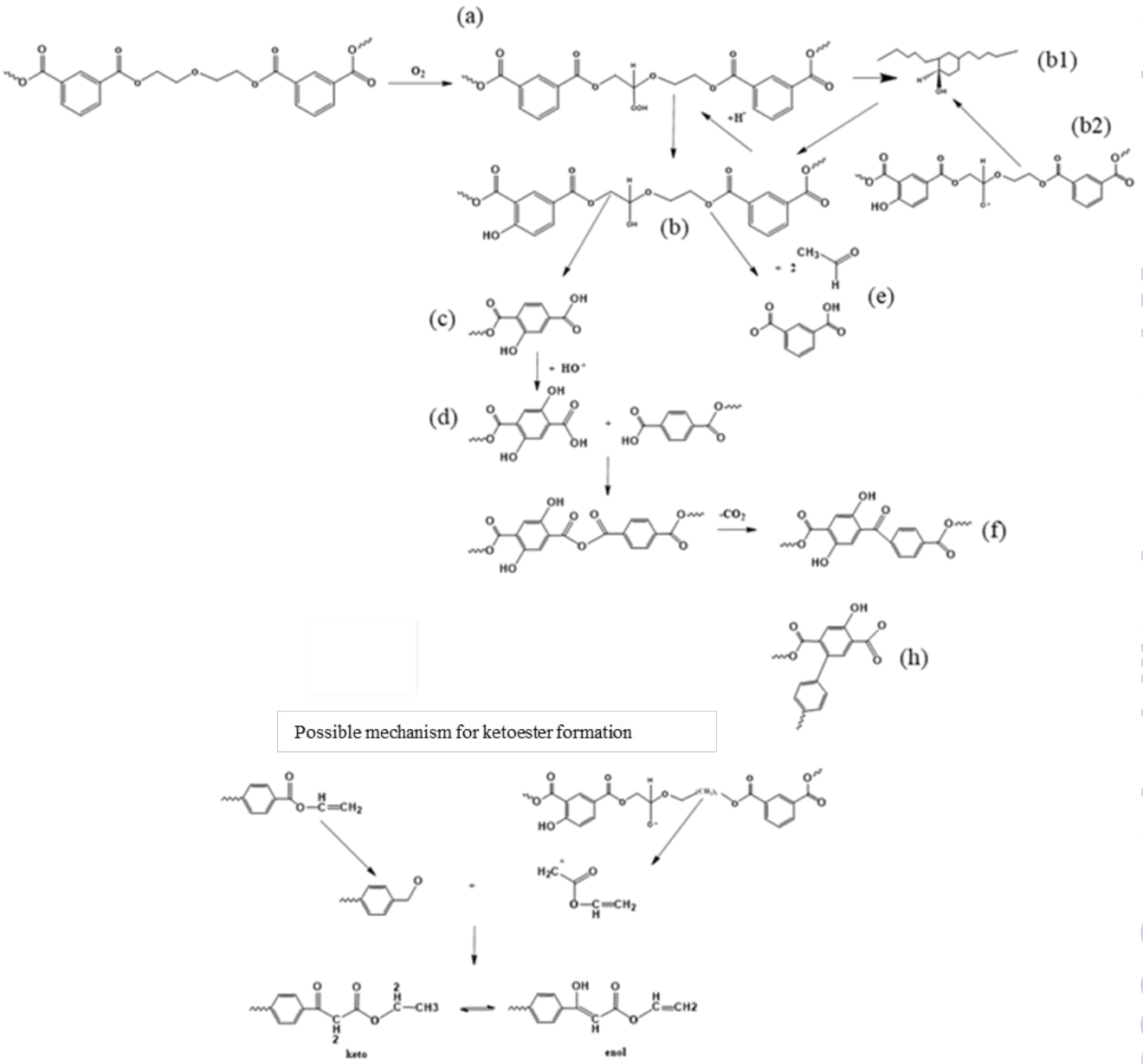

Figure 14. A second mechanism of thermo-oxidative degradation of PET. This mechanism is based on the work of Ciolacu et al. [123]

Figure 14 depicts that the weakest ether link is prone to hydroperoxide formation ((a) label), and that the OH-radical produced via decomposition of peroxides can not only abstract H from -CH_2- groups of the ester linkage (as in any other polymer) but also react with the phenyl ring ((b1) label). After H-

View Article Online
DOI: 10.1039/D4SU00485J

abstraction by another radical, a hydroxylated compound ((c) label) is yielded which is the main source of PET discoloration.[124] The hydroperoxide can also undergo chain scission, forming hydroxyl and carboxyl end groups as well as acetaldehyde (label (e)). Further reactions during thermal and thermo-oxidative degradations lead to the formation of new carbonyl functionalities, being ketoesters or hydroxylated ketoesters containing a conjugated system of double bonds (label (f) and (g)). In parallel, the buildup of conjugated aromatic structures has been proposed (label (h)) as further described in literature.[103,124,125]

Several authors also mention that oxygen plays an important role in the post-condensation reactions of PET, increasing the average chain length and, hence, can contribute to crosslinking instead of scission. In particular, de Souza *et al.*[126] link the thermo-oxidative degradation to the increase of melt viscosity after the drying step. This phenomenon was also reported by Assadi *et al.*,[102] who studied the crosslinking behavior of PET according to the reactions listed in **Figure 15**. The presence of oxygen leads to extra radical formation and chain crosslinking in case the concentration of oxygen is low. However, once the oxygen concentration is above a certain threshold scission of PET is promoted, as the reactions listed in **Figure 13** and **Figure 14** start to be dominant.

Initiation	$\lambda POOH \rightarrow \alpha P^{\circ} + \beta PO_2^{\circ} + \gamma_1 s\ (k_1)$	(I)
Propagation	$P^{\circ} + O_2 \rightarrow PO_2^{\circ}\ (k_2)$	(II)
Propagation	$PO_2^{\circ} + PH \rightarrow POOH + P^{\circ}\ (k_3)$	(III)
Termination	$P^{\circ} + P^{\circ} \rightarrow \text{inactive products} + \gamma_4 x\ \ (k_4)$	(IV)
Termination	$P^{\circ} + PO_2^{\circ} \rightarrow \text{inactive products}\ \ (k_5)$	(V)
Termination	$PO_2^{\circ} + PO_2^{\circ} \rightarrow \text{inactive products} + O_2\ (k_6)$	(VI)

Figure 15. Mechanism of PET crosslinking in the presence of oxygen. POOH is the initiator generated by the oxidation process, PH is a methyl group, and *s* indicates chain scission and *x* crosslinking, as reported in the work of Assadi *et al.* [102]

The presence of comonomers also plays an important role in the thermo-oxidative (and thermal degradation) of PET-btg, as e.g. shown by Romão *et al.*[127] Particularly DEG is prone to the attack by molecular oxygen on the methylene protons adjacent to the ether oxygen atom. As shown in **Figure 16**,

View Article Online
DOI: 10.1039/D4SU00485J

this causes the release of hydroxyl radicals in the polymer matrix, thereby producing mono- and di-hydroxyl substituted species. These authors also pointed out the formation of cyclic oligomers, as also discussed before via thermal means. Similarly, Lecomte and Liggat [12] compared the cascade of reactions for pure PET and copolymer-containing DEG units to point out the importance of cyclization toward DEG units, forming cyclic oligomers that are released early in the degradation. DEG units are thus easily pushed out during recycling, as they are more likely involved in the formation of cyclic oligomers than the rest of the PET backbone, due to their chemical structure and flexibility.

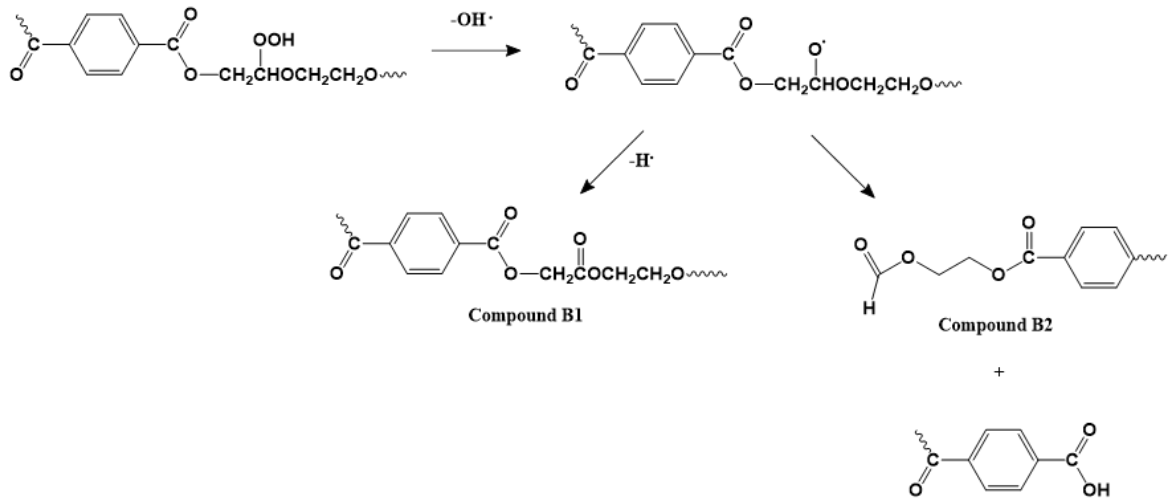

Figure 16. Thermo-oxidative degradation mechanism with a DEG comonomer unit, as based onht the work of Romão *et al*.[127]

The presence of oxygen has also an effect on the reprocessing potential and stability of PET. This has for instance been highlighted in the study of Badia *et al.*, [128] showing that the reprocessing of partially degraded PET in an inert atmosphere requires more energy due to the (remaining) presence of certain functional groups. However, in case the reprocessing occurs in the presence of oxygen, the decomposition of the resulting oxidized PET proceeds faster. These results are similar to those of Das and Tiwari [129] who observed a faster decomposition of PCW PET. The effect of the environment on the recycling of PET was also pointed out by Schyns *et al.*[130] In case the authors performed melt extrusion under a nitrogen atmosphere instead of an oxygen atmosphere, they observed an increase of the PET average chain length by 20%. In the presence of oxygen they observed chain scission as the predominant degradation mechanism with ca. an 8% decrease of the mass average molar mass (M_m) value.

View Article Online
DOI: 10.1039/D4SU00485J

Photo-oxidative degradation

Polymers can undergo faster degradation in contact with UV- and visible light irradiation, implying a role of so-called photo-oxidative degradation next to thermal and thermomechanical degradation. This contact for instance provokes C-H bond homolysis with subsequent radical species formation. Consequently, all the reactions typical for thermo(-oxidative) degradation (**Figure 5** - **Figure 16**) can take place at accelerated speed if sunlight is available. A disclaimer is that the effect of photo-oxidative degradation is only noticeable if a sufficiently long irradiation time of e.g. weeks or months is applied. Hence, photo-oxidative degradation is only relevant for polymer-based appliances with long use-times or waste which stays sufficiently long in open dumps or in the environment, e.g. marine plastics.

It has been indicated that multiple polymers release degradation products that might be harmful for the environment if they are exposed to sunlight and atmospheric oxygen. This seems to be especially true if they contain no stabilizer molecules,[131] which is more likely toward the end-of-life as these small molecules tend to degrade and lose their functions during prolonged exposure to irradiation. A special case are microplastics carried out from the water to the sea shore, with likely a strong photodegradation effect due to a polymeric material being in a resting mode at high temperature and in contact with air for a long time.[132]

According to the classification of Rabek,[133] PET is moderately photostable so that it should be able to be used without photostabilizer. However, photo-oxidative reactions do still take place, as for instance demonstrated by Abboudi *et al.*[134] considering the degradation of PET water bottles. As shown in **Figure 17**, these authors compared the leaching of e.g. formaldehyde and acetaldehyde into the water poured in the PET bottles in the presence of sunlight as well as in the dark. It follows that the concentration of acetaldehyde increases until 100 days of storage after which a saturation is reached. Notably in the presence of UV more degradation occurs compared to aging in the dark. Interestingly, PET is claimed to be more photo-oxidative stable then other common plastics such as polystyrene and polypropylene.[135]

View Article Online
DOI: 10.1039/D4SU00485J

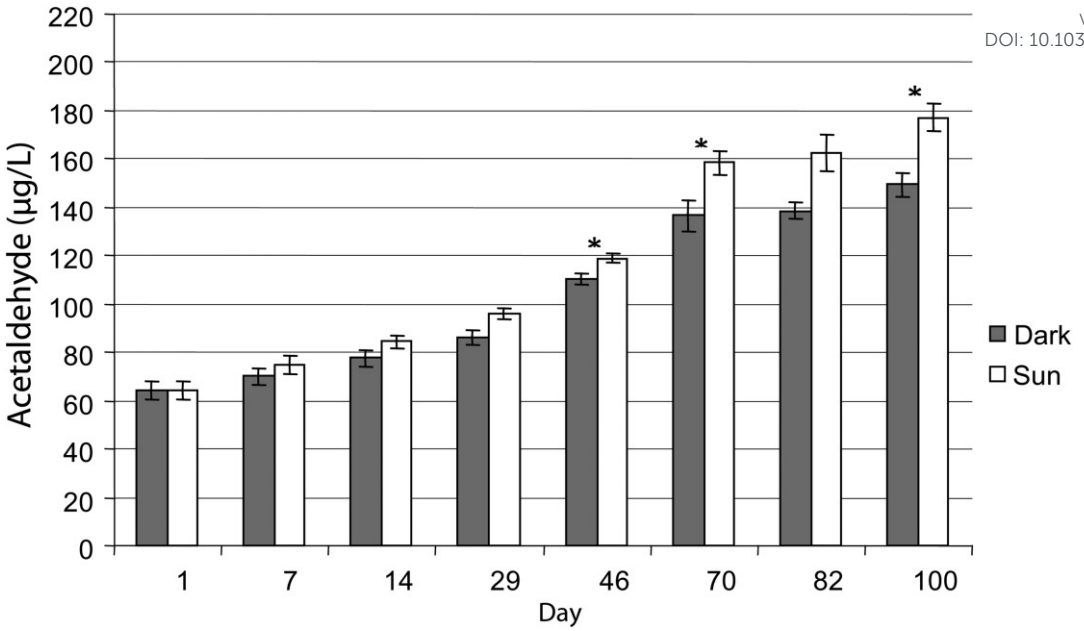

Figure 17. Concentration of acetaldehyde in PET bottled water samples during 100 days of storage in the laboratory (dark) and under sun exposure (UV-light). Under UV-light more acetaldehyde is observed, highlighting the relevance of photo-oxidative degradation at long exposure times. Plot made based on the work of Abboudi *et al.* [134] Reproduced with permission from the copyright holders IWA Publishing.

For PET, the absorbing chromophore is part of the main chain and the ester carbonyl groups absorb light in the wavelength region of 280 to 400 nm[136] so that that the degradation involves chain scission reactions. The detailed mechanism of photo-oxidative degradation has been elaborated by several groups, with the main results from Fox and Cozzens[137] and Murayama et al.,[138] delivering the overall reactions in **Figure 18** (top).

One can identify in **Figure 18** (top) hydroperoxide formation and cleavage to form hydroxyl radicals and alkoxyl radicals, with the latter also undergoing several reactions leading to chain scission, the formation of monohydroxy terephthalate groups, and CO and CO_2 as volatile products.[139] As shown in **Figure 18** (bottom), Day *et al*.[135] proposed a complementary mechanism for both photolysis and photo-oxidation. They verified that the production of COOH end groups was independent from the UV wavelength, as well as the production of CO.

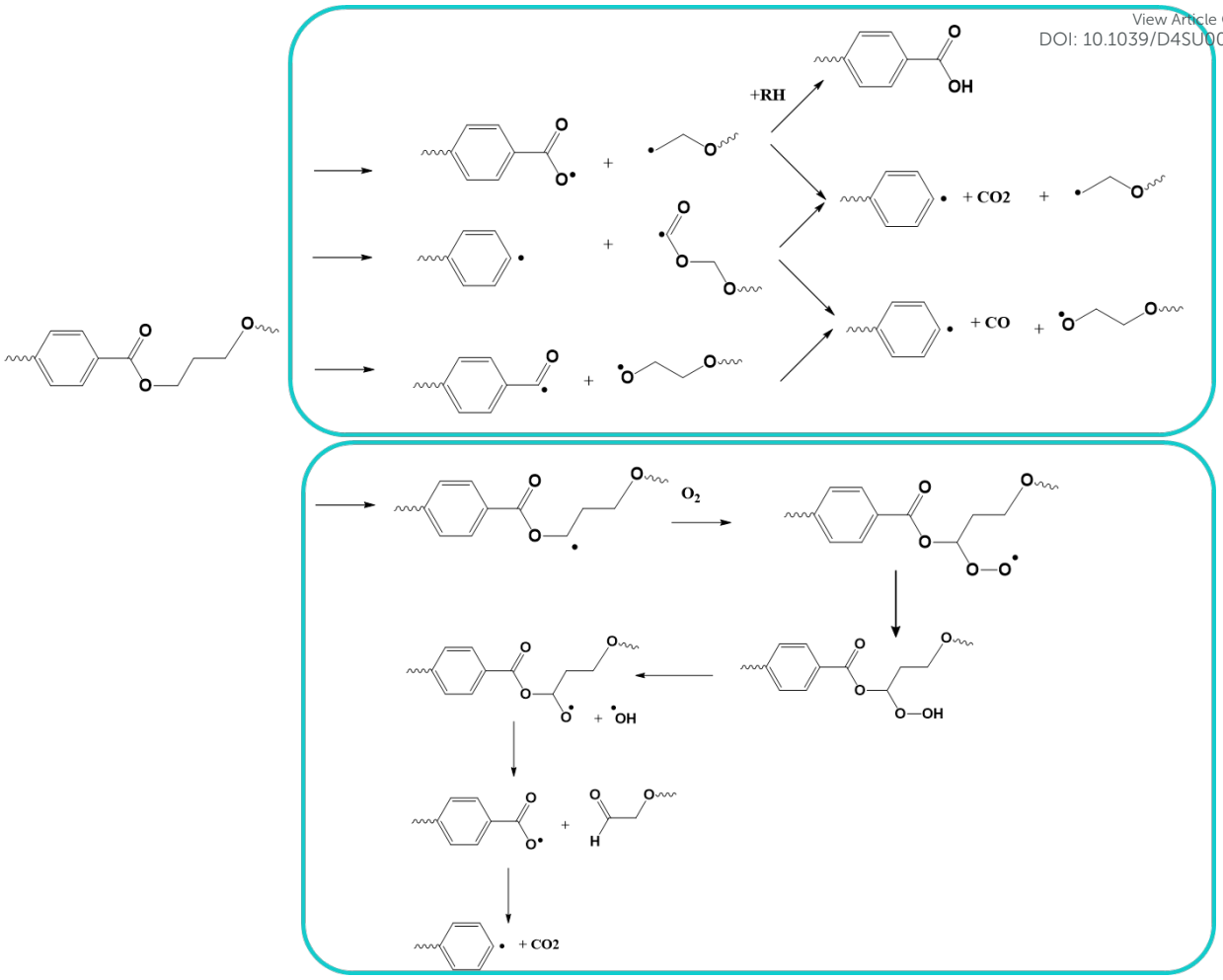

Figure 18. Top: Reported overall mechanisms for photo-oxidative degradation; Bottom: specific mechanism for vacuum photolysis and photo-oxidation. Reactions based on the work of Day *et al.* [135]

Hydrolytic degradation

Polyesters contain by default ester groups in the backbone so that they are susceptible to hydrolytic degradation. [140] As shown in **Figure 19**, water reacts with these groups resulting in the formation of carboxylic acid and hydroxyl functional groups, hence, a lowering of the chain length by chain scission. [141] For copolyesters, the hydrolytic degradation is faster than for conventional PET because of the more amorphous structure of the former. [142]

View Article Online
DOI: 10.1039/D4SU00485J

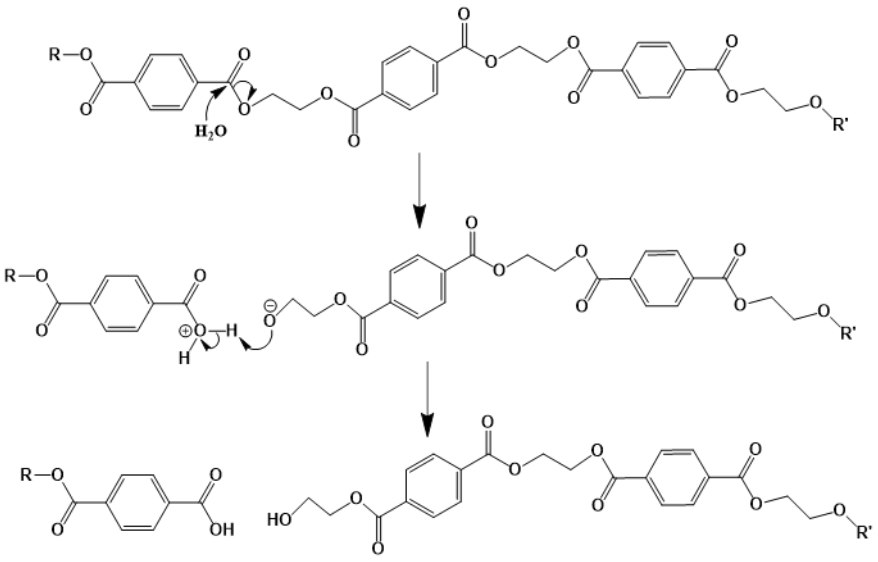

Figure 19. Mechanism of PET hydrolytic degradation, as based on the work of Sammon *et al.* [141]

The pH of the water has shown to play an important role in the polyester hydrolytic degradation mechanism.[143] As shown in **Figure 20**, Woodard *et al.* [142] for instance showed that in a basic environment the ester carbonyl reacts with hydroxide ions, while in acid environment the functional group is protonated before reacting with water. Depending on the level of acidity the degradation rates vary, as e.g. shown in the work of Rowe *et al*. [143] Increasing the pH increases the mass loss rate of PET compared to samples in de-ionized water. The reason is that the addition of e.g. KOH interferes with the mechanism driven by the acidic medium, stabilizing the carboxylate anion and leading to carbonyl protonation.[143] However, many studies have indicated that a dedicated change for the degradation rate of polyesters only happens for extremely acid or basic systems.[140]

It should be noted that the acid and alkaline hydrolysis process are deliberately exploited for chemical recycling of polyesters.[142,144] Carta *et al.*[145] for instance highlighted that acidic hydrolysis proceeds via a so-called shrinking core model, meaning that the reaction occurs mainly close to the chain end. As a result, in the presence of excess of acid, the final products are TPA, EG and inorganic salts. On the other hand, under basic conditions, random chain scission reactions take dominantly place, eventually also leading to the formation of TPA and EG. Hence, in the limit the hydrolysis of PET results in the release of the valuable compound TPA, justifying chemical recycling technology research. [145]

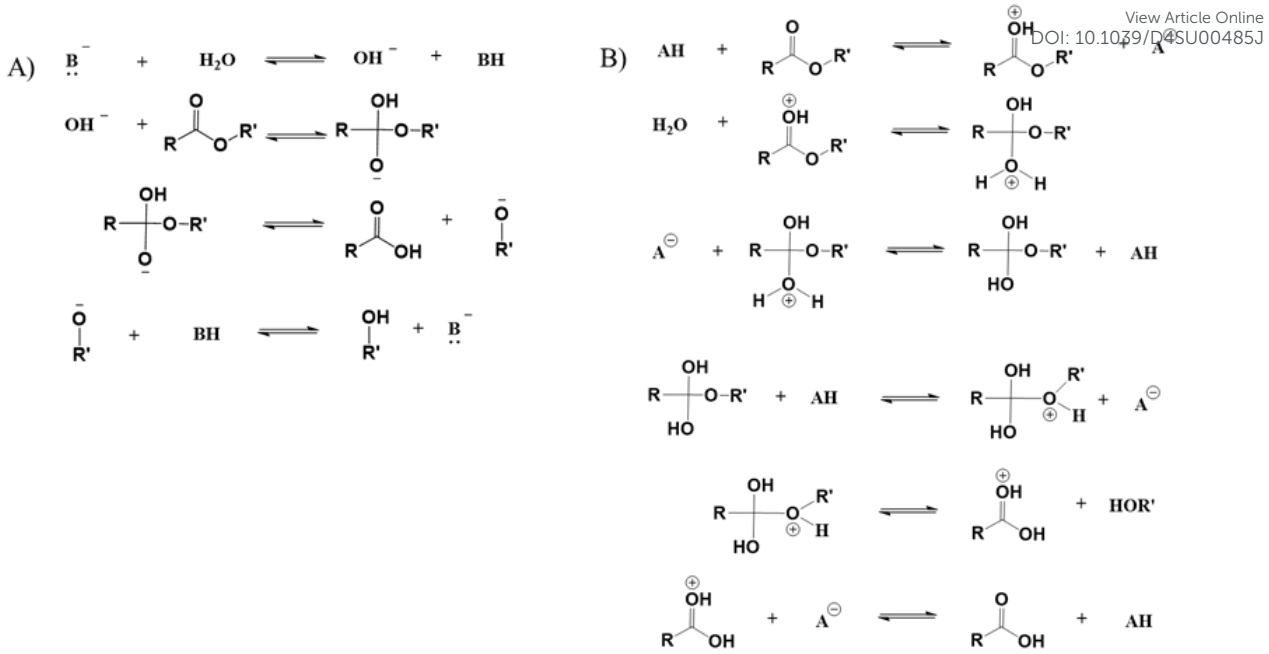

Figure 20. Mechanism of hydrolysis in (top) basic environment and (bottom) acid environment, based on the work of Woodard and Grunlan. [142]

Enzymatic degradation

More recently, for PET, recycling biological methods, which have been also grouped as enzymatic degradation techniques, have been developed alongside the more traditional chemical and mechanical methods (**Figure 6 - Figure 20**), as conceptually shown in **Figure 21**.[146,147] Biological methods have been postulated to be promising and environmentally friendly solutions for the decomposition of PET waste, provided that appropriate scale up strategies can be developed. Despite that PET is labelled as non-biodegradable, significant research has been devoted to the use of microorganisms or enzymes to break it down via natural means. [148]

Enzymes are biocatalysts which participate in a reaction, act on a particular substrate, and accelerate the process of conversion of that substrate into a valuable (or targeted) product. All the enzymes that are known to degrade polymers belong to the class of hydrolases, classified as EC 3 in the EC numbering of enzymes. To date, the enzymes mostly employed for PET depolymerization are cutinase (EC 3.1.1.74), lipase (EC 3.1.1.3), carboxylesterase (EC 3.1.1.1), PETase (EC 3.1.1.101), MHETase (EC 3.1.1.102), and esterase (EC 3.1.1.1).[148,149]

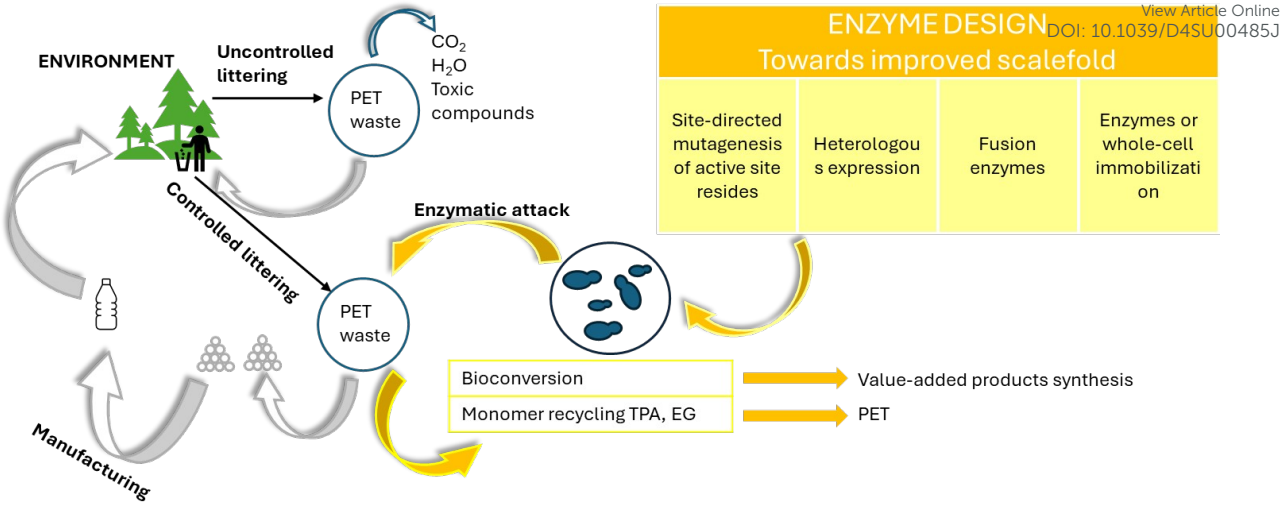

Figure 21. Potential of enzymatic degradation for polyester circularity; overview made based on Urbanek et al.[146]

The most relevant degradation takes place with the help of enzymes that are present in microbial cells (extracellular/intracellular), which causes breakdown of polymer chains through assimilation within the cells and releasing metabolic products such as CO_2, H_2O, methane (CH_4), and nitrogen (N_2).[150] The enzymatic degradation occurs in two stages, including (i) adsorption of enzymes on the polymer surface and (ii) hydro-peroxidation/hydrolysis of the bonds.[149,151] For illustration purposes, the mechanism of PET degradation, as catalyzed by PETase or cutinase under mild conditions, is highlighted in **Figure 22**. The enzyme PETase first converts PET into oligomers and monomers such as BHET, mono(2-hydroxyethyl) terephthalate (MHET), TPA, and EG. MHET is then further hydrolyzed by a second enzyme, MHETase, to again yield TPA and EG. [149] Once the monomers and constituents are separated out, they can be used and repolymerized to create plastics or other petrochemical products.

The enzymatic degradation process usually requires less energy and has the potential to extend the life of PET by recycling the polymer multiple times while producing virgin-like quality. However, in some cases extensive heat might be needed as a pre-treatment step to prepare the (mixed) plastic waste for the enzymatic reaction. This can negatively impact the life cycle assessment (LCA) and overall emissions, depending on the sources of energy used. Furthermore, the crystallinity (higher being less accessible for enzymes), temperature (higher enabling flexibility, e.g. 343 K, but not too high enabling enzyme stability), pH (more TPA formation with increasing acidity), buffer strength, and the nature of substituent/additives present (as plasticizers) affect the enzymatic degradation efficiency of PET.[152] In

View Article Online
DOI: 10.1039/D4SU00485J

general, one does need to avoid that a process design does not alter the enzyme activity or inhibits the accessibility to the ester linkage.[153] Moreover, the necessity of long PET chains penetrating into the active sites of hydrolases, which are often located in rather deep cavities, makes the sufficient mobility of the chains the most important factor for controlling the polyester degradability.[154] Hence, as for conventional degradation of PET in the melt or solid state diffusional limitations are essential to be grasped in a sufficiently fundamental detail.

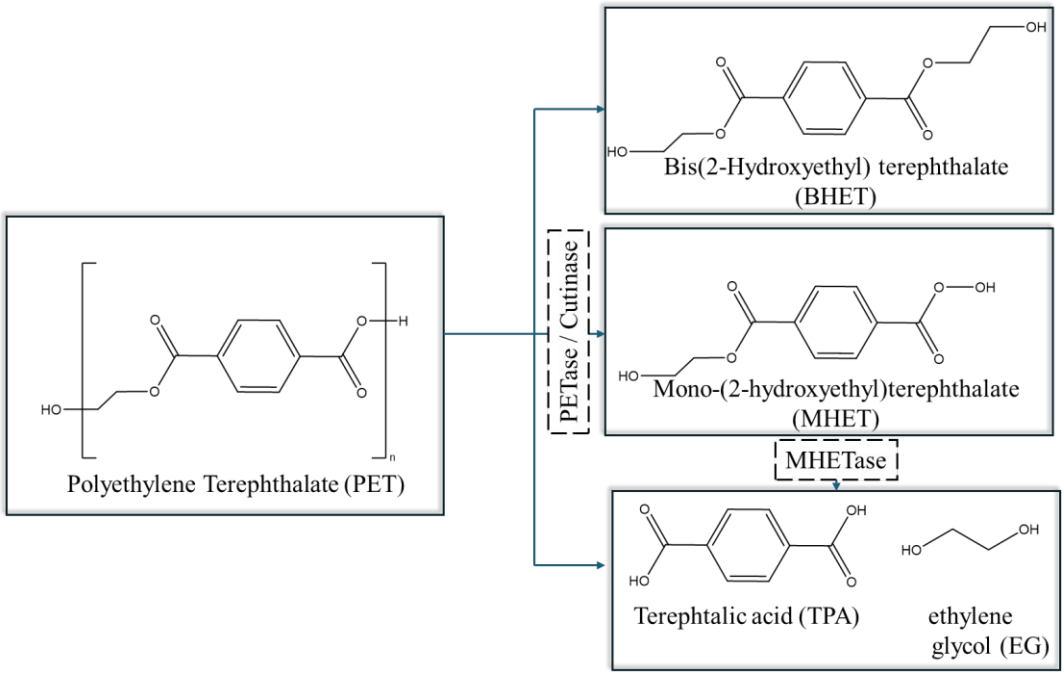

Figure 22. Overall reactions for PET degradation catalysed by PETase or cutinase based on the work of Khairul Anuar[149]

In addition, the degradation enzymes need to be efficiently produced and their activity needs to increase to ensure the industrial relevance of enzymatic degradation.[155] In this context, metabolic engineering provides certain opportunities such as engineering of the substrate binding pocket as well as the hydrolase specificity, or relieving product inhibition of PET hydrolases. Other methods include developing a surface display for PET hydrolases and mutations of enzymes to create more space for the active sites to fit the large, inaccessible polymer particles and to construct more hydrophobic substrate-binding sites.[155]

View Article Online
DOI: 10.1039/D4SU00485J

Rate coefficients and kinetic parameters

In view of modelling the kinetics for mechanical recycling one can ideally rely on a library of Arrhenius (and diffusivity) parameters of the elementary reactions of relevance, or at least the representative (apparent) kinetic parameters should be available at the relevant temperature(s). For example, Launay *et al.*[156] analyzed the weight loss over time of PET aged in distilled water at 100°C to quantify the hydrolytic degradation kinetics. Assuming a random mechanism of chain attack, they deduced a second order hydrolytic degradation rate coefficient k_{hydro} of 1.83×10^{-8} L mol^{-1}s^{-1}. The dependency of k_{hydro} on the percentage of relative humidity (RH) was studied by McMahon *et al.*,[157] with the associated Arrhenius plots provided in **Figure 23**.

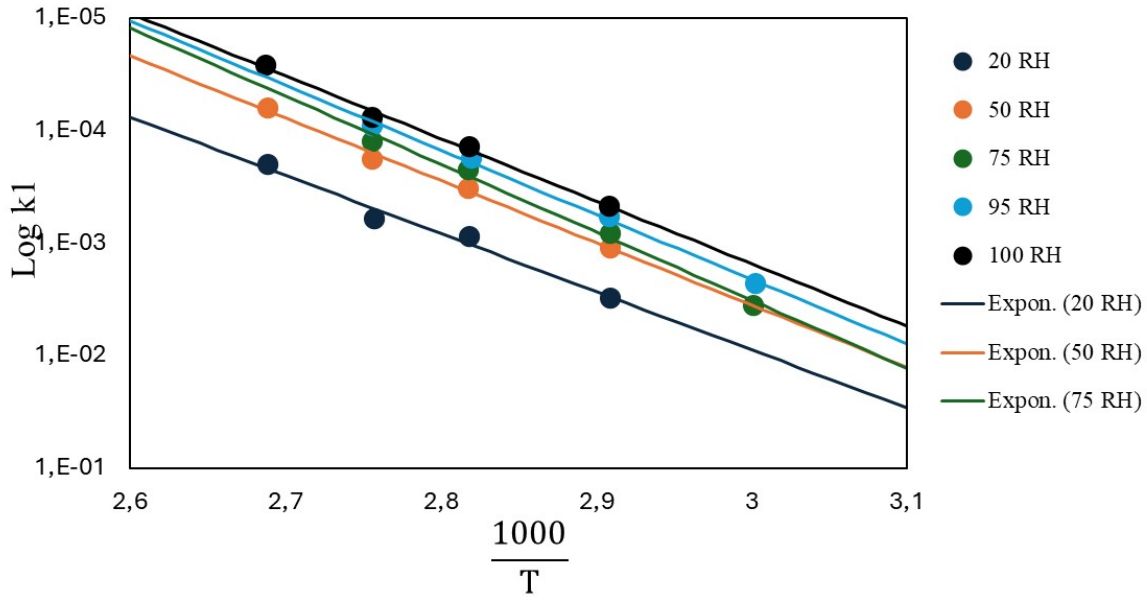

Figure 23. Arrhenius parameter plots for PET hydrolysis at different relative humidity (RH) percentages.[157] The figure is constructed based on the data from McMahon et al [157].

However, in many recycling studies lumped (or apparent) rate coefficients have been determined, with most emphasis on chemical and not mechanical recycling, as emphasis is on thermogravimetric analysis (TGA) aiming at full conversion of the polymer into small molecules. Lumped activation energies (*E* values) typically follow from describing the evolution of the conversion α with time *t* as the product of a lumped rate coefficient *k*, following an Arrhenius law, and a to be determined function *f* depending on this α. As shown in Moens *et al.*, [158] one focusses for the determination of *E* at a given α on:

View Article Online
DOI: 10.1039/D4SU00485J

$$\left[\frac{d\ln\left(\frac{d\alpha}{dT}\right)}{d\left(\frac{1}{T}\right)}\right]_{\alpha} = -\left[\frac{E}{R}\right]_{\alpha} + \left[\frac{d\ln(f(\alpha))}{d\left(\frac{1}{T}\right)}\right]_{\alpha}$$

For example, Jenekhe *et al.*[90] investigated the pyrolysis of PET in an inert atmosphere through TGA with heating rates ranging from 0.31 to 10 K min^{-1} and covering temperatures between 25 and 600 K, defining at first a mechanism of A to B and then B to C, with A being the polymer, B being a mixture of TPA and vinyl ester oligomers, and C volatile compounds. A further lumping could although be performed so that only one set of Arrhenius parameters was finally needed. Depending on the heating rate, different Arrhenius parameters were although found, further highlighting the apparent nature of this approach. For the slowest and fastest rate, an E of 48.14 kcal mol^{-1} and 55.56 kcal mol^{-1} and a pre-exponential factor A of 3.16 10^{12} s^{-1} and 7.84 10^{14} s^{-1} respectively resulted.

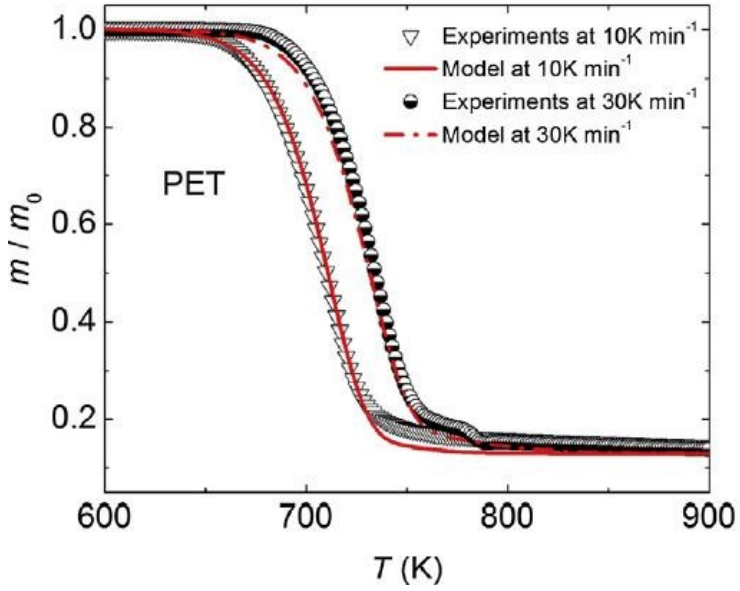

Figure 24. Example of application of TGA to obtain lumped kinetic parameters, typically for chemical recycling (or very strong degradation) of polyesters.[159] Reproduced with permission from the publisher Elsevier.

A similar study was performed by Li *et al.*[159] also considering differential scanning calorimetry (DSC) analysis. As shown in **Figure 24** two dominant mechanisms could be identified at a heating rate of 10 K min^{-1}, one corresponding to an E of 235 kJ mol^{-1} and an A of 1.6 10^{15} s^{-1} (first step), and one corresponding to an E of 96 kJ mol^{-1} and an A of 3.53 10^{4} s^{-1} (second step).

View Article Online
DOI: 10.1039/D4SU00485J

More special TGA treatments are the formal use of f=1, defining a conversional method, the use of iso-conversional methods according to certain standards, or the use of integrated forms, as also mathematically elaborated on in Moens *et al.*[158] For example, Osman *et al.*[160] used the American Society for Testing and Materials (ASTM) method to obtain an E of 165.6 kJ mol^{-1}, whereas the Flynn-Wall and Ozawa method gave an E of 166-180 kJ mol^{-1} and the iso-conversional method delivered an E of 165-195 kJ mol^{-1}. Das *et al.*[129] additionally performed TGA experiments for PET at heating rates between 5 and 50 K min^{-1} for a temperature span from 303 K to 973 K, as well as isothermal experiments. Using the isoconversional method, they found an E of 203-355 kJ mol^{-1} and a log (A; s^{-1}) of 33.3 – 59.3 under nitrogen atmosphere, whereas in air they observed a decrease toward an E of 145-2318 kJ mol^{-1} and a log (A; s^{-1}) of 28.5 – 51.8 s^{-1}.

Table 4: Kinetic parameters from TGA analysis for PET and copolymers; *E*: activation energy; *A*: pre-exponential factor. [103]

	PET			
	Rate coeff. for loss of C-H (s^{-1})	Rate coeff. for loss of C=O (s^{-1})	Rate coeff. for loss of ester (s^{-1})	Rate coeff. for loss of ethylene glycol end group (s^{-1})
E (kJ mol^{-1})	230 ± 10	220 ± 10	220 ± 10	160 ± 10
A (s^{-1})	(3.62 ± 0.35) x 10^{15}	(2.05 ± 0.2) x 10^{15}	(3.58 ± 0.39) x 10^{14}	(9.37 ± 1.0) x 10^{9}
	Copolymer			
	Rate coeff. for loss of C-H (s^{-1})	Rate coeff. for loss of C=O (s^{-1})	Rate coeff. for loss of ester (s^{-1})	Rate coeff. for loss of ethylene glycol end group (s^{-1})
E (kJ mol^{-1})	260 ± 10	260 ± 10	260 ± 10	160 ± 10
A (s^{-1})	(2.56 ± 0.27) x 10^{16}	(1.16 ± 0.14) x 10^{18}	(2.92 ± 0.30) x 10^{17}	(3.77 ± 0.40) x 10^{9}

A comparison of the TGA degradation kinetics of PET and its copolymers has been performed by Holland *et al.*[103] under argon atmosphere at temperatures between 473 K and 643 K. The copolymer contained 2-4 mol% DEG and 1.3-2.6 mol% IPA. These authors reported (for simplicity independently assumed) Arrhenius parameters for the loss of functional groups and bonds, as specified in **Table 4**. Specifically higher pre-exponential factors have been measured for the copolymer consistent with the aforementioned results regarding (basic) thermal degradation involving DEG.

View Article Online
DOI: 10.1039/D4SU00485J

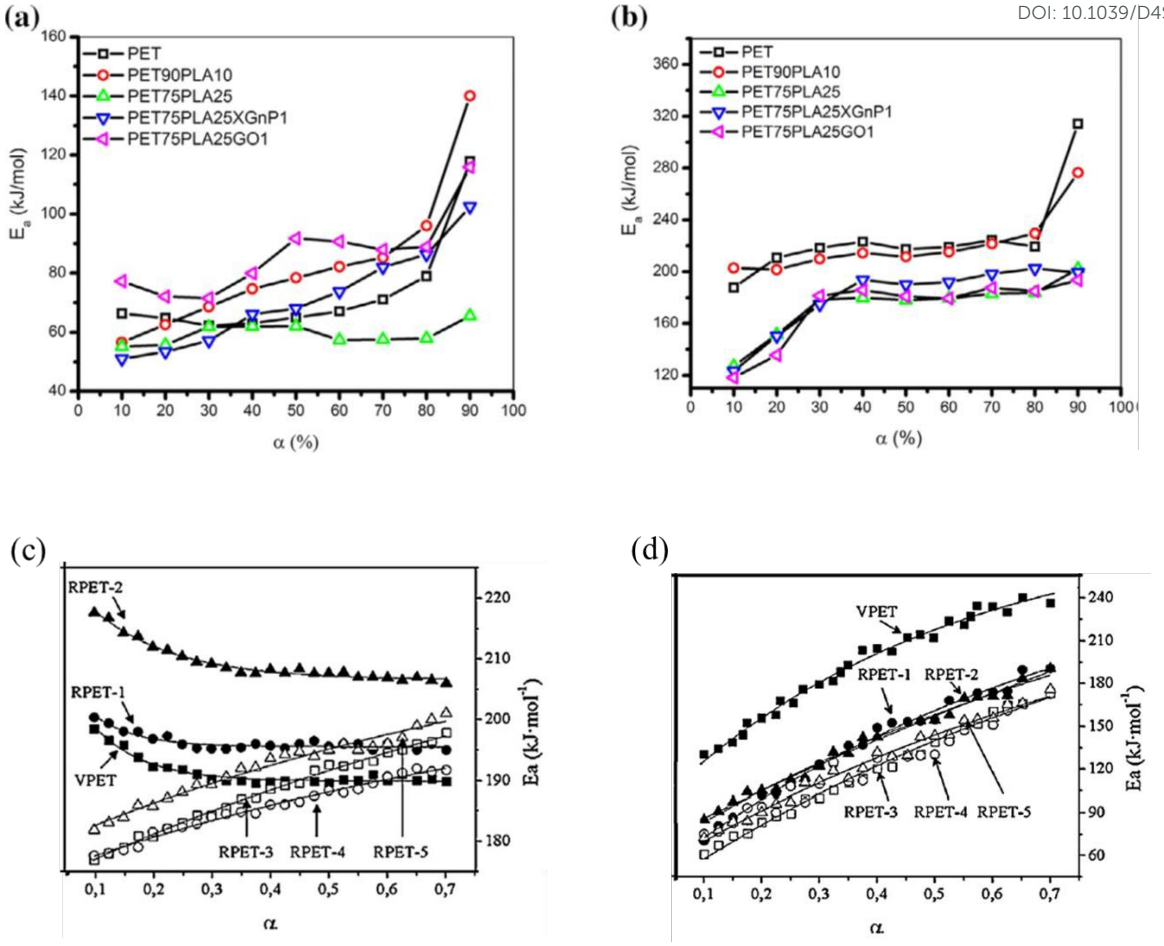

Figure 25: TGA results for blends with PET (top row; a and b) and comparing virgin and recycled PET (bottom row; c and d).[105,161] Reproduced with permissions from the publishers Elsevier and John Wiley & Sons; α is conversion (either in % (top) or as fraction (bottom)).

For blends, TGA has also been applied with for instance Jafari *et al.*[161] analyzing PET/PLA blends potentially containing graphene oxide (GO) and exfoliated graphite (xGnP). These authors applied heating rates between 2.5 and 20 K min^{-1}, with the results for the *E* variation with mass loss percentage presented in **Figure 25** (top row; a: air, b: N_2 atmosphere). It again follows that *E* is lower in air than under inert conditions; more in detail a factor 2 difference is identified. Similar experiments dealing with PET and recycled PET (up to 5 times) have been performed by Badia *et al.*,[105] except that instead of air an O_2 atmosphere has been applied. **Figure 25** (bottom row) shows a comparison between TGA results under N_2 and O_2 atmosphere.[105] Consistently with the previous discussion, lower *E* values are found in case O_2 is present. This effect is even more significant if reprocessed materials are considered.

(1o) Initiation $PH + O_2 \rightarrow 4P^{\cdot}$ (k_{1o})

(1u)Initiation $POOH \rightarrow 2P^{\cdot} + \gamma_1 POH = O + \gamma_1 S$ (k_{1u})

(2) Propagation $P^{\cdot} + O_2 \rightarrow PO_2^{\cdot}$ (k_2)

(3) Propagation $PO_2^{\cdot} + PH \rightarrow POOH + F$ (k_3)

(4) Termination $P^{\cdot} + P^{\cdot} \rightarrow \gamma_4 PP + (1-\gamma_4)PH + (1-\gamma_4)F + \gamma_4 X$ (k_4)

(5) Termination $P^{\cdot} + PO_2^{\cdot} \rightarrow POOH + F$ (k_5)

(60) Activated complex formation (k_{60})

$PO_2^{\cdot} + PO_2^{\cdot} \rightarrow [PO^{\cdot} + {}^{\cdot}OP]_{cage} + O_2$

(62) Termination $[PO^{\cdot} + {}^{\cdot}OP]_{cage} \rightarrow O(P=O)_2 + POH$ (k_{62})

(63) Non terminating combination $[PO^{\cdot} + {}^{\cdot}OP]_{cage} \rightarrow O(P=O)_2 + POH$ (k_{63})

(0i)Decomposition Irreg $\rightarrow$ $POH = O + F_V + S$ (k_{0i})

(7)Condensation $POH = O + POH = O \rightarrow O(P=O)_2 + H_2O - S$ (k_7)

Parameter	Value	Unit
k_{0i}	7.1×10^{-4}	s^{-1}
k_{1o}	9×10^{-4}	$L\,mol^{-1}s^{-1}$
k_{1u}	5×10^{-1}	s^{-1}
k_2	1×10^{8}	$L\,mol^{-1}s^{-1}$
k_3	1.9×10^{3}	$L\,mol^{-1}s^{-1}$
k_4	6×10^{13}	$L\,mol^{-1}s^{-1}$
k_5	4×10^{11}	$L\,mol^{-1}s^{-1}$
k_{60}	1×10^{10}	$L\,mol^{-1}s^{-1}$
k_{62}	4×10^{5}	s^{-1}
k_{63}	1×10^{8}	s^{-1}
k_7	1.7×10^{-6}	$L\,mol^{-1}s^{-1}$
γ_1	8.3×10	%
γ_4	1.71×10	%

Parameters used for kinetic modeling at 280°C

Figure 26: Example of a kinetic study for thermo-oxidative degradation in which a set of rate coefficients is determined as linked to a more detailed reaction scheme; example with tuning based on a macroscopic property; based on the work of Nait-Ali *et al.*[162]

It should be stressed that only in more isolated kinetic studies sets of rate coefficients have been reported so that a link to a detailed reaction mechanism driven by elementary reactions is more within reach. For example, as shown in **Figure 26**, Nait-Ali *et al.*[162] reported several kinetic parameters for thermo-oxidative degradation at 280°C, deriving rate coefficients from rheological data, specifically describing changes in the Newtonian viscosity. Hence, the kinetic model has been built on a macroscopic property

View Article Online
DOI: 10.1039/D4SU00485J

variation, as opposed to a typical model for chemical kinetics in which (molar) concentration variations are modeled. Similarly, Härth *et al.*[163] conducted an oscillatory rheological study under a nitrogen atmosphere to describe kinetic changes in zero-shear viscosity, according to a so-called build-up reaction, lumping esterification and transesterification, and a so-called break-down reaction, being a lumped chain scission reaction. E values of 93 kJ mol^{-1} and 176 kJ mol^{-1} have been respectively reported.

Another study treating the degradation kinetics at the level of viscosity variations is the one of Launay *et al.* [156] These authors dealt with the hydrolytic degradation of PET by exposing it to boiling distilled water at 100 °C for a period of 25 days, after which the samples became brittle. A second order (apparent) rate coefficient of 1.83 10^{-8} kg mol s^{-1} (unconventional units) could be determined, assuming random chain scission. Oreski *et al.*[164] further reported a significantly larger drop in average chain length of PET samples exposed to a temperature of 95 °C and a humidity of 85% compared to samples exposed to 125°C in a dry environment. This shows that next to thermo-oxidative degradation, hydrolytic degradation should be considered in the presence of water, at least if the temperature is above T_g knowing that the hydrolysis will be mainly relevant in the amorphous part. The authors reported an E of 86 kJ mol^{-1} and 96 kJ mol^{-1} depending on the grade but lower than the E value of Arhant *et al.* [165] being 115 kJ mol^{-1}.

More recently, Fiorillo *et al.* [16] compared Arrhenius values for hydrolytic degradation for PETG both based on (molecular) chain length variations via SEC and (macroscopic) rheological variations, including the Newtonian viscosity and shear thinning parameters. It was highlighted that M_n is a key parameter to be considered and that fitting with the relaxation time parameter provided more rheological sensitivity.

View Article Online
DOI: 10.1039/D4SU00485J

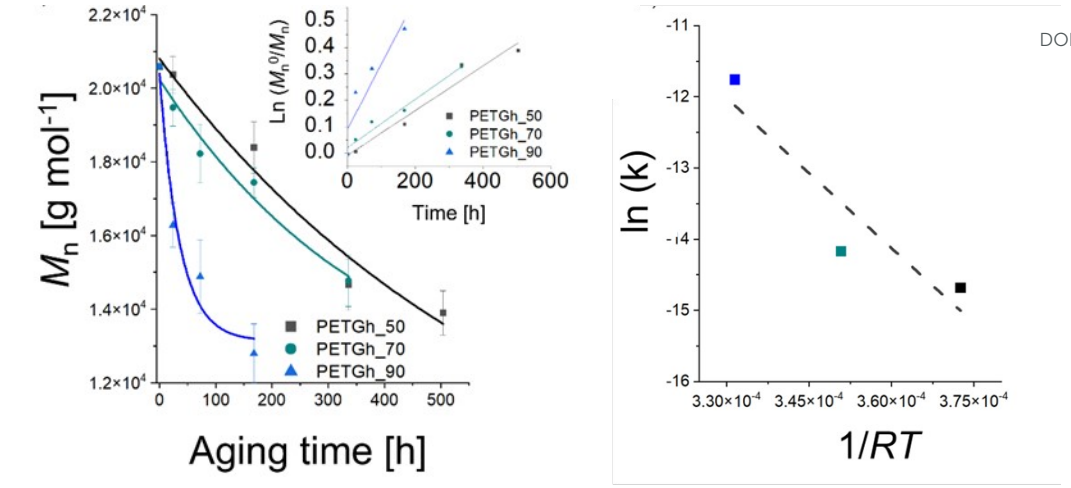

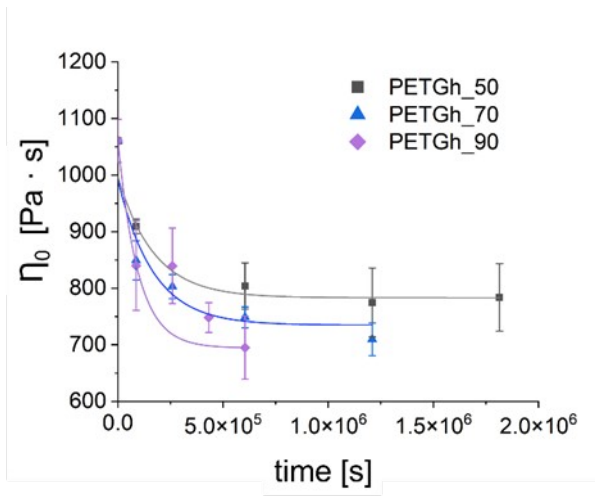

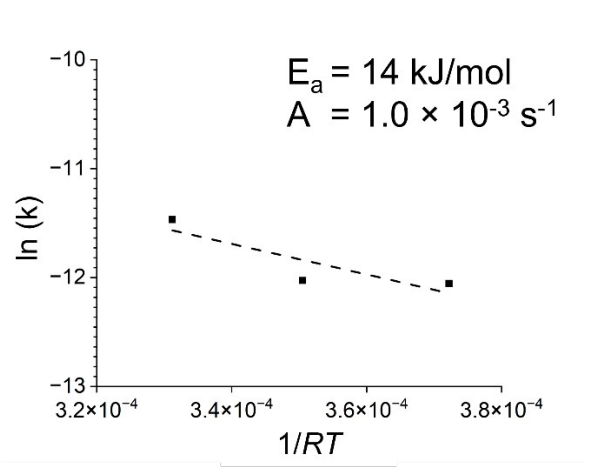

Method	Temperature [K]	τ [s]	k [s^{-1}]	A [s^{-1}]	E_a [kJ/mol]
SEC (k_{M_n})	323	2.3 × 10^6	4.2 × 10^{-7}	6.8 × 10^4	70
	343	1.4 × 10^6	7.0 × 10^{-7}		
	363	1.3 × 10^5	7.8 × 10^{-6}		
SAOS zero shear viscosity (k_η)	323	1.7 × 10^5	5.8 × 10^{-6}	1.0 × 10^{-3}	14
	343	1.7 × 10^5	6.0× 10^{-6}		
	363	9.6 × 10^4	1.05× 10^{-5}		
SAOS relaxation time (k_λ)	323	1.6 × 10^5	6.3 × 10^{-6}	1.6 × 10^{-4}	8.8
	343	1.5 × 10^5	6.7 × 10^{-6}		
	363	1.1 × 10^5	9.1 × 10^{-6}		

Figure 27: Example of hydrolytic rate coefficient determination for PETG using either a macroscopic or molecular property variation.[16] Parameters of the exponential interpolation for degradation at different scales thus via different measuring techniques: τ is the characteristic time parameter and k is an apparent degradation coefficient for the decrease of the number-average molar mass, viscosity and characteristic relaxation time. Arrhenius parameters for k values also included. Reproduced with permissions from the publisher Elsevier.

View Article Online
DOI: 10.1039/D4SU00485J

In this work of Fiorillo et al. [16] the highest (Newtonian) viscosity drop was reached after an ageing in water of 7 days at 90 °C. By extrapolation a k_{hydro} of about 3.4 10^{-6} L mol^{-1} s^{-1} was obtained at 25°C, resulting in a half-life of decomposition of *ca.* 3 days under storage conditions (excess of water). Jung *et al.*[166] determined, following a similar approach, k_{hydro} via viscosity measurements including a pH variation. More in detail, these authors found that the relative viscosity dropped more rapidly with time at a higher pH, as shown in **Figure 28**. Coupled with GPC analysis and assuming first order kinetics, k_{hydro} in the presence of acids could be assessed as 0.05 day^{-1} at 30 °C. The study of Jung *et al.*[166] additionally compared polyester and poly(propylene carbonate) (PPC) water contact, pointing out that in a strong acid environment polyesters are less degraded than PPC.

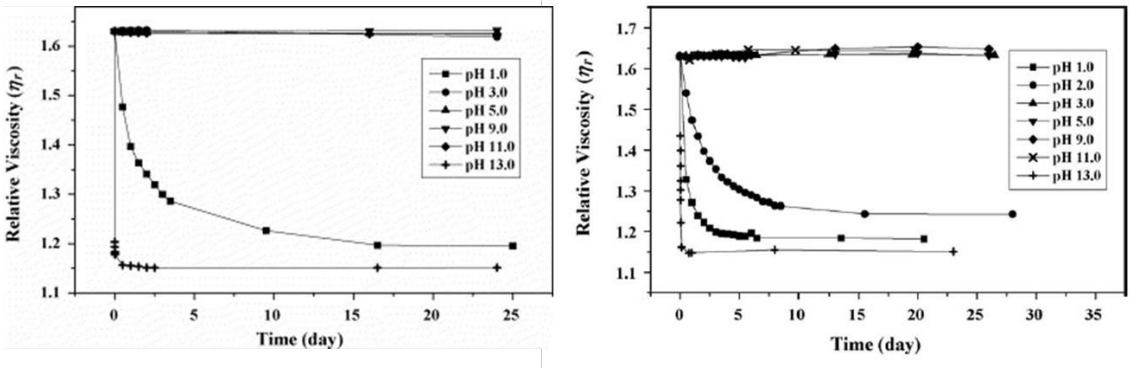

Figure 28. Relative viscosity of solution with PLA (left) and PPC (right; 0.5 wt.% polymer) at different pH.[166] Reproduced with permissions from the publisher Elsevier

Alternatively, computational chemistry can be applied to assess (or determine) degradation rate coefficients (or kinetic parameters). Specifically, density functional theory (DFT) calculations have been performed to assess degradation reaction energies. For example, Huang *et al.*[91] et al. put forward the likelihood of concerted reaction mechanisms, and more specifically those with a six-membered transition state compared to cleavage of C-C and C-O bonds in the main chain.

Hence, the current section has highlighted that several methods exist to retrieve (apparent) degradation kinetic parameters. This is further illustrated in **Table 6**, giving an overview of typical rate coefficients according to the reaction type and method applied. One can specifically notice a large difference in *E* values, highlighting the use of apparent or lumped methods that are less desirable, as the molecular scale is not recognized in sufficient detail with many elementary reactions with different relative importances dependent on the boundary conditions at play. Otherwise said, it is clear that the number of data is

View Article Online
DOI: 10.1039/D4SU00485J

limited and effort should be undertaken to retrieve more elementary driven rate coefficients and kinetic parameters seeing the plethora of reactions mentioned in the previous sections.

Table 6: Overview of (lumped) rate coefficients for PET degradation reactions; *E*: activation energy; *A*: pre-exponential factor.

Degradation reaction type	(Apparent) kinetic parameter	Reference
Thermal	E = 48.14 - 55.56 kcal mol^{-1} A = 3.16 10^{12} - 7.84 10^{14} s^{-1}	90
Thermal	First step: E = 235 kJ mol^{-1} A = 1.610^{15} s^{-1} Second step E = 96 kJ mol^{-1} A = 3.53 10^{4} s^{-1}	167
Thermal	ASTM method E = 165.6 kJ mol^{-1} Flynn-Wall-Ozawa method E = 166-180 kJ mol^{-1} Iso-conversional method E = 165-195 kJ mol^{-1}	160
Thermal	E = 161.23 kJ mol^{-1} A = 3.8510^{9} s^{-1}	168
Thermal	Activation energies in Table 4	103
Thermo-mechanical	Rate coefficients in Table 4	162
Thermo-mechanical	Build-up reaction E = 93 kJ mol^{-1} Chain scission E = 176 kJ/mol^{-1}	169
Thermal	E = 203-355 kJ mol^{-1} Log A = 33.3-59.3 s^{-1}	129
Thermo-oxidative (air)	E = 145-218 kJ mol^{-1} Log A = 28.5-51.8 s^{-1}	129
Thermal	Activation energies in Figure 5b	161
Thermo-oxidative (air)	Activation energies in Figure 5a	161
Thermal	Activation energies in Table 4	105
Thermo-oxidative (oxygen)	Activation energies in Table 4	105
Hydrolytic	E = 1.83 10^{-8} kg mol^{-1}s^{-1} at 100°C	156
Hydrolytic	E = 86 - 96 kJ mol^{-1}	164
Hydrolytic	E = 115 kJ mol^{-1}	170

View Article Online
DOI: 10.1039/D4SU00485J

Relevance to support life cycle assessment and environmental footprint data

The mechanical recycling process aligns with at least three out of the twelve principles of Green Chemistry, [171] i.e. "Prevent Waste", "Avoid Auxiliaries", and "Energy Efficiency". Indeed, with the help of mechanical recycling, we can prevent landfilling of polymer products, avoid the use of solvents and achieve energy efficiency compared to other processes such as chemical recycling, at least if the recycled polymer product quality is sufficient. These features can be better demonstrated in case LCA is applied to evaluate and compare from a more environmental point of view all the possibilities for closing the loop for polymer products.

LCA is potentially a powerful approach to identify green technologies in polymer production and processing, comparing industrial processes and technologies. LCA can also recognize PET and bio-based PET as materials with high "adherence to green design principles" and low "life-cycle environmental impacts", as demonstrated by Tabone *et al.*[172] However, most of the LCA studies on polyesters and PET in particular still focus on overall CO_2 equivalents per treated mass of waste, hence, the carbon footprint (CF) calculations are still to be seen with a certain degree of uncertainty. Such LCA studies consider only overall process manipulations, hence, more apparent (lumped) chemical modifications, with overall the claim that mechanical recycling can be beneficial in several cases.

For example, for bottle-to-bottle mechanical recycling, Ncube and Borodin[173] put forward the use of 3.33 kg CO_2 eq. CF as opposed to the landfill mode of operation with a value as high as 47 CO_2 eq. Furthermore, Meys *et al.*[174] indicated that PET chemical recycling could potentially enable improvements up to 4.3 kg CO_2 eq. compared to energy recovery. Allen and James[31] in turn have demonstrated that mechanical recycling is preferred over chemical recycling but the latter is still beneficial versus virgin production. Work of Dormer et al.[176] in addition reveals that the CF of PET-based packaging production decreases by 58%, i.e. from 2.1 to 1.6 kg CO_2 eq., by manufacturing the trays with 85% recycled content compared to the use of pure virgin material. Furthermore, the CF value can be further reduced by 24%, i.e. from 1.6 to 1 kg CO_2 eq. in case the fraction of recycled PET becomes 100%, highlighting an important environmental goal for the PET recycling industry.

View Article Online
DOI: 10.1039/D4SU00485J

It is also well recognized that LCA should be combined with green metrics, e.g. E-factor calculations,[177,178] to provide a more complete understanding of the environmental impact of polymer production and disposal identifying areas for improvement and developing sustainable practices.[179–181] E-factor analysis can be linked to the the total mass of waste generated by the mass of the product manufactured, with e.g. a recent review by Fadlallah and Allais[181] tackling the possibilities and limitations of E-factors based analysis. Uekert et al.[182] in turn provided environmental, economic and technical comparison of existing technologies. In particular, they reported an E-factor of 0.8 for the production of virgin PET, 0.9 for mechanical recycling and 0.4 for methanolysis, although a further refinement of calculation methods is still desirable to make more substantial comparisons. Enzymatic hydrolysis has likely a high E-factor, generating ca. 5.5 kg of waste water per 1 kg of PET made. Other reports have shown that mechanical recycling has lower greenhouse gas emissions than chemical recycling, landfilling, or incineration.[183,184]

Interestingly, Shen *et al.*[175] studied the relevance of consecutive recycling for bottle-to-fiber recycling. An advantage regarding environmental impact could only be confirmed by up to three generations of waste. These authors also put forward that more data on molecular properties is needed and the link to material properties should be incorporated for the genuine exploitation of the bottle to bottle recycling technique. More fundamentally it follows that chemical reactions underlying the mechanical recycling technique result in the modification of the polymer molecules involved. A too severe modification upon mechanical recycling makes it a non-trivial task to repair those transformations toward the desired material properties (e.g. IV) by performing post-processing steps, e.g. SSP. LCA should thus ideally be linked to the molecular scale and the type of reactions covered in the present work, e.g. differentiating between the use of dry and wetted flakes.

It should be also emphasized that the recognition of the molecular scale is not the only LCA challenge but we also need to develop more defined boundary conditions to establish the environmental preference of mechanical or chemical recycling, as for instance indicated in the work of Nakatini *et al.*[185]

A more in-depth discussion of the state of the art on LCA analysis is included in our follow-up contribution also dealing in detail with the role of contaminants as well as the use of alternative bio-based feedstocks.

View Article Online
DOI: 10.1039/D4SU00485J

Material property variations in view of final applications

The impact of reactions is ultimately translated in variations at the material scale. In the present section, an overview is given of the most important rheological, thermal and mechanical properties for polyester materials and applications in view of their (mechanical) recycling potential. Examples are included in which an explicit link is made to a molecular scale variation as discussed in the previous section, being a key novelty of the present work.

Rheological properties

Rheological properties of polymer melts, describing variations in flow behavior due to deformations, are essential macroscopic characteristics in view of polymer processing and recycling design.[186] These properties are typically obtained in offline mode via various equipment tools relying on a well-defined flow pattern in a confined lab-scale environment. So-called constitutive models are used to describe the experimental observations, enabling a better coupling to software packages simulating the flow behavior in actual (industrial) equipment and devices. For such packages one can distinguish between (i) computational fluid dynamic (CFD) packages dealing with very fine mesh calculations for the application scale but treating lower scales in lower detail; and (ii) molecular scale-driven software packages employing for the application axis a more basic mesh but otherwise considering a detailed implementation of lower scale phenomena.

The most common lab polymer melt rheological set-up is a rotational rheometer equipped with a parallel plate geometry, as shown in **Figure 29** (top left).[186] This set-up consists of two plates, one fixed and the other one rotating, generating a laminar flow defined by a gap that can alter defining a shear rate as the product of the angular speed, the (local) radius *r* and the reciprocal of the gap height *H*. The upper limit in shear rate is determined by the ability to reach uniformity of the shear stress in the sample in the shortest time possible, whereas the lower limit is linked to the accuracy of the machine. The gap error is about 30 μm so that one recommends to not go below 200 μm for *H*. Furthermore, to assure homogeneity *H* should be much smaller than the maximal radius *R*, *e.g.* for *R* equal to 25 mm *H* should be maximally 1 mm. In the presence of particles, hence, blends one advises that *H* should be at least 5 time the particle diameter.[187]

View Article Online
DOI: 10.1039/D4SU00485J

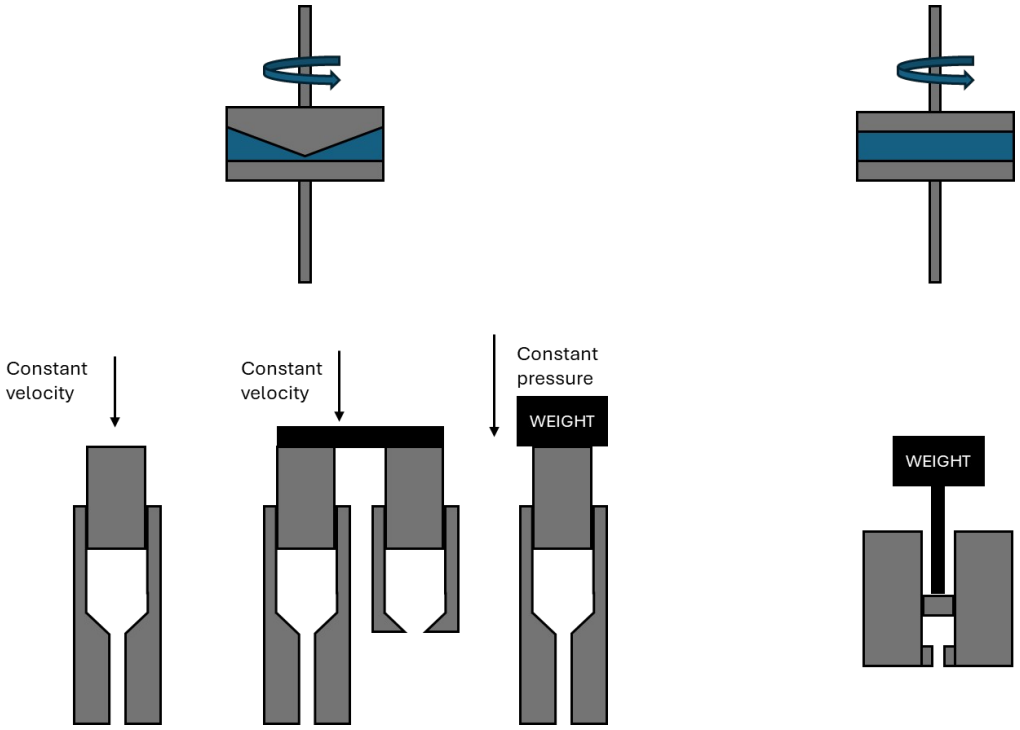

Figure 29. Conceptual design of parallel plate rotational rheometer, cone-plate rotational rheometer, capillary rheometer(s), and melt-flow index device. Figure based on general configurations mentioned in the literature.[188]

The cone-plate geometry, as depicted in **Figure 29** (top right), is an alternative to the parallel plate geometry. The advantage is the generation of a shear flow in a gap characterized by a constant shear rate along the radius, due to a constant cone-plate angle α being the ratio of *r* and the (local) height. For normal stress difference measurements, the cone-plate geometry is preferred over the parallel plate one. A disadvantage is the difficulty in the filling of the complete system. In any case, rotational rheometers are more restricted to low shear rate data.

A way to obtain shear viscosity data at higher shear rates is by means of a capillary rheometer, in which as depicted in **Figure 29** (bottom left), a piston is employed to push the melt through a capillary die e.g. up to a shear rate of 10^{-7} s^{-1} but likely above 1 s^{-1} to avoid complications such as surface tension and gravity, which can interfere with the measured accuracy.[186] Several capillary rheometer configurations exist, e.g. one can distinguish those based on a constant velocity, a twin barrel principle, and a constant pressure (left to right in **Figure 29** (bottom left)). The advantage of capillary rheometer measurements is the possibility to mimic higher shear rate processes such as injection molding.[189]

View Article Online
DOI: 10.1039/D4SU00485J

Note that a somewhat related piston configuration also exists for application at very low shear rates, defining a melt-flow index (MFI) device, as shown in **Figure 29** (bottom right). An MFI device allows to measure the amount of material exiting for a given period of 10 minutes, with a larger amount implicitly implying a lower (Newtonian) viscosity. MFI measurements are thus very implicit and do not allow for a dedicated rheological analysis. [113]

Furthermore, one of the most popular rheological testing approaches is based on conducting small amplitude oscillatory sweep (SAOS) analysis, considering the (parallel plate) rotational rheometer at different frequencies (ω values). This dynamic testing under melt conditions allows to obtain information about the elastic and viscous contribution, respectively known as the (shear) storage modulus (*G*' or G_1) and the (shear) loss modulus (*G*'' or G_2). Plotting both *G*' and *G*'' as a function ω allows to assess the overall material composition, with a possible derived property being a characteristic relaxation time λ, e.g. defined as ω_c^{-1} with ω_c denoting the crossover frequency.

Polymer melts are very likely characterized by both a non-zero *G*' and *G*'' and for a sufficiently low ω a linear viscoelastic regime results. They thus behave differently like for instance the Newtonian fluid water being a perfectly viscous material (vanishing *G*') and a perfectly elastic solid obeying Hooke's law (vanishing *G*"). Polymer materials possess in general a deformation behavior between that of a purely viscous material and a purely elastic material, as also measurable in the solid state with a swapping of the symbol *G* into *E* in the scientific community.[186]

As shown in **Figure 30** (top row), for PET and PETG, *G*" is higher than *G*' at any ω, meaning that the viscous behavior is dominant and no ω_c is obtained.[16,190] In **Figure 30** (left middle), for PLA, one does obtain such ω_c at higher frequencies so that only at the lower to intermediate ω a dominant viscous contribution is established.[191,192] A more branched/crosslinked polymer system has an ω_c at lower frequencies, as depicted in **Figure 30** (right middle) for the multiphase acrylonitrile-butadiene-styrene polymer (ABS).[111] With increasing ω the material behavior now changes from a viscous liquid to that of a solid.

View Article Online
DOI: 10.1039/D4SU00485J

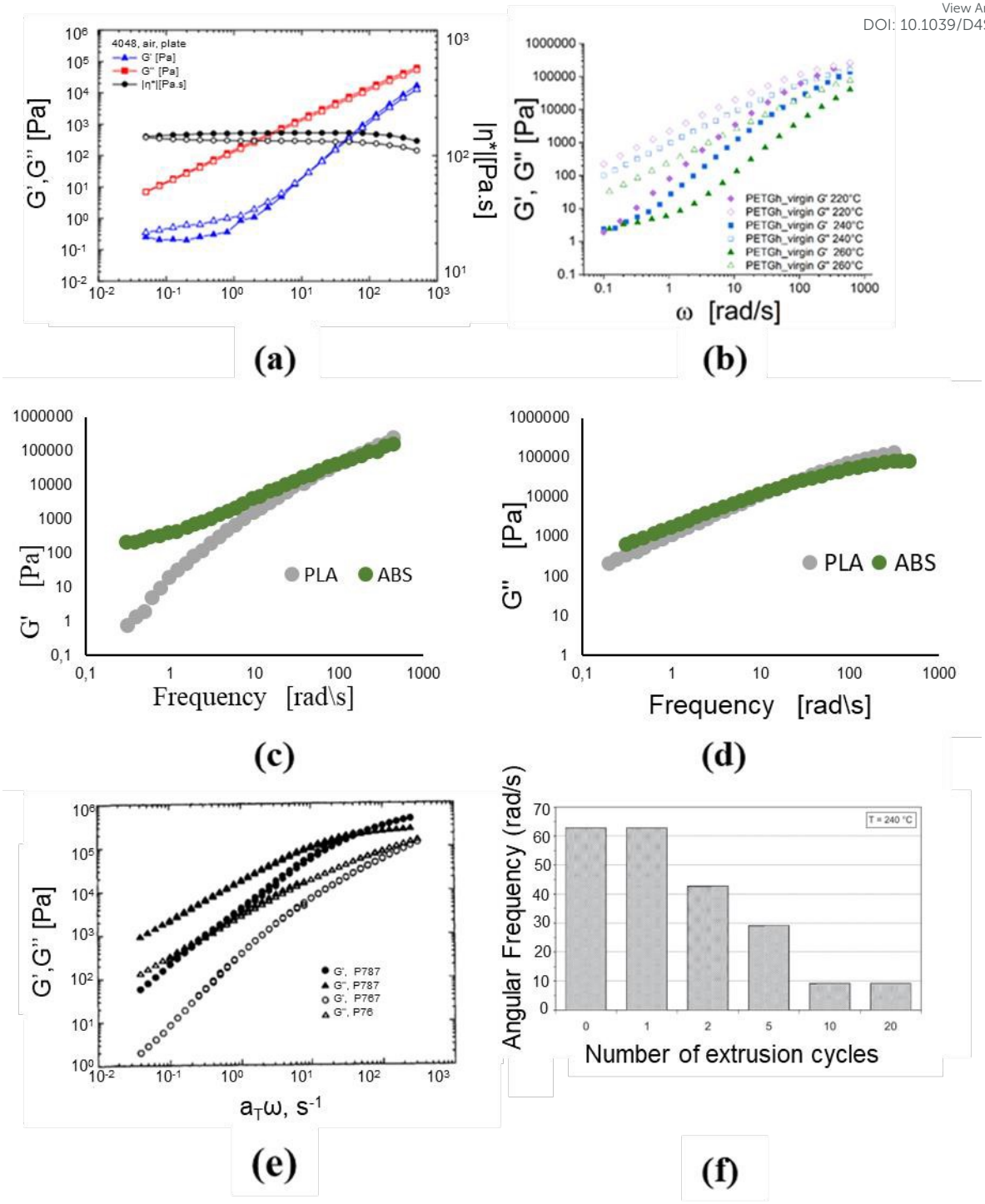

Figure 30. Data on storage and loss (shear) modulus (G' and G") as a function of frequency ω, so-called frequency sweeps. (a): PET (also depicting the complex viscosity) and PETG (temperature effect).[16,190] (c): Data on the storage modulus of PLA and ABS [191] (d) complementary data on the Loss modulus of PLA and ABS. (e): Data on storage and loss (shear) modulus (G' and G") as a function of frequency ω, so-called frequency sweeps. The material is PCL (100°C; variation of via number average molar mass: P787 M_n "0.64" and P767 M_n "0.43", a_T: shift factor;[193] (f): LDPE only displaying the cross over point for G' and G" for different extrusion cycles. [111] Subfigure a, b, e and f: feproduced with permissions from the publisher: Elsevier, AIP Publishing and John Wiley and Sons. Data of Figure c and d from Sanchez et al.[191]

View Article Online
DOI: 10.1039/D4SU00485J

This relation between macromolecular properties and rheology is further illustrated in **Figure 30** (left bottom), selecting poly(caprolactone) PCL. After modification of the chains due to scission reactions, M_n decreases (labeling in legend), which is translated in a decrease of the absolute values of the moduli. Furthermore, ω_c shifts to a higher ω. For a lower average molar mass material, e.g. by a dominant scission due to extensive degradation, a faster relaxation is therefore expected. Oppositely if the degradation induces mainly a shift toward higher average molar masses ω_c becomes lower. For example, Jin *et al.*[111] analyzed the degradation of LDPE after multiple reprocessing and revealed the formation of crosslinks, with the storage module increasing along the complete interval of frequencies. The latter increase implies that the material shows an improved elastic behavior. A delay of the relaxation time has thus been established, as shown in **Figure 30** (right bottom) based on a shift of ω_c to lower frequencies.

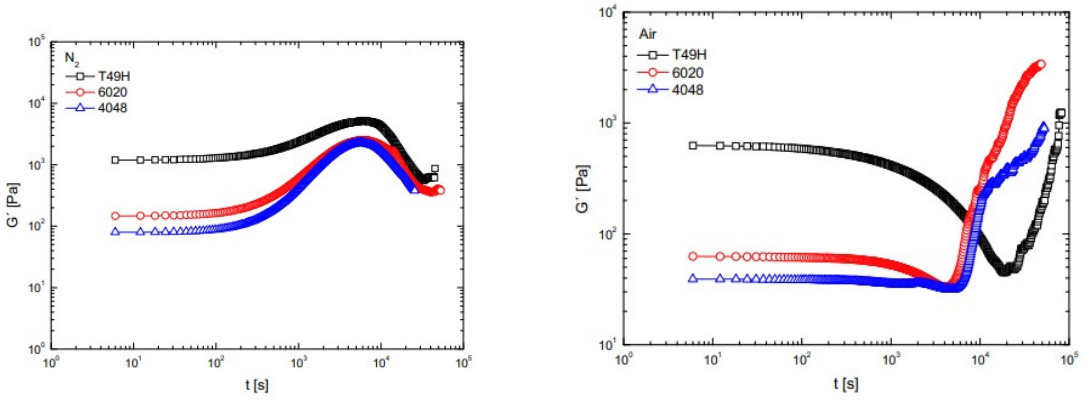

Figure 31. Storage modulus (*G*') measured as a function of time in the presence of nitrogen (left) and air (right) of 3 different PET grade: PET T49H (black), 6020 (red) and 4048 (blue). Temperature of 280 °C , frequency of 10 rad s^{-1} and deformation of 10%.[190] Reproduced with permission from the publisher AIP Publishing.

A different reaction environment can also imply a different variation of *G* values. The comparison between a purely thermal degradation effect and a thermo-oxidative effect on the PET melt behavior was for instance investigated by Kruse *et al.*[190] by comparing temporal *G*' variations in an air and nitrogen atmosphere. Based on the experimental data in **Figure 31**, these authors concluded that in the inert atmosphere chain scission and post-condensation reach a steady-state giving nearly a zero net effect on the average chain length. However, the behavior in air is totally different, with the post-condensation reaction overcompensating the chain scission leading to the increase of the elastic contribution.

View Article Online
DOI: 10.1039/D4SU00485J

Additional rheological properties coming from SAOS measurements are the variation of the (absolute value of the) complex modulus $|G^*|$ and the phase angle δ, which are defined as:

$$|G^*| = \sqrt{(G')^2 + (G'')^2}$$

$$\tan(\delta) = \frac{G''}{G'}$$

Based on the latter two rheological properties a so-called Van Gurp-Palmen (vGP)-plot can be created. [194] Such plot displays the variation of δ with $|G^*|$ at a given T, with the minimum of the curve denoted as the plateau modulus G_N^0. The latter modules is linked to the entanglement molar mass M_e for a given density ρ and the universal gas constant denoted as:

$$G_N^0 = \frac{\rho R_u \mathrm{T}}{M_e}$$

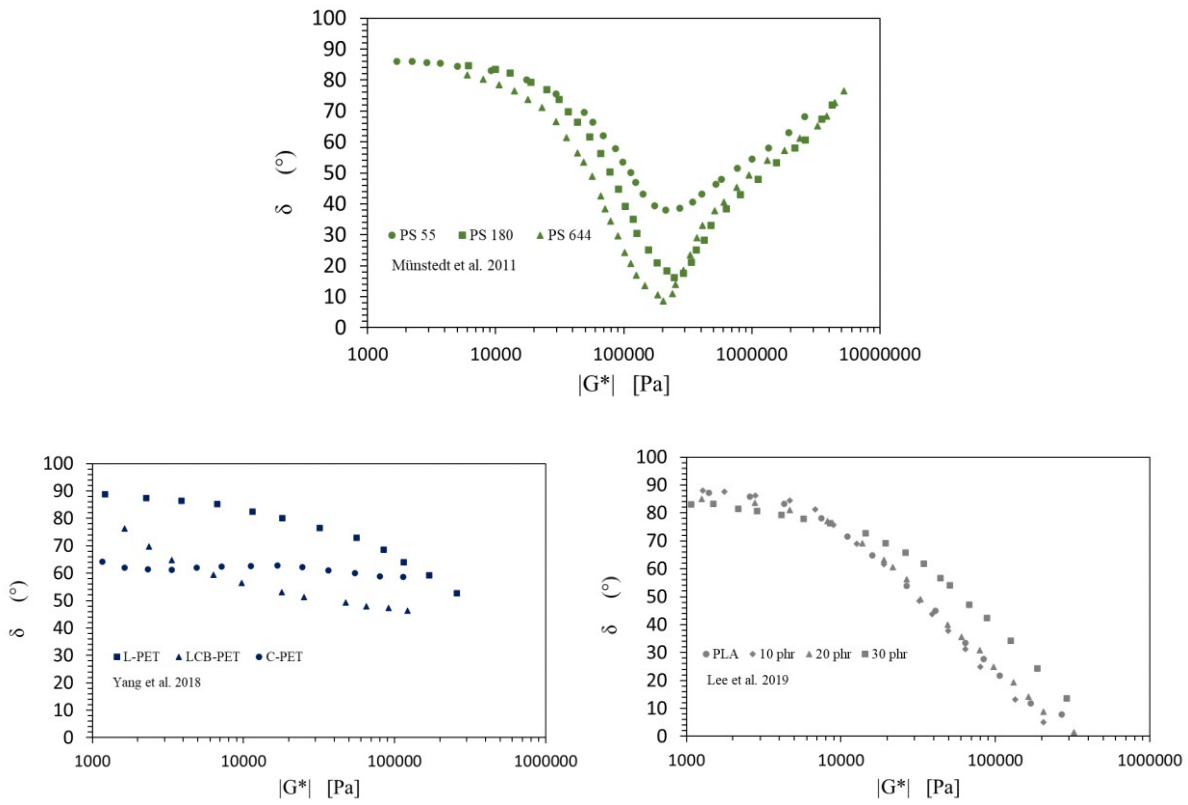

Figure 32. Van Gurp-Palmen (vGP) plots (phase angle δ as a function of complex modulus |G* |) for (top) three polystyrene (PS) samples with different average molar mass; for (bottom left) linear PET (L-PET), branched PET (LCB-PET) and cross-linked PET (C-PET); and for (bottom right) neat PLA and PLA modified with acrylic core–shell rubber (filler content in phr). Data to construct the subfigures taken from following references: [194–196]

As shown in **Figure 32** (top), for polystyrene (PS) with a higher average molar mass the minimum of the vGP plot drops. Furthermore, Yang *et al.* [195] employed such a vGP plot to show that PET materials

View Article Online
DOI: 10.1039/D4SU00485J

with different molecular properties behave differently in rheological properties, as shown in **Figure 32** (bottom left). For linear PET (L-PET) the aforementioned minimum is absent, while PET modified with long chain branches via reactive extrusion (LCB-PET) reveals a different trend toward the establishment of such minimum. The minimum is actually obtained upon considering the PET modified with a crosslinking agent (C-PET).

An extra example on molecular variation in vGP configuration is included in **Figure 32** (bottom right), emphasizing on the difference of unmodified linear PLA and PLA modified with acrylic core–shell rubber at different concentrations. A lower δ results for a higher filler mass concentration, highlighting the enhancement of the viscous behavior of the material.[196]

Another important rheological property following from SAOS measurements is the complex viscosity of which the absolute value $|\eta^*|$ follows from:

$$|\eta^*| = \sqrt{\left(\frac{G'}{\omega}\right)^2 + \left(\frac{G''}{\omega}\right)^2}$$

For low ω, for a viscosity dominated polymer melt, the real or conventional viscosity η is obtained, and in several cases the Cox-Merz rule holds so that frequency and shear rate can be interchanged.[197] In general, the (complex) viscosity can be investigated in a range of shear rates and we can observe at a given temperature for a given ω range either shear thinning, being a lowering of the (complex) viscosity with increased shear rate, shear thickening, being the opposite, or Newtonian behavior.[198]

The majority of polymer melts exhibits shear thinning behavior,[199] due to a variation of molecular variations as conceptually highlighted in **Figure 33 (top)**.[199] For low shear stress, as relevant at low frequencies, the chains cannot easily move since they are too entangled or interactive. Higher shear forces in contrast can free the chains from their constraints so that they can undergo reptation diffusion, leading to a pathway of less resistance and a (complex) viscosity decrease. Exemplary curves of shear thinning with PET and PLA materials are depicted in **Figure 33 (bottom)**, [198,200] differentiating between the effect of processing environment, contamination level, and temperature. It follows that with more contamination the viscosities drop but a certain repair by SSP is possible.

View Article Online
DOI: 10.1039/D4SU00485J

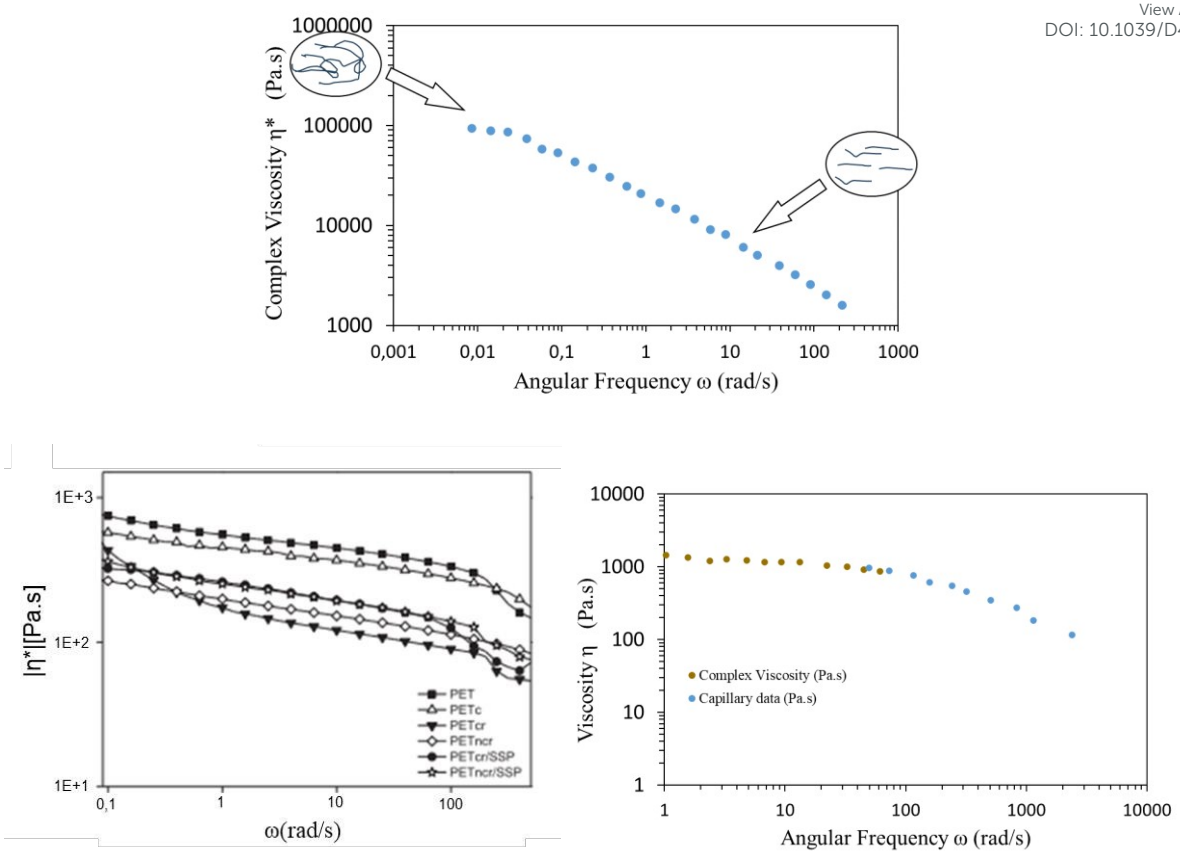

Figure 33. Top: Mechanistic interpretation at the molecular level for the variation of the complex viscosity with frequency ω; Bottom left (Reproduced with permission from the publisher Elsevier): actual data blends of PET and chemical contaminants vs. a reference PET and with fitting according to a Cross model (reference denoted as PET, PETc: contaminated, PETcr: contaminated and reprocessed, PETncr: non-contaminated and reprocessed, PETcr/SSP: contaminated and re-copolymerized with solid state polymerization; PETncr/SSP: non-contaminated and recopolymerized with solid state polymerization) [198]**; Bottom right: actual data with PLA showing data at lower frequencies and higher shear rates. Data to make top and bottom right subfigure from following references:** [199,200]

Through rotational rheological measurements it is in many cases possible to obtain this Newtonian viscosity by directly identifying or by extrapolation accessing the limiting value at very low (zero) shear rate,[201] the latter exemplified in **Figure 33** (bottom right).[200] Interestingly, Münstedt [194] highlighted the variation of η_0 with M_m (also known as the weight average molecular weight M_w), as highlighted in **Figure 34** dealing with linear polymers. The overall dependency changes greatly if we are above a certain average molar mass to manifest entanglements. Higher exponents in the associated power law fits, as also included in this figure by lines, are implying a more effective restriction by entanglements in the higher average molar mass range.

View Article Online
DOI: 10.1039/D4SU00485J

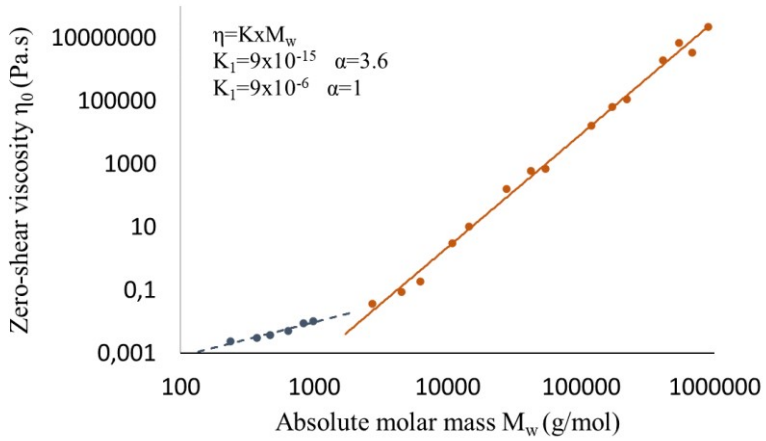

Figure 34. Zero-shear viscosity as a function of mass (weight) average molar mass for linear polyethylenes, considering a wide range of such molar masses and dispersities. Data to construct the figure from Münstedt [194]

Notably, Nait-Ali *et al.*[162] used temporal η_0 data to study the effect of oxygen presence for PET degradation, having in mind that in the hopper and die unit a more oxygen-rich environment exists, expecting more scission and less crosslinking. Consistently, **Figure 35** displays that at low oxygen partial pressures η_0 rises as a function of time, indicating the importance of chain coupling. However, once a critical oxygen partial pressure threshold is reached (9%) η_0 decreases, meaning that chain scission is more relevant.

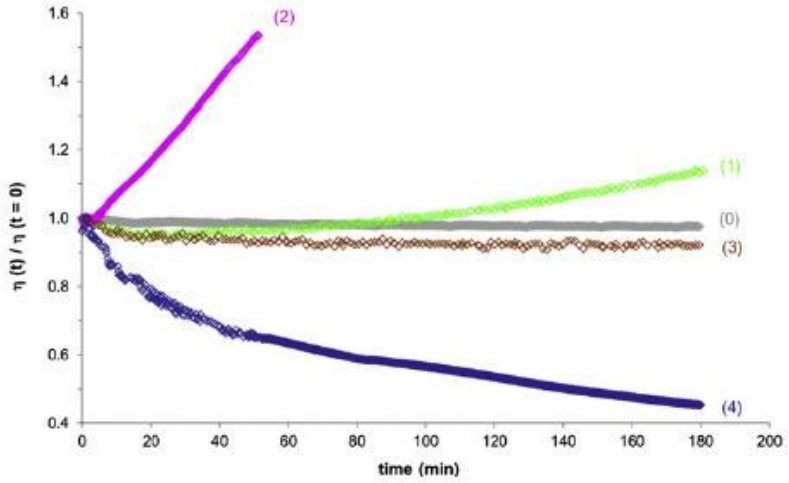

Figure 35. PET Zero-shear or Newtonian viscosity as a function of time (divided by the initial value) at oxygen partial pressures of 0%, 0.6%, 1%, 9%, and 21% of atmospheric pressure (at 280° C). [162] **Reproduced with permission from the publisher Elsevier.**

The results in **Figure 30** to **Figure 35** highlight the link of the molecular scale and the rheological properties as measured at the material scale. During degradation or recycling, as explained in the

View Article Online
DOI: 10.1039/D4SU00485J

previous section, molecular changes take place and thus the rheological properties should also alter. Consistently, one can try to attribute the occurrence of certain reactions during mechanical recycling to changes in material properties, as illustrated in the following paragraphs in the current section.

For a first example on connecting the molecular and material scale, emphasis is on the reprocessing of PLA for which it has been indicated that η_0 decreases with more recycling steps as collaborated by a shortening of the chains through a (dominant) chain scission process.[202] This shortening of chains is evident from the molecular data in **Table 7**, highlighting a drop in M_n and M_m. While the average molar masses are both decreasing the dispersity is increasing, highlighting the relevance of the formation of shorter chains. In parallel, the η_0 values are decreasing, also shown in the same table.

Table 7. Effect of number of extrusions on the number average molar mass (M_n), mass average mass molar mass (M_m) and dispersity of PLA, also displaying the variation of the zero-shear viscosity (η_0).[202]

Extrusion number	M_n [g/mol]	M_w [g/mol]	Dispersity (-)	Zero-shear viscosity η_0 (Pa s)
Virgin	85000	110000	1.29	-
1	75000	104000	1.39	2729
2	66600	88200	1.32	930
3	57500	80600	1.402	520
4	45800	68600	1.50	314
5	37300	58400	1.55	219

A second example connecting the molecular and material scale is the activated nature of degradation reactions, as evident upon inspecting apparent viscosity plots. As shown in **Figure 36**, Peinado *et al* [203] analyzed recycling of bio-based PLA at three temperatures for several recycling cycles. It follows that after each extrusion cycle the viscosity diminishes, however, at 190°C the viscosity decreases are much more pronounced so that one can postulate that scission reactions are then more relevant chemistry wise. This also highlights again the need to have better *E* values, as mentioned upon the discussion of **Table 6**.

View Article Online
DOI: 10.1039/D4SU00485J

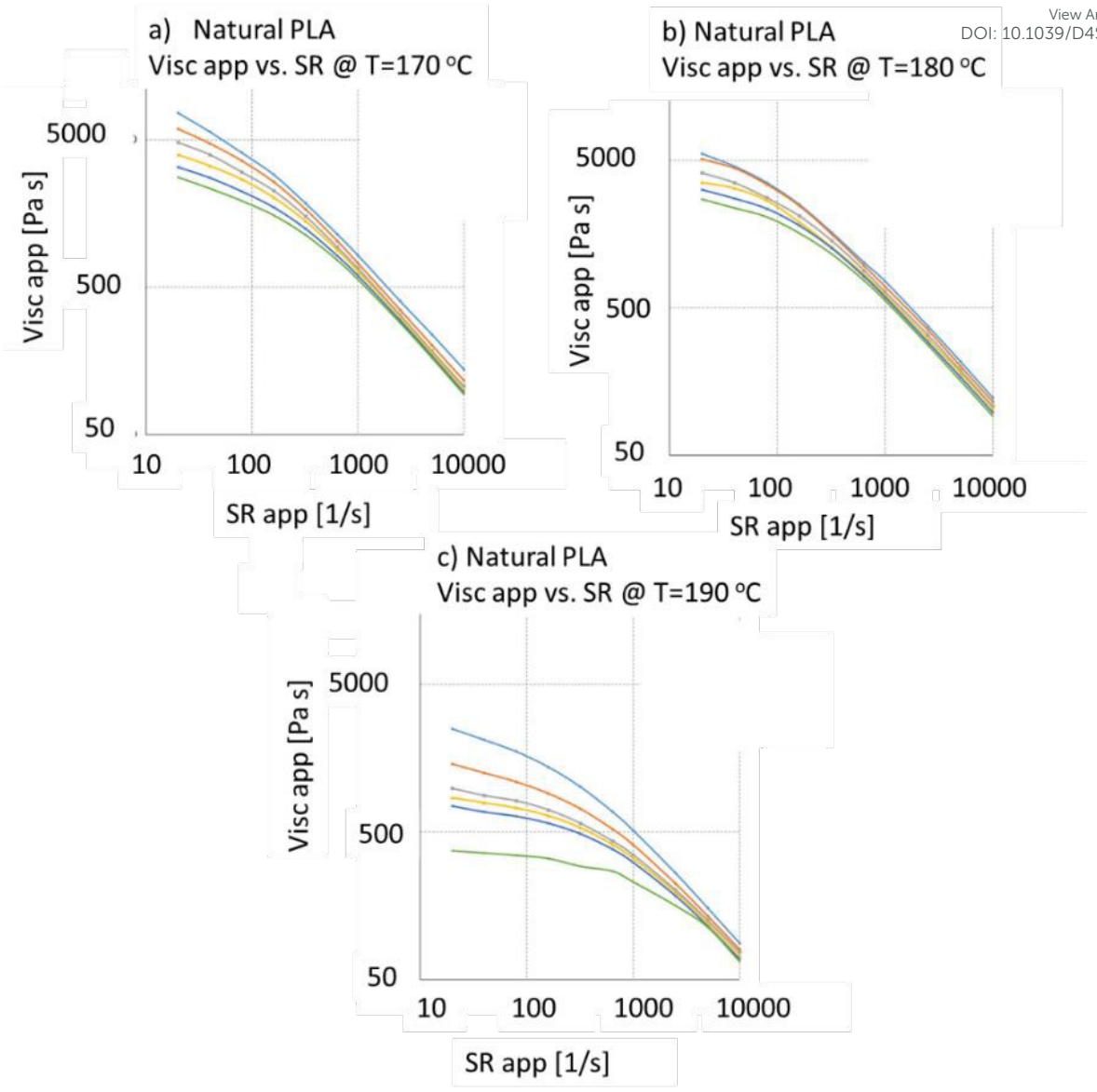

Figure 36. Variation of apparent viscosity with frequency ω for neat PLA measured at three different temperatures: 170°C, 180°C and 190°C: light-blue – virgin, orange – 4 extrusions, grey – 8 extrusions, yellow – 12 extrusions, dark-blue – 16 extrusions, green – 20 extrusions. [203]

A related third example connecting the molecular and material scale is the work of Kruse *et al.* [204] who analyzed the effect of temperature on the melt properties through time-resolved mechanical spectroscopy (TRMS) in the air, as shown in **Figure 37**. These authors found that crosslinking occurs at larger exposure times but that for a decreasing temperature this phenomenon diminishes, as evident from the more dynamic *G*' variations in the right subplot compared to the left one.

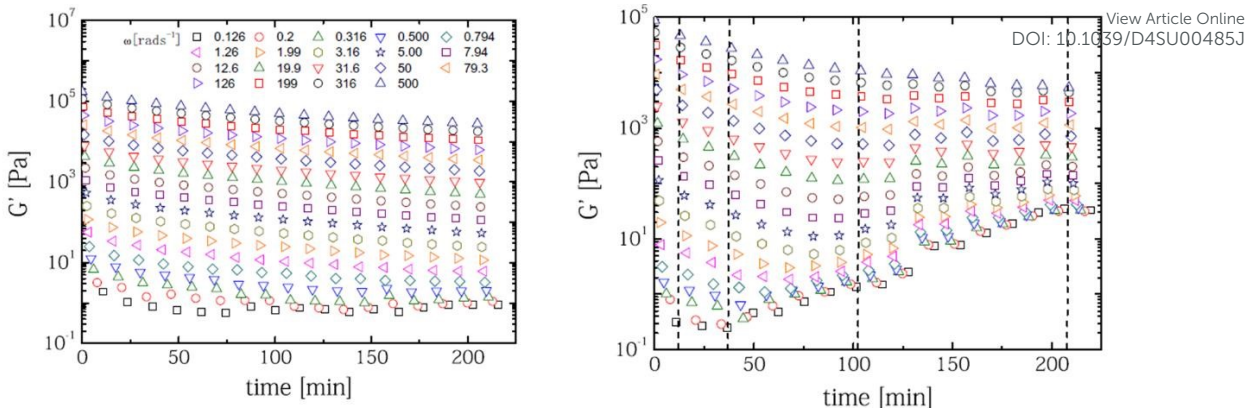

Figure 37. Time-resolved mechanical spectroscopy (TRMS) of the storage modulus *G'* at different frequencies (ω values): left 265°C and right 288°C. Measurement performed in the air. [204] **Reproduced with permission from the publisher Springer Nature.**

Using capillary rheometer data, the apparent viscosity variations for PET and recycled PET at different temperatures are highlighted in **Figure 38** (left; [205]), providing a fourth example on the connection of the molecular and material scale. The decline of the (apparent) viscosity values at a given temperature for recycled PET can be attributed to molecular degradation according to the reactions specified in the upper part of the previous section.

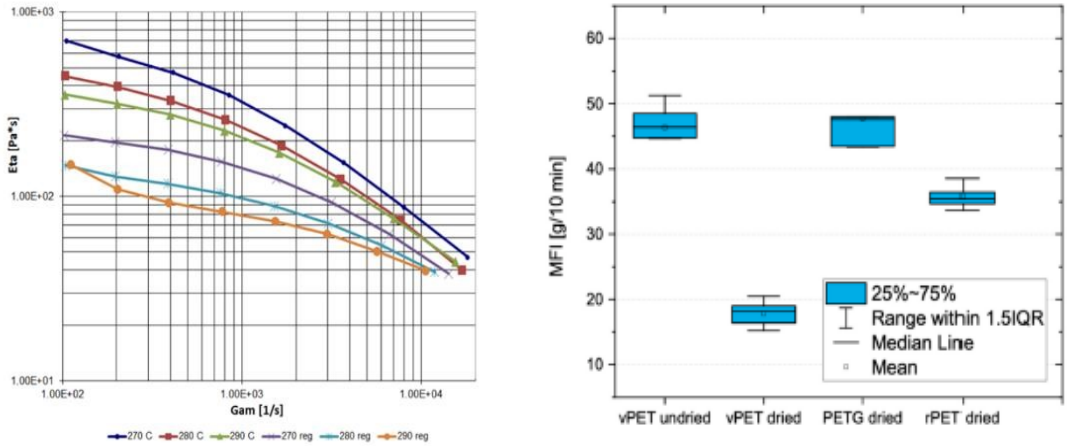

Figure 38. Left: Variation of apparent viscosity with frequency ω for PET and recycled PET at 270°C, 280°C and 290°C (capillary rheometer) [205]**; Right: melt flow index (MFI) data for PET and recycled PET, dried or not.** [206] **Both subfigures are reproduced in open access redistribution mode.**

A fifth example on the connection of the molecular and material scale is devoted to MFI measurements as industrially often employed to assess the degradation state of polymers. As explained above, this is a cheaper experimental method employing a heated channel in which the material is extruded by means of a piston equipped with a known weight to determine the mass in a known interval of time and to

View Article Online
DOI: 10.1039/D4SU00485J

assess one relative point of the (apparent) viscosity curve.[207] Specifically, for PET, Bustos Seibert *et al.* [206] measured a higher MFI for undried virgin PET versus both dried virgin PET and dried recycled PET, as highlighted in **Figure 38** (right).

Consistently, the effect of the hydrolysis on the melt viscosity was studied by Seo *et al.*, [208] showcasing a steeper decrease in melt viscosity for undried PET samples compared to dried PET samples, further demonstrating the importance of moisture for the chain scission reaction. Additionally, for 3D printing of PLA blends, the MFI technique has been used to make a first analysis of the flowability for the composite deposition.[209] Spinace and De Paoli [210] in turn showed that MFI measurements revealed more PET degradation (higher MFI values) consistent with the carboxylic end group trend in **Figure 10**.

In parallel the melt flow rate (MFR) measurement has been performed, accounting (in principle) for the flow rate and density compared to an MFI measurement. Badia *et al.* [211] for instance evaluated the relevance of thermo-mechanical degradation on recycled PET and came to similar results as Spinace et *al.* [210] upon conducting MFI measurements. As highlighted in **Figure 39**, a continuous and exponential increase of MFR is observed with consecutive reprocessing cycles, which almost increased with a factor 4 after the sixth recycling step. This increase in fluidity is related to the progressive diminution of the average molar mass through multiple processing cycles.

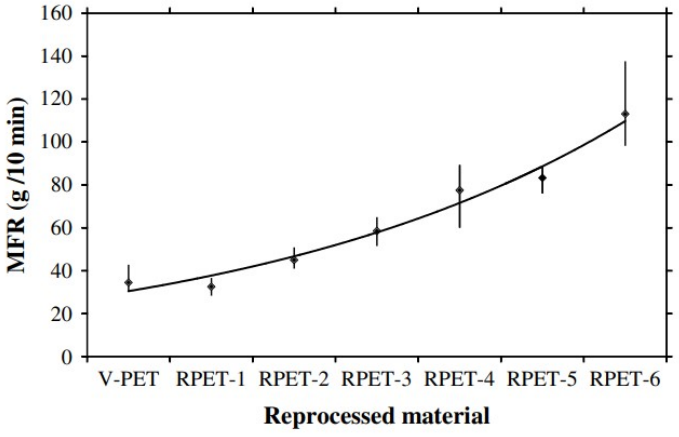

Figure 39: Evolution of melt-mass flow rate (MFR) through reprocessing simulation. [211] **Reproduced with permission from the publisher Elsevier.**

Connected in a broader context one also has the residence time in a processing unit as an important variable. It has been indicated that with more (screw) speed the average molar mass goes down because

View Article Online
DOI: 10.1039/D4SU00485J

of the impact of mechanical forces, implying higher shear rates.[212] However, higher speeds imply also lower residence times so that for instance scission reactions are less likely. Overall the relevance of computational tools comes forward, capable of mapping competitive phenomena[213].

Thermal properties

In the aforementioned subsection on the determination of rate coefficients it has been highlighted that TGA is a common technique to study to the thermal stability of polyesters. Critical TGA parameters are the heating rate, the starting temperature, the end temperature, and the type of atmosphere.[214]

Complementary to the already covered examples, in the present subsection, focus is first on the work of Baida *et al*.[105] investigating differences for virgin PET and recycled PET with(out) oxygen. As shown in **Figure 40**, TGA was conducted under inert atmosphere (case 1) to establish that both materials decomposed around 400°C. The difference between virgin and recycled material was only about 5°C. However, in the presence of oxygen (case 2), the decomposition of the material is faster and the leftover mass rather negligible. The second degradation step observed in this case is followed by a greater production of CO_2. While the first decomposition step results in both atmospheres, the second decomposition step only with oxygen again highlights the complexity of the environment in studying the relation of material properties and molecular changes.

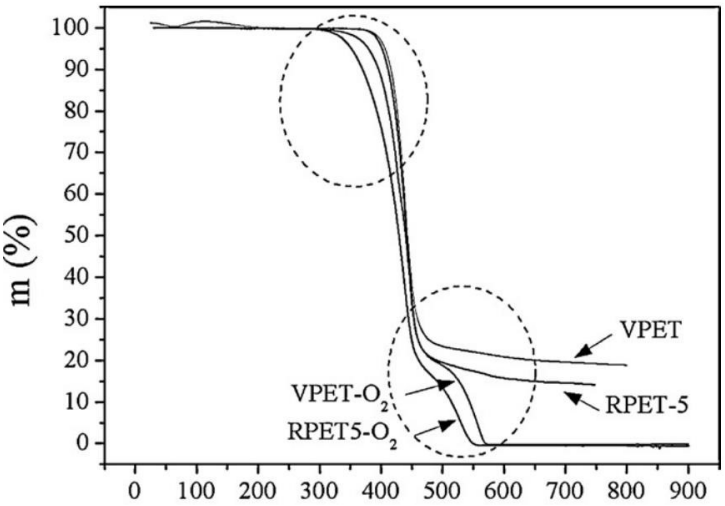

Figure 40. TGA analysis of virgin PET (VPET) and PET reprocessed for 5 times (RPET-5). Two cases are considered, an inert atmosphere and under oxygen.[105] Reproduced with permission from the publisher Elsevier.

View Article Online
DOI: 10.1039/D4SU00485J

An additional example on the relevance of TGA is included in **Figure 41**, considering different types of copolyester that maintain the maximum value of residual mass at a different temperature (in the presence of oxygen). In the top part of this figure, the beginning of the gravimetric curves are shown for modified polyethylene terephthalate (PETM) and PETg (a PETG grade with low amount of modifications), and the bottom part of this figure covers the temperature at which 97.5% of the initial mass is hold as a function of the residence time.

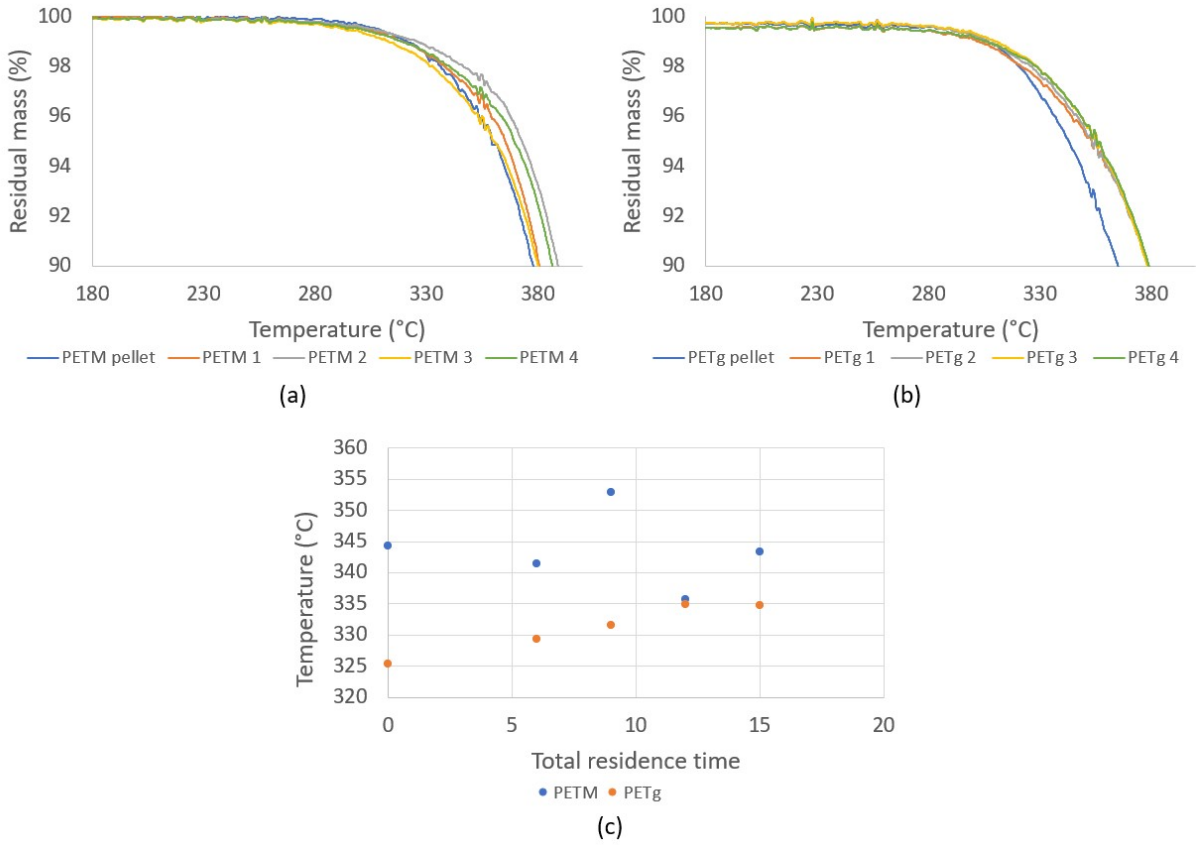

Figure 41. Top: TGA analysis results for PETM (a) and PETg (b) samples with different recycling; (c), temperature at 97.5 % of the initial weight of the sample for a given total residence time (min). Own work of the authors.

Small but significant changes can be observed. For PETM, the sample has e.g. lost 2.5 % of its mass between 335.7 and 352.9 °C, 5 % between 359.0 and 372,.4 °C, and 10 % between 379.4 and 389.0 °C. PETg has lost in turn 2.5 % of its mass between 325.4 and 334.9 °C, 5 % between 342.9 and 355,8 °C, and 10 % between 365.1 and 379.0 °C. Moreover, for PETg, a clear trend is visible for every residual mass, with the longer the residence time the higher the temperature at which the sample has lost mass. It can be further deduced that the thermal stability of PETM is larger than for PETg. Note that the higher

View Article Online
DOI: 10.1039/D4SU00485J

thermal stability of the acyclic units has been also stated by Thompson *et al.*[215] Consistently, TGA measurements that have been carried out under a nitrogen atmosphere at which PET was modified with bicyclohexyldimethanol showed a large loss of weight starting from 390 °C.

Another important technique for thermal analysis is differential scanning calorimetry (DSC), in which in many cases emphasis is on the determination of the crystallinity level, T_g and T_m. Specifically for PET such analysis is crucial, bearing in mind that it is a semi-crystalline material with a faster degradation in the amorphous phase. For example, Panowicz *et al.*[88] focused on the effect of thermo-oxidative degradation on the morphological and thermal properties of PET. They reported that the amount of the crystalline phase increases by about 8%, which translates into the properties of the aged material. The T_g and T_m. of lamellar crystals formed during the first and second crystallization increase with aging as well.

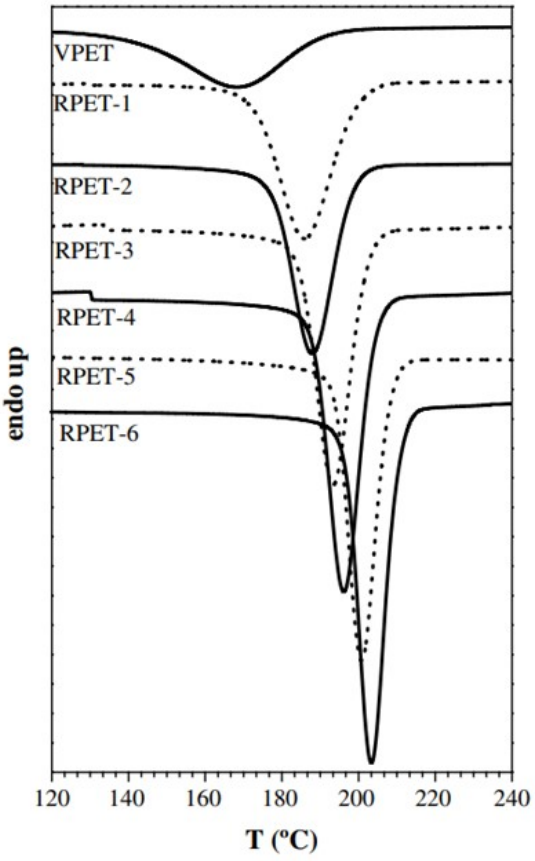

Figure 42. DSC curves of PET during the first cooling cycle.[211] Reproduced with permission from the publisher Elsevier.

Furthermore, in the study of Alves *et al.*[216] the objective was the better understanding of PET structural relaxation as a function of the crystallinity degree. The T_g was monitored for a totally amorphous PET (cooled down at 40°C min^{-1}) and for PET with different degrees of crystallinity. The higher is the percentage of crystallinity the broader is the T_g range, implying a broader range of relaxation times. If the amount of crystals is small the mobility of the amorphous phase is more uniform. However once this number increases, one can assess the diversification of the amorphous phases. For instance the chains closer to the crystals lamellae have a higher relaxation time.[216]

In the context of mechanical recycling several groups have dealt with how the crystallinity changes during multiple reprocessing.[106,217] For example, as shown in **Figure 42**, after multiple reprocessing steps the crystallinity peaks of the first cooling appear sharper and shift to higher temperature values. This can be explained through the improved arrangement of the chains after the first heating. Degradation of PET results in a higher number of shorter chains, promoting better mobility during the cooling step.[211] Overall it follows that chain scission reactions induced under thermo-mechanical degradation may result in a heterogeneous distribution of chain lengths in the molten state, altering the subsequent amorphous and crystalline microstructure in recycled PET after chain rearrangement during cooling.

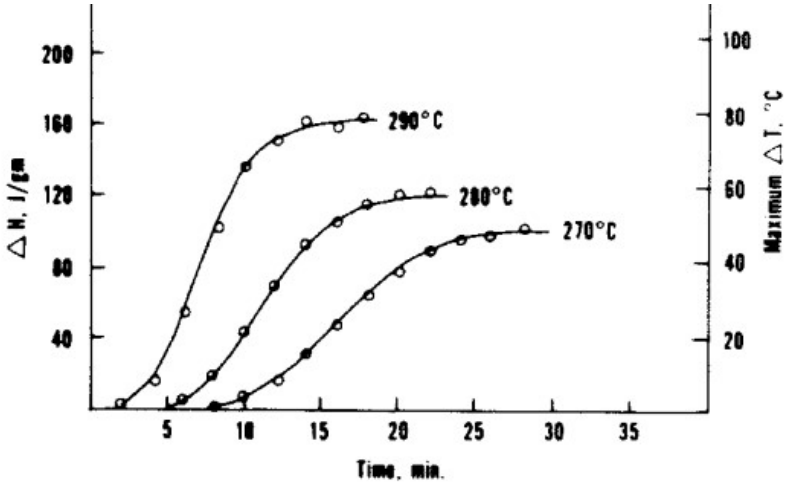

Figure 43. DSC enthalpies data regarding the exothermic peak of PET. The measurements were conducted at an isothermal mode for a certain time. The curves are parametric to the melting temperature. [121] **Reproduced with permission from the publisher John Wiley and Sons.**

View Article Online
DOI: 10.1039/D4SU00485J

Thermal analysis has been also applied for the investigation of the onset oxidation peak (OOP), which is a method for the determination of the thermo-oxidative stability of a polymeric material. The procedure follows the standard ASTM E2009 and consists in heating the sample at a constant heating rate and registering the temperature in case the first exothermic peak appears.[218] Specifically, Jabarin and Lofgren [121] analyzed the degradation of PET under an air environment. Several PET samples were vacuum dried and kept at a fixed melting temperature in an air atmosphere. The study reported the (absolute) enthalpy difference (ΔH) for oxidative degradation and its evolution during time. As shown in **Figure 43**, an S shape is obtained, with a higher induction time if the melting temperature is higher.

Analysis of the oxidative offset has also been more recently performed for copolyesters, as shown by Trossaert *et al.*,[219] considering PETM and PETg. The oxidation onset temperature (OOT) was found by analysing the DSC signal of the TGA instrument. In **Figure 44** (left), the relevant part of the DSC curves for PETM are given. It is clear that the OOT is lower if the sample has been exposed to a longer residence time in the extruder. The difference between the pellet and the processed samples is the most striking. The reason of the OOT decrease can be found in the presence of more shorter chains as result of a longer processing time. In fact more chain ends are present, and oxygen has more easily accessible sites to attack functional groups prone to oxidation, for instance the alcohol groups. Shorter chains also lead to a higher chain mobility as a whole, which results in a higher reactivity.

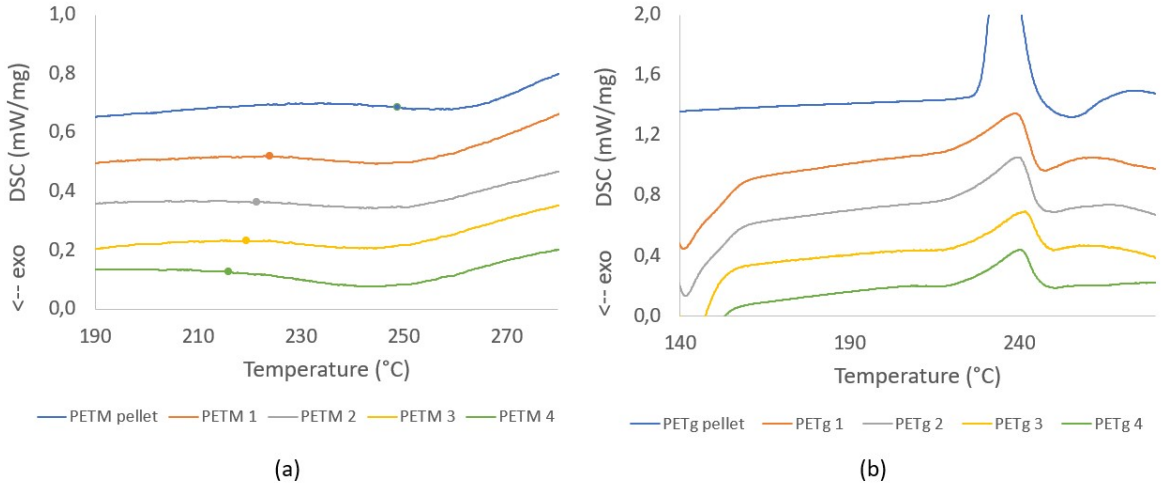

Figure 44. DSC curves for TGA analysis of PETM (a) and PETg (b) residence time samples with a highlighted oxidation onset temperature, based on Trossaert *et al.* [219] Both subplots are reproduced in open access redistribution mode

View Article Online
DOI: 10.1039/D4SU00485J

For PETg, as shown in **Figure 44** (right), the DSC signal is more complex. As PETg is a crystalline material, an exothermal cold crystallization peak (left side of the graph) and a melt peak results. It is visible that there is a drop in the signal just after melting. This means that the OOT occurs at approximately the same time or just after melting occurs. Although no OOT could be determined, a slight trend is visible upon looking at the graph. For the pellets, a large drop is situated after the melt peak. However, this drop becomes smaller in case the residence time increases. Moreover, the melt peak seems to be smaller if the residence time increases. This implies that once the residence time increases the OOT moves to lower temperatures and has a larger overlap with the melt peak. The melt peak is thus somewhat compensated for, resulting in a smaller endothermal peak.[219]

Mechanical properties

Besides rheological and thermal properties also mechanical properties matter. An overview of important mechanical properties for PET is given in **Table 8**. Depending on the grade, e.g. the presence of comonomers, the mechanical properties can vary providing more or less stiffness to the material and determining its further applications.

Table 8: Mechanical properties of PET

Property	Test method	Value (unit)	Reference
Breaking strength	Tensile	50 (MPa)	[220]
Tensile strength (Young's modulus)		1700 (MPa)	[220]
Yield strain	Tensile	4 (%)	[220]
Impact strength	ASTM D256-86	90 (J m^{-1})	[220]
Heat of fusion	DSC	166 (J/g)	[221]
Breaking strength	Tensile	50 (MPa)	[220]
Tensile strength (Young's modulus)		1700 (MPa)	[220]
Yield strain	Tensile	4 (%)	[220]
Impact strength	ASTM D256-86	90 (J m^{-1})	[220]

Importantly to explain most of the properties in this table a link to lower scale phenomena is required. Hence, to understand the evolution of mechanical properties during PET simulated extrusion, i.e. repetitive processing, one needs to think about micro-scale (e.g. crystallinity) and molecular (e.g. chain length) variations as well.

View Article Online
DOI: 10.1039/D4SU00485J

For example, Badia *et al.* [211] observed a strong increase in the degree of crystallinity during consecutive extrusion cycles for PET, leading to significant embrittlement and complete loss of its plastic deformation properties after four reprocessing cycles. A related example is the variation of the mechanical properties by hydrolytic degradation, leading to chain scission and a decrease of M_n. Due to this degradation, the crystallinity increases, which makes the material more brittle [222].

Similarly, as shown in **Figure 45**, La Mantia *et al.* [110] reported that together with the M_m decrease, the elongation at break (EB) diminishes. In addition, Frounchi [223] showed that the tensile properties and the impact resistance are affected by degradation with multiple reprocessing in a twin-screw extruder. This author specifically observed more than 50% decrease of M_m (mass average molar mass; also known as M_w) for 5 reprocessing cycles, and a 10% and 12% decrease of the tensile strength and impact strength respectively.

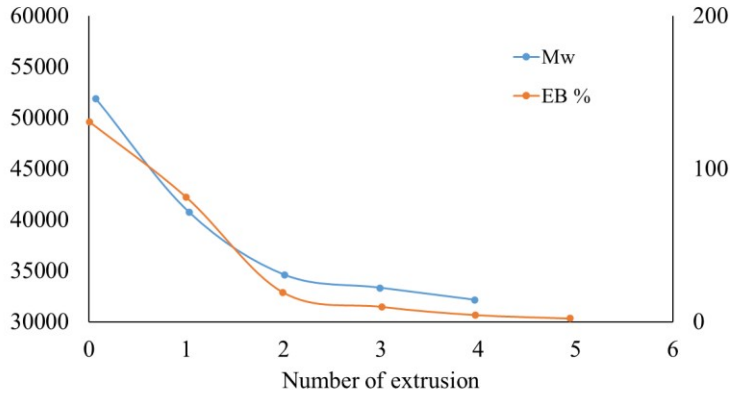

Figure 45. The mass average molar mass (or molecular weight; M_w) and elongation (EB) at the brake after different extrusion cycles of PET. Data to construct the figure taken from La Mantia et al. [110]

The opposite trend for crystallinity, i.e. a decrease with more recycling, and the same trend for the tensile properties, i.e loss of tensile strength, was reported by Müller *et al.* [224] for PCW beverage PET bottles. The authors reprocessed virgin pellets and shredded bottles via injection molding under the same conditions and compared the average molar mass, crystallinity with a link to crystallite size and transparency, as well as the tensile properties. The authors observed a 30% smaller value for the average molar mass and a 50% smaller stress at break for the recycled material. Furthermore, a brittle behavior

View Article Online
DOI: 10.1039/D4SU00485J

for the virgin specimens in contrast to the ductile behavior of the recycled specimens was observed, which was linked to the now opposite evolution of crystallinity. The authors emphasized that the virgin material was initially more crystalline than the post-consumer one due to different grades. This highlights once again the broadness of the properties that can be achieved for PET.

In addition, Giannotta *et al.*[225] and Torres *et al.*[226] mentioned that contaminants such as PVC and adhesives play a significant role in the material properties of the recycled PET. In particular, Giannotta *et al.*[225] listed several factors that can affect crystallization of PCW PET, i.e. (i) the presence of impurities and the increased content of cyclic or linear oligomers that act as nucleating agents,[227] (ii) the decrease in IV and average molar mass, (iii) the different thermal and mechanical histories, with the scraps coming from bottles crystallized by mechanical stretching, and the pellets crystallized by heating, (iv) the presence of residual moisture coming in the shape of scraps, and (v) the molecular orientation of material during the injection molding. Specifically, PCW PET being more contaminated than post-industrial PET is more sensitive to thermal and hydrolytic degradation, leading to a decrease in IV and average molar mass. This facilitates for PCW PET spherulitic crystallization, which strongly reduces the elongation at break and the impact strength.

It should be reminded that for the recycling of PCW the influence of photo-oxidative and hydrolytic degradation needs to be assessed. In this scope, the effect on PET morphology after UV aging has been investigated by Feng *et al.*, [228] who compared aging of PET with polypropylene and poly(vinyl chloride) through SEM imaging. Increasing the UV irradiation time revealed physical changes at the surface of the plastics, especially after 84 to 168 days. On the PET surface one can notice the formation of pits, flakes and adhering particles, hence, plastic fragmentation occurred.[228] Another example is the crystallinity increase reported by Panowicz *et al.*,[88] as discussed before in the context of thermo-oxidative degradation, inducing an increase in Young's modulus and a decrease in elongation at break.

View Article Online
DOI: 10.1039/D4SU00485J

Conclusions

Poly(ethylene terephthalate) (PET) is an important polymer in our society. In view of its circular use it is paramount to establish guidelines to decide on the most suited recycling technology. It is essential to establish the boundaries within which mechanical recycled solutions are fit for use in a variety of applications. While mechanical recycling is a lower energy process as compared to chemical recycling, it is less well-suited to process hard to recycle inputs and the quality of the outputs may not match that of chemically recycled solutions, specifically for multiple recycling generations.

The present overview focuses on the impact of chemical modifications for PET and polyester materials in general during its (re)processing under melt conditions, ideally in a (lab) extruder with a limited disturbance of contaminations. It has been demonstrated that molecular scale variations need to be mapped and preferably linked to variations at the material or application scale. The consideration of a detailed reaction scheme is strongly recommended, bearing in mind that degradation reactions not only alter the chain lengths but also the functional groups and potentially the topology of the chains. Depending on the environment and contact time a wide spectrum of degradation reactions can be active, with influence of temperature, UV light and moisture. Specifically chain repair relies on the presence of the correct functional groups and chain length reductions cannot be to severe to enable a more efficient mechanical recycling.

It has been explained under which circumstances which reactions (pathways) are dominant and how a consecutive number of extrusion cycles can have an impact on molecular and macroscopic key parameters defining the polymer material at hand. Model-based design is put forward as an interesting platform to identify all these variations and to facilitate the identification of optimal processing conditions. A main challenge remains the reliable determination of (input) kinetic parameters on the level of the elementary reaction, as most current kinetic studies report only apparent or lumped kinetic parameters. Interesting is to connect the chemical changes to the material changes, to enable a more science driven evaluation of the best (mechanical) recycling technology.

A follow-up contribution will situate the findings of the present work in a more general industrial framework in which emphasis is also on the role of contaminants as well as the overall mechanical

View Article Online
DOI: 10.1039/D4SU00485J

recycling process, hence, from pre-treatment to finishing thus beyond the melt-based processing sections only. Overall both contributions aim at a representative reflection of the state of the art for polyester mechanical recycling technology, acknowledging both chemistry and transport phenomena, as well as addressing lower and higher Technology Readiness Levels (TRLs).

Acknowledgements

C.F. and H.O. acknowledge the agency for Flanders Innovation & Entrepreneurship (VLAIO) via the Green AM project. L. T. acknowledges the Research Foundation – Flanders (FWO) via a scholarship: FWO.SPB.2021.0036.01. D.R.D. acknowledges FWO via the project G027122N. All authors thank Eastman for valuable input on PET-based materials and their market relevance.

References

View Article Online
DOI: 10.1039/D4SU00485J

1 Polyethylene Terephthalate Market Size Analysis Report, 2025, https://www.grandviewresearch.com/industry-analysis/polyethylene-terephthalate-market, (accessed 8 January 2024).

2 PET Bottles Market, https://www.transparencymarketresearch.com/pet-bottles-market.html, (accessed 23 July 2024).

3 J. A. Glaser, E. Sahle-Demessie and L. R. Te'ri, *Waste Material Recycling in the Circular Economy-Challenges and Developments*.

4 H. K. Webb, J. Arnott, R. J. Crawford and E. P. Ivanova, *Polymers (Basel)*, 2012, **5**, 1–18.

5 T. Grossetête, A. Rivaton, J. L. Gardette, C. E. Hoyle, M. Ziemer, D. R. Fagerburg and H. Clauberg, *Polymer (Guildf)*, 2000, **41**, 3541–3554.

6 T. Meyer and J. T. F. Keurentjes, *Handbook of polymer reaction engineering*, Wiley-VCH Verlag, 2005.

7 F. Awaja and D. Pavel, *Eur Polym J*, 2005, 41, 1453–1477.

8 J. M. Asua, *Polymer Reaction Engineering*, 2008, 1–367.

9 B. J. Holland and J. N. Hay, *Analysis of comonomer content and cyclic oligomers of poly(ethylene terephthalate)*, .

10 S. R. Turner, *J Polym Sci A Polym Chem*, 2004, 42, 5847–5852.

11 W. Romao, M. F. Franco, Y. E. Corilo, M. N. Eberlin, M. A. S. Spinace and M.-A. De Paoli, *Polym Degrad Stab*, 2009, **94**, 1849–1859.

12 H. A. Lecomte and J. J. Liggat, *Polym Degrad Stab*, 2006, **91**, 681–689.

13 S. R. Turner, *J Polym Sci A Polym Chem*, 2004, **42**, 5847–5852.

14 S. Fakirov, I. Seganov and E. Kurdowa, *Die Makromolekulare Chemie: Macromolecular Chemistry and Physics*, 1981, **182**, 185–197.

15 S. G. Hovenkamp and p J. P. Munting, *J Polym Sci A1*, 1970, **8**, 679–682.

16 C. Fiorillo, H. Ohnmacht, P. Reyes, P. H. M. Van Steenberge, L. Cardon, D. R. D'hooge and M. Edeleva, *Polym Degrad Stab*, 2023, **217**, 110511.

17 N. Vidakis, M. Petousis, L. Tzounis, A. Maniadi, E. Velidakis, N. Mountakis and J. D. Kechagias, *Materials*, 2021, **14**, 466.

18 European Green Deal: Putting an end to wasteful packaging, https://ec.europa.eu/commission/presscorner/detail/en/ip_22_7155, (accessed 8 January 2024).

19 F. Awaja and D. Pavel, *Eur Polym J*, 2005, **41**, 1453–1477.

20 Plastic pollution is growing relentlessly as waste management and recycling fall short, says OECD, https://www.oecd.org/environment/plastic-pollution-is-growing-relentlessly-as-waste-management-and-recycling-fall-short.htm, (accessed 8 January 2024).

View Article Online
DOI: 10.1039/D4SU00485J

21 A. Siddiqua, J. N. Hahladakis and W. A. K. A. Al-Attiya, *Environmental Science and Pollution Research*, 2022, **29**, 58514–58536.

22 A. Asadi, M. Miller, R. J. Moon and K. Kalaitzidou, *Express Polym Lett*.

23 Y.-H. V. Soong, M. J. Sobkowicz and D. Xie, *Bioengineering*, 2022, **9**, 98.

24 A. Vozniak, R. Hosseinnezhad, I. Vozniak and A. Galeski, *Sustainable Materials and Technologies*, 2024, **40**, e00886.

25 M. H. Ghasemi, N. Neekzad, F. B. Ajdari, E. Kowsari and S. Ramakrishna, *Environmental Science and Pollution Research*, 2021, **28**, 43074–43101.

26 S. M. Al-Salem, P. Lettieri and J. Baeyens, *Waste Management*, 2009, 29, 2625–2643.

27 N. Singh, D. Hui, R. Singh, I. P. S. Ahuja, L. Feo and F. Fraternali, *Compos B Eng*, 2017, **115**, 409–422.

28 E. Barnard, J. J. R. Arias and W. Thielemans, *Green Chemistry*, 2021, **23**, 3765–3789.

29 A. Aguado, L. Martínez, L. Becerra, M. Arieta-Araunabeña, S. Arnaiz, A. Asueta and I. Robertson, *J Mater Cycles Waste Manag*, 2014, **16**, 201–210.

30 M. Han, in *Recycling of polyethylene terephthalate bottles*, Elsevier, 2019, pp. 85–108.

31 R. D. Allen and M. I. James, in *Circular Economy of Polymers: Topics in Recycling Technologies*, ACS Publications, 2021, pp. 61–80.

32 D. E. Nikles and M. S. Farahat, *Macromol Mater Eng*, 2005, **290**, 13–30.

33 K. Ragaert, L. Delva and K. Van Geem, *Waste management*, 2017, **69**, 24–58.

34 C. Nerìn, J. Albiñana, M. R. Philo, L. Castle, B. Raffael and C. Simoneau, *Food Addit Contam*, 2003, **20**, 668–677.

35 Damayanti and H.-S. Wu, *Polymers (Basel)*, 2021, **13**, 1475.

36 P. Benyathiar, P. Kumar, G. Carpenter, J. Brace and D. K. Mishra, *Polymers (Basel)*, 2022, **14**, 2366.

37 D. Paszun and T. Spychaj, *Ind Eng Chem Res*, 1997, **36**, 1373–1383.

38 I. Taniguchi, S. Yoshida, K. Hiraga, K. Miyamoto, Y. Kimura and K. Oda, *ACS Catal*, 2019, **9**, 4089–4105.

39 S. Joo, I. J. Cho, H. Seo, H. F. Son, H.-Y. Sagong, T. J. Shin, S. Y. Choi, S. Y. Lee and K.-J. Kim, *Nat Commun*, 2018, **9**, 382.

40 E. Barnard, J. J. R. Arias and W. Thielemans, *Green Chemistry*, 2021, **23**, 3765–3789.

41 N. Torres, J. J. Robin and B. Boutevin, *Eur Polym J*, 2000, **36**, 2075–2080.

42 M. K. Eriksen, J. D. Christiansen, A. E. Daugaard and T. F. Astrup, *Waste management*, 2019, **96**, 75–85.

43 A. Elamri, K. Zdiri, O. Harzallah and A. Lallam, *Polyethylene Terephthalate: Uses, Properties and Degradation*.

View Article Online
DOI: 10.1039/D4SU00485J

44 Damayanti and H.-S. Wu, *Polymers (Basel)*, 2021, **13**, 1475.

45 T. Liu, X. Gu, J. Wang and L. Feng, *Chemical Engineering and Processing - Process Intensification*, 2019, **135**, 217–226.

46 R. M. R. Wellen and M. S. Rabello, *J Mater Sci*, 2005, **40**, 6099–6104.

47 R. C. Roberts, *Polymer (Guildf)*, 1969, **10**, 117–125.

48 Z. Bashir, I. Al-Aloush, I. Al-Raqibah and M. Ibrahim, *Polym Eng Sci*, 2000, **40**, 2442–2455.

49 S. N. Vouyiouka, V. Filgueiras, C. D. Papaspyrides, E. L. Lima and J. C. Pinto, *J Appl Polym Sci*, 2012, **124**, 4457–4465.

50 J. E. Mark, *New York*.

51 N. B. Sanches, M. L. Dias and E. B. A. V. Pacheco, *Polym Test*, 2005, **24**, 688–693.

52 C. W. Chen, P. H. Liu, F. J. Lin, C. J. Cho, L. Y. Wang, H. I. Mao, Y. C. Chiu, S. H. Chang, S. P. Rwei and C. C. Kuo, *J Polym Environ*, 2020, **28**, 2880–2892.

53 S. Makkam and W. Harnnarongchai, *Energy Procedia*, 2014, **56**, 547–553.

54 S. Farah, T. Tsach, A. Bentolila and A. J. Domb, *Talanta*, 2014, **123**, 54–62.

55 S. H. Park and S. H. Kim, *Fashion and Textiles*, 2014, **1**, 1–17.

56 W. Thodsaratpreeyakul, P. Uawongsuwan and T. Negoro, *Materials Sciences and Applications*, 2018, **09**, 174–190.

57 M. Del Mar Castro López, A. I. Ares Pernas, M. J. Abad López, A. L. Latorre, J. M. López Vilariño and M. V. González Rodríguez, *Mater Chem Phys*, 2014, **147**, 884–894.

58 M. R. Milana, M. Denaro, L. Arrivabene, A. Maggio and L. Gramiccioni, *Food Addit Contam*, 1998, **15**, 355–361.

59 A. Gooneie, P. Simonetti, K. A. Salmeia, S. Gaan, R. Hufenus and M. P. Heuberger, *Polym Degrad Stab*, 2019, **160**, 218–228.

60 S. Japon, Y. Leterrier and J. A. E. Månson, *Polym Eng Sci*, 2000, **40**, 1942–1952.

61 M. Xanthos, R. Dhavalikar, V. Tan, S. K. Dey and U. Yilmazer, *http://dx.doi.org/10.1177/073168401772678562*, 2001, **20**, 786–793.

62 S. Yao, T. Guo, T. Liu, Z. Xi, Z. Xu and L. Zhao, *J Appl Polym Sci*, 2020, **137**, 49268.

63 Ł. Pyrzowski and M. Miśkiewicz, *International Multidisciplinary Scientific GeoConference: SGEM*, 2017, **17**, 9–16.

64 T. Y. Liu, P. Y. Xu, Dan Huang, B. Lu, Z. C. Zhen, W. Z. Zheng, Y. C. Dong, X. Li, G. X. Wang and J. H. Ji, *J Hazard Mater*, 2023, **446**, 130670.

65 H. Ohnmacht, L. Trossaert, M. Edeleva, D. D'hooge and L. Cardon, *Faculty of Engineering and Architecture Research Symposium 2022 (FEARS 2022), Abstracts*, , DOI:10.5281/ZENODO.7400513.

66 K. Wang, J. Shen, Z. Ma, Y. Zhang, N. Xu and S. Pang, *Polymers 2021, Vol. 13, Page 452*, 2021, **13**, 452.

View Article Online
DOI: 10.1039/D4SU00485J

67 K. Matyjaszewski and M. Möller, *(No Title)*.

68 G. J. P. Bex, B. L. J. Ingenhut, T. ten Cate, M. Sezen and G. Ozkoc, *Polym Compos*, 2021, **42**, 4253–4264.

69 J. Kaiser and C. Bonten, *AIP Conf Proc*, , DOI:10.1063/5.0028415/597929.

70 E. García, P. J. Núñez, M. A. Caminero, J. M. Chacón and S. Kamarthi, *Compos B Eng*, 2022, **235**, 109766.

71 F. Adrian Rodriguez Lorenzana, D. Espalin, C. Yirong Lin, A. Lopes and S. L. Crites, .

72 NETZSCH-Gerätebau, *NETZSCH Handbook DSC.*, GmbH, 2015.

73 Y. Zhou, J. G. P. Goossens, R. P. Sijbesma and J. P. A. Heuts, *Macromolecules*, 2017, **50**, 6742–6751.

74 S. Bhagia, K. Bornani, S. Ozcan and A. J. Ragauskas, *ChemistryOpen*, 2021, **10**, 830–841.

75 I. Pillin, S. Pimbert, J. F. Feller and G. Levesque, *Polym Eng Sci*, 2001, **41**, 178–191.

76 S. V. Levchik and E. D. Weil, *Polym Int*, 2005, **54**, 11–35.

77 Isophthalic Acid - Chemical Economics Handbook (CEH) | S&P Global, https://www.spglobal.com/commodityinsights/en/ci/products/isophthalic-acid-chemical-economics-handbook.html, (accessed 9 January 2024).

78 J. Zhang, *J Appl Polym Sci*, 2004, **91**, 1657–1666.

79 Characteristics of Triexta PTT Carpet Fiber, https://www.thespruce.com/triexta-ptt-carpet-fiber-2908799, (accessed 9 January 2024).

80 D. P. R. Kint and S. Muñoz-Guerra, 2003.

81 B. Demirel, A. Yaraş and H. Elcicek, .

82 K. Pang, R. Kotek and A. Tonelli, *Prog Polym Sci*, 2006, **31**, 1009–1037.

83 M. Konstantopoulou, Z. Terzopoulou, M. Nerantzaki, J. Tsagkalias, D. S. Achilias, D. N. Bikiaris, S. Exarhopoulos, D. G. Papageorgiou and G. Z. Papageorgiou, *Eur Polym J*, 2017, **89**, 349–366.

84 F. Hannay, *Rigid plastics packaging: materials, processes and applications*, iSmithers Rapra Publishing, 2002, vol. 151.

85 H. C. A. Lim, in *Brydson's plastics materials*, Elsevier, 2017, pp. 527–543.

86 T. Chen, W. Zhang and J. Zhang, *Polym Degrad Stab*, 2015, **120**, 232–243.

87 B. Fayolle, L. Audouin and J. Verdu, *Polym Degrad Stab*, 2000, **70**, 333–340.

88 R. Panowicz, M. Konarzewski, T. Durejko, M. Szala, M. Łazińska, M. Czerwińska and P. Prasuła, *Materials 2021, Vol. 14, Page 3833*, 2021, **14**, 3833.

89 J. L. Gardette, A. Colin, S. Trivis, S. German and S. Therias, *Polym Degrad Stab*, 2014, **103**, 35–41.

90 S. A. Jenekhe, J. W. Lin and B. Sun, *Thermochim Acta*, 1983, **61**, 287–299.

91 J. Huang, H. Meng, X. Luo, X. Mu, W. Xu, L. Jin and B. Lai, *Chemosphere*, 2022, **291**, 133112.

View Article Online
DOI: 10.1039/D4SU00485J

92 H. Zimmerman and N. T. Kim, *Polym Eng Sci*, 1980, **20**, 680–683.

93 I. Marshall and A. Todd, .

94 D. V. A. Ceretti, M. Edeleva, L. Cardon and D. R. D'hooge, *Molecules*, 2023, 28.

95 T. M. Kruse, S. Woo and L. J. Broadbelt, *Detailed mechanistic modeling of polymer degradation: application to polystyrene*, .

96 S. Foti, M. Giuffrida, P. Maravigna and G. Montaudo, *Journal of Polymer Science: Polymer Chemistry Edition*, 1984, **22**, 1217–1229.

97 I. Lüderwald, *Pure and Applied Chemistry*, 1982, **54**, 255–265.

98 K. Yoda, A. Tsuboi, M. Wada and R. Yamadera, *J Appl Polym Sci*, 1970, **14**, 2357–2376.

99 I. C. McNeill and M. Bounekhel, *Polym Degrad Stab*, 1991, **34**, 187–204.

100 G. Montaudo, C. Puglisi and F. Samperi, *Polym Degrad Stab*, 1993, **42**, 13–28.

101 F. Samperi, C. Puglisi, R. Alicata and G. Montaudo, *Polym Degrad Stab*, 2004, **83**, 11–17.

102 R. Assadi, X. Colin and J. Verdu, *Polymer (Guildf)*, 2004, **45**, 4403–4412.

103 B. J. Holland and J. N. Hay, *Polymer (Guildf)*, 2002, **43**, 1835–1847.

104 W. Romao, M. F. Franco, Y. E. Corilo, M. N. Eberlin, M. A. S. Spinace and M.-A. De Paoli, *Polym Degrad Stab*, 2009, **94**, 1849–1859.

105 J. D. Badia, A. Martinez-Felipe, L. Santonja-Blasco and A. Ribes-Greus, *J Anal Appl Pyrolysis*, 2013, **99**, 191–202.

106 H. Wu, S. Lv, Y. He and J.-P. Qu, *Polym Test*, 2019, **77**, 105882.

107 M. A. S. Spinacé and M. A. De Paoli, *J Appl Polym Sci*, 2001, **80**, 20–25.

108 K. Weisskopf, *J Polym Sci A Polym Chem*, 1988, **26**, 1919–1935.

109 Z. O. G. Schyns and M. P. Shaver, *Macromol Rapid Commun*, 2021, **42**, 2000415.

110 F. P. La Mantia, *Recycling of PVC and mixed plastic waste. Chem Tec Publishing*, 1996, 63–76.

111 H. Jin, J. Gonzalez-Gutierrez, P. Oblak, B. Zupančič and I. Emri, *Polym Degrad Stab*, 2012, **97**, 2262–2272.

112 P. Oblak, J. Gonzalez-Gutierrez, B. Zupančič, A. Aulova and I. Emri, *Polym Degrad Stab*, 2015, **114**, 133–145.

113 A. V Shenoy, S. Chattopadhyay and V. M. Nadkarni, *Rheol Acta*, 1983, **22**, 90–101.

114 W. R. Waldman and M. A. De Paoli, *Polym Degrad Stab*, 1998, **60**, 301–308.

115 F. Cruz, S. Lanza, H. Boudaoud, S. Hoppe and M. Camargo, in *2015 International Solid Freeform Fabrication Symposium*, University of Texas at Austin, 2015.

116 F. Bueche, *J Appl Polym Sci*, 1960, **4**, 101–106.

117 S. J. Blanksby and G. B. Ellison, *Acc Chem Res*, 2003, **36**, 255–263.

118 V. B. Oyeyemi, J. M. Dieterich, D. B. Krisiloff, T. Tan and E. A. Carter, *J Phys Chem A*, 2015, **119**, 3429–3439.

119 A. B. Bestul, *Rubber Chemistry and Technology*, 1960, **33**, 909–920.

120 I. Marshall and A. Todd, *Transactions of the Faraday Society*, 1953, **49**, 67–78.

121 S. A. Jabarin and E. A. Lofgren, *Polym Eng Sci*, 1984, **24**, 1056–1063.

122 G. Botelho, A. Queirós, S. Liberal and P. Gijsman, *Polym Degrad Stab*, 2001, **74**, 39–48.

123 C. F. L. Ciolacu, N. Roy Choudhury and N. K. Dutta, *Polym Degrad Stab*, 2006, **91**, 875–885.

124 M. Edge, R. Wiles, N. S. Allen, W. A. McDonald and S. V Mortlock, *Polym Degrad Stab*, 1996, **53**, 141–151.

125 S. A. Jabbarin, *Polymeric materials encyclopaedia*, 1996, **8**, 6114.

126 A. M. C. de Souza, D. S. Leprêtre, N. R. Demarquette, M.-F. Lacrampe and P. Krawczak, *J Appl Polym Sci*, 2010, **116**, 3525–3533.

127 W. Romão, M. F. Franco, Y. E. Corilo, M. N. Eberlin, M. A. S. Spinacé and M. A. De Paoli, *Polym Degrad Stab*, 2009, **94**, 1849–1859.

128 J. D. Badia, A. Martinez-Felipe, L. Santonja-Blasco and A. Ribes-Greus, *J Anal Appl Pyrolysis*, 2013, **99**, 191–202.

129 P. Das and P. Tiwari, *Thermochim Acta*, 2019, **679**, 178340.

130 Z. O. G. Schyns, A. D. Patel and M. P. Shaver, *Resour Conserv Recycl*, 2023, **198**, 107170.

131 M. Abboudi, A. Odeh and K. Aljoumaa, *Toxicol Environ Chem*, 2016, **98**, 167–178.

132 M. Niaounakis, *Management of Marine Plastic Debris*, 2017, 127–142.

133 J. F. Rabek and J. F. Rabek, *Photostabilization of Polymers: Priciples and Applications*, 1990, 1–41.

134 M. Abboudi and A. Odeh, *Journal of Water Supply: Research and Technology - AQUA*, 2015, **64**, 149–156.

135 M. Day and D. M. Wiles, *J Appl Polym Sci*, 1972, **16**, 203–215.

136 J. Scheirs and J.-L. Gardette, *Polym Degrad Stab*, 1997, **56**, 339–350.

137 R. B. Fox, T. R. Price, R. F. Cozzens and J. R. McDonald, *J Chem Phys*, 1972, **57**, 534–541.

138 S. Yano and M. Murayama, *Polymer Photochemistry*, 1981, **1**, 177–190.

139 J. E. Potts, *Encyclopedia of Chemical Technology*, 1984, 626.

140 S. Li, *Journal of Biomedical Materials Research: An Official Journal of The Society for Biomaterials, The Japanese Society for Biomaterials, and The Australian Society for Biomaterials*, 1999, **48**, 342–353.

141 C. Sammon, J. Yarwood and N. Everall, *Polym Degrad Stab*, 2000, **67**, 149–158.

142 L. N. Woodard and M. A. Grunlan, *ACS Macro Lett*, 2018, 7, 976–982.

View Article Online
DOI: 10.1039/D4SU00485J

143 M. D. Rowe, E. Eyiler and K. B. Walters, *Polym Test*, 2016, **52**, 192–199.

144 T. El Darai, A. Ter-Halle, M. Blanzat, G. Despras, V. Sartor, G. Bordeau, A. Lattes, S. Franceschi, S. Cassel and N. Chouini-Lalanne, *Green Chemistry*.

145 D. Carta, G. Cao and C. D'Angeli, *Environmental Science and Pollution Research*, 2003, **10**, 390–394.

146 A. K. Urbanek, K. E. Kosiorowska and A. M. Mirończuk, *Front Bioeng Biotechnol*, 2021, **9**, 771133.

147 R. Brackmann, C. de Oliveira Veloso, A. M. de Castro and M. A. P. Langone, *3 Biotech*, 2023, **13**, 135.

148 F. Degli-Innocenti, T. Breton, S. Chinaglia, E. Esposito, M. Pecchiari, A. Pennacchio, A. Pischedda and M. Tosin, *Biodegradation*, 2023, 1–30.

149 N. F. S. Khairul Anuar, F. Huyop, G. Ur-Rehman, F. Abdullah, Y. M. Normi, M. K. Sabullah and R. Abdul Wahab, *Int J Mol Sci*, 2022, **23**, 12644.

150 J. Kaushal, M. Khatri and S. K. Arya, *Clean Eng Technol*, 2021, **2**, 100083.

151 R. Gao, H. Pan and J. Lian, *Enzyme Microb Technol*, 2021, **150**, 109868.

152 S. N. Dimassi, J. N. Hahladakis, M. N. D. Yahia, M. I. Ahmad, S. Sayadi and M. A. Al-Ghouti, *J Hazard Mater*, 2023, **447**, 130796.

153 A. Maurya, A. Bhattacharya and S. K. Khare, *Front Bioeng Biotechnol*, 2020, **8**, 602325.

154 R.-J. Mueller, *Process Biochemistry*, 2006, **41**, 2124–2128.

155 K. N. Fotopoulou and H. K. Karapanagioti, *Hazardous chemicals associated with plastics in the marine environment*, 2019, 71–92.

156 A. Launay, F. Thominette and J. Verdu, *Polym Degrad Stab*, 1994, **46**, 319–324.

157 W. McMahon, H. A. Birdsall, G. R. Johnson and C. T. Camilli, *J Chem Eng Data*, 1959, **4**, 57–79.

158 E. K. C. Moens, K. De Smit, Y. W. Marien, A. D. Trigilio, P. H. M. Van Steenberge, K. M. Van Geem, J. L. Dubois and D. R. D'hooge, *Polymers (Basel)*, 2020, 12.

159 J. Li and S. I. Stoliarov, *Polym Degrad Stab*, 2014, **106**, 2–15.

160 A. I. Osman, C. Farrell, A. H. Al-Muhtaseb, A. S. Al-Fatesh, J. Harrison and D. W. Rooney, *Environ Sci Eur*, 2020, **32**, 1–12.

161 S. M. A. Jafari, R. Khajavi, V. Goodarzi, M. R. Kalaee and H. A. Khonakdar, *J Appl Polym Sci*, 2020, **137**, 48466.

162 L. K. Nait-Ali, X. Colin and A. Bergeret, *Polym Degrad Stab*, 2011, **96**, 236–246.

163 M. Härth, J. Kaschta and D. W. Schubert, *Macromolecules*, 2014, **47**, 4471–4478.

164 G. Oreski, B. Ottersböck, C. Barretta, P. Christöfl, S. Radl and G. Pinter, *Polym Test*, 2023, 108130.

165 M. Arhant, M. Le Gall, P. Y. Le Gac and P. Davies, *Polym Degrad Stab*, 2019, **161**, 175–182.

View Article Online
DOI: 10.1039/D4SU00485J

166 J. H. Jung, M. Ree and H. Kim, *Catal Today*, 2006, **115**, 283–287.

167 J. Li and S. I. Stoliarov, *Combust Flame*, 2013, **160**, 1287–1297.

168 J. M. Encinar and J. F. González, *Fuel Processing Technology*, 2008, **89**, 678–686.

169 M. Härth, J. Kaschta and D. W. Schubert, *Polym Degrad Stab*, 2015, **120**, 70–75.

170 M. Arhant, M. Le Gall, P.-Y. Le Gac and P. Davies, *Polym Degrad Stab*, 2019, **161**, 175–182.

171 E. J. Lenardão, R. A. Freitag, M. J. Dabdoub, A. C. F. Batista and C. da C. Silveira, *Quim Nova*, 2003, **26**, 123–129.

172 M. D. Tabone, J. J. Cregg, E. J. Beckman and A. E. Landis, *Environ Sci Technol*, 2010, **44**, 8264–8269.

173 A. Ncube and Y. Borodin, in *2012 7th International Forum on Strategic Technology (IFOST)*, IEEE, 2012, pp. 1–6.

174 R. Meys, F. Frick, S. Westhues, A. Sternberg, J. Klankermayer and A. Bardow, *Resour Conserv Recycl*, 2020, **162**, 105010.

175 L. Shen, E. Worrell and M. K. Patel, *Resour Conserv Recycl*, 2010, **55**, 34–52.

176 A. Dormer, D. P. Finn, P. Ward and J. Cullen, *J Clean Prod*, 2013, **51**, 133–141.

177 R. A. Sheldon, *Green Chemistry*, 2007, **9**, 1273–1283.

178 R. A. Sheldon, *Green Chemistry*, 2017, **19**, 18–43.

179 S. Fadlallah, P. S. Roy, G. Garnier, K. Saito and F. Allais, *Green Chemistry*, 2021, **23**, 1495–1535.

180 S. Fadlallah, L. M. M. Mouterde, G. Garnier, K. Saito and F. Allais, in *Sustainability & Green Polymer Chemistry Volume 2: Biocatalysis and Biobased Polymers*, ACS Publications, 2020, pp. 77–97.

181 H. El Itawi, S. Fadlallah, F. Allais and P. Perré, *Green Chemistry*, 2022, **24**, 4237–4269.

182 T. Uekert, A. Singh, J. S. DesVeaux, T. Ghosh, A. Bhatt, G. Yadav, S. Afzal, J. Walzberg, K. M. Knauer and S. R. Nicholson, *ACS Sustain Chem Eng*, 2023, **11**, 965–978.

183 R. Volk, C. Stallkamp, J. J. Steins, S. P. Yogish, R. C. Müller, D. Stapf and F. Schultmann, *J Ind Ecol*, 2021, **25**, 1318–1337.

184 A. E. Schwarz, T. N. Ligthart, D. G. Bizarro, P. De Wild, B. Vreugdenhil and T. Van Harmelen, *Waste Management*, 2021, **121**, 331–342.

185 J. Nakatani, M. Fujii, Y. Moriguchi and M. Hirao, *Int J Life Cycle Assess*, 2010, **15**, 590–597.

186 T. Osswald and N. Rudolph, *Carl Hanser, München*.

187 G. A. Davies and J. R. Stokes, *J Rheol (N Y N Y)*, 2005, **49**, 919–922.

188 M. R. Mackley and R. P. G. Rutgers, in *Rheological Measurement*, Springer, 1998, pp. 167–189.

189 G. Trotta, B. Stampone, I. Fassi and L. Tricarico, *Polym Test*, 2021, **96**, 107068.

190 M. Kruse, V. H. Rolón-Garrido and M. H. Wagner, in *AIP Conference Proceedings*, American Institute of Physics, 2013, vol. 1526, pp. 216–229.

View Article Online
DOI: 10.1039/D4SU00485J

191 L. C. Sanchez, C. A. G. Beatrice, C. Lotti, J. Marini, S. H. P. Bettini and L. C. Costa, *International Journal of Advanced Manufacturing Technology*, 2019, **105**, 2403–2414.

192 C. Liu, J. He, E. van Ruymbeke, R. Keunings and C. Bailly, *Polymer (Guildf)*, 2006, **47**, 4461–4479.

193 D. H. S. Ramkumar and M. Bhattacmya, *Steady Shear and Dynamic Properties of B i od eg ra da b l e Po l y est e rs*, .

194 H. Münstedt, *Soft Matter*, 2011, **7**, 2273–2283.

195 Z. Yang, C. Xin, W. Mughal, Z. Wang, X. Bai and Y. He, *Advances in Polymer Technology*, 2018, **37**, 2344–2353.

196 J. Y. Lee, S. H. Kwon, I.-J. Chin and H. J. Choi, *Polymer Bulletin*, 2019, **76**, 5483–5497.

197 R. Rathner, W. Roland, H. Albrecht, F. Ruemer and J. Miethlinger, *Polymers (Basel)*, 2021, **13**, 1218.

198 S. A. Cruz, C. H. Scuracchio, L. B. Fitaroni and É. C. Oliveira, *Polym Test*, 2017, **60**, 236–241.

199 J. M. Dealy and J. Wang, *Melt Rheology and its Applications in the Plastics Industry*, 2013.

200 D. Kanev, E. Takacs and J. Vlachopoulos, *International Polymer Processing*, 2007, **22**, 395–401.

201 P. O. Brunn and J. Vorwerk, *Rheol Acta*, 1993, **32**, 380–397.

202 F. Cruz, S. Lanza, H. Boudaoud, S. Hoppe and M. Camargo, *Proceedings - 26th Annual International Solid Freeform Fabrication Symposium - An Additive Manufacturing Conference, SFF 2015*, 2020, 1591–1600.

203 V. Peinado, P. Castell, L. García and Á. Fernández, *Materials*, 2015, **8**, 7106–7117.

204 M. Kruse and M. H. Wagner, *Rheol Acta*, 2016, **55**, 789–800.

205 A. Bata, G. Toth, D. Nagy and K. Belina, in *Journal of Physics: Conference Series*, IOP Publishing, 2018, vol. 1045, p. 012007.

206 M. Bustos Seibert, G. A. Mazzei Capote, M. Gruber, W. Volk and T. A. Osswald, *Recycling*, 2022, **7**, 69.

207 S. Yin, R. Tuladhar, F. Shi, R. A. Shanks, M. Combe and T. Collister, *Polym Eng Sci*, 2015, **55**, 2899–2909.

208 K. S. Seo and J. D. Cloyd, *J Appl Polym Sci*, 1991, **42**, 845–850.

209 S. Wang, L. Capoen, D. R. D'hooge and L. Cardon, *Plastics, Rubber and Composites*, 2018, **47**, 9–16.

210 M. A. S. Spinacé and M. A. De Paoli, *J Appl Polym Sci*, 2001, **80**, 20–25.

211 J. D. Badia, F. Vilaplana, S. Karlsson and A. Ribes-Greus, *Polym Test*, 2009, **28**, 169–175.

212 T. Villmow, B. Kretzschmar and P. Pötschke, *Compos Sci Technol*, 2010, **70**, 2045–2055.

213 K. De Smit, T. Wieme, Y. W. Marien, P. H. M. Van Steenberge, D. R. D'hooge and M. Edeleva, *React Chem Eng*, 2022, **7**, 245–263.

View Article Online
DOI: 10.1039/D4SU00485J

214 S. M. Al-Salem, P. Lettieri and J. Baeyens, *Waste management*, 2009, **29**, 2625–2643.

215 T. N. Thompson, A. S. Coley and M. D. Schulz, *Polym Chem*, 2020, **11**, 2485–2491.

216 N. M. Alves, J. F. Mano, E. Balaguer, J. M. M. Dueñas and J. L. G. Ribelles, *Polymer (Guildf)*, 2002, **43**, 4111–4122.

217 S. D. Mancini and M. Zanin, *J Appl Polym Sci*, 2000, **76**, 266–275.

218 J. E. Volponi, L. H. I. Mei and D. dos S. Rosa, *J Polym Environ*, 2004, **12**, 11–16.

219 L. Trossaert, M. De Vel, L. Cardon and M. Edeleva, *Polymers 2022, Vol. 14, Page 196*, 2022, **14**, 196.

220 D. B. Jaquiss, W. F. H. Borman and R. W. Campbell, *edited by M. Grayson, John Wiley and Sons, New York*, 1982, **18**, 549.

221 O. Olabisi and K. Adewale, *Handbook of thermoplastics*, CRC press, 2016, vol. 41.

222 S. J. A. Hocker, W. T. Kim, H. C. Schniepp and D. E. Kranbuehl, *Polymer (Guildf)*, 2018, **158**, 72–76.

223 M. Frounchi, in *Macromolecular Symposia*, Wiley Online Library, 1999, vol. 144, pp. 465–469.

224 A. J. Müller, J. L. Feijoo, M. E. Alvarez and A. C. Febles, *Polym Eng Sci*, 1987, **27**, 796–803.

225 G. Giannotta, R. Po', N. Cardi, E. Tampellini, E. Occhiello, F. Garbassi and L. Nicolais, *Polym Eng Sci*, 1994, **34**, 1219–1223.

226 N. Torres, J. J. Robin and B. Boutevin, *Eur Polym J*, 2000, **36**, 2075–2080.

227 G. Giannotta, R. Po, N. Cardi, E. Occhiello and F. Garbassi, in *Proc Int Recyc Congress, Geneva, Switzerland*, 1993, p. 225.

228 W. Feng, C. Huang, X. Tan, N. Tang, L. Zhang, H. Li, X. Xu and J. Peng, *Ecotoxicology*, 2022, 1–10.

View Article Online
DOI: 10.1039/D4SU00485J

Biblio

Chiara Fiorillo is senior PhD student at the Center for Polymer and Material Technologies (CPMT) and the Laboratory for Chemical Technology (LCT) at Ghent University. She focuses in her research on the degradability of polyester-based materials, including a detailed rheological characterization. She is a co-author of 3 peer-reviewed research articles and currently preparing 3 more publications on the field of polyester sustainability and manufacturing design.

Prof. Dagmar R. D'hooge is the elected Chair for the Department "Materials, Textiles and Chemical Engineering" at Ghent University. His research emphasizes on multi-scale design of polymerization, polymer processing and polymer recycling. He uniquely performs research in chemical engineering, materials science, polymer science, and mechanics/rheology. He was a postdoctoral researcher at Carnegie Mellon University and Karlsruhe Institute of Technology, Karlsruhe. He is a visiting scientist at Stanford University. He is a co-author of 200 peer-reviewed full length research articles, 6 book chapters, 2 books, and 3 patents. He is a co-founder of two spin-offs.

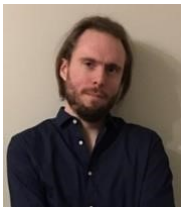

Prof. Mariya Edeleva is a tenure-track professor at the Center for Polymer and Material Technologies (CPMT) at Ghent University. She focuses in her research on the development of polymeric materials and their recycling to promote polymer circularity. She applies chemical and material design for sustainable polymer manufacturing, including mechanical recycling and reactive modification. She was a postdoctoral researcher at Aix-Marseille University. She is a co-author of 65 peer-reviewed research articles, 4 book chapters, and several patents.

.

View Article Online
DOI: 10.1039/D4SU00485J

Seeing the review nature of the current contribution data is reported as available in literature.